The control of fixational eye movements

Dissertation

zur Erlangung des akademischen Grades
Doktor der Naturwissenschaften (Dr. rer. nat.)
in der Wissenschaftsdisziplin Nichtlineare Dynamik

eingereicht an der
Mathematisch-Naturwissenschaftlichen Fakultät
Universität Potsdam

von
Konstantin Mergenthaler

Potsdam, Oktober 2008

Published online at the
Institutional Repository of the University of Potsdam:
http://opus.kobv.de/ubp/volltexte/2009/2939/
urn:nbn:de:kobv:517-opus-29397
[http://nbn-resolving.de/urn:nbn:de:kobv:517-opus-29397]

Acknowledgments

I thank Professor Ralf Engbert for accepting me as his doctoral student, for providing me with a very productive environment, and for his great support in all kinds of questions related to the preparation of the thesis. He helped me to go the large step from pure physics into modeling in the cognitive sciences.

I thank Professor Reinhold Kliegl and Professor Jürgen Kurths for offering me a position within the Promotionskolleg "Helmholtz center for mind and brain dynamics" and the financial support of the MWFK Brandenburg. I thank Maria Carmen Romano for her outstanding efforts to organize meetings, colloquia and financial backing of the Promotionskolleg.

I thank the members of the groups "Computational neuroscience" and "Cognitive psychology" for their fruitful discussions and support in the preparation of the experiments. Especially, I thank Hans Trukenbrod, Martin Rolfs and Michael Dambacher who heartily included me into the field of cognitive psychology. Further, I thank the student assistants who helped me with the realization of the experiments.

I thank James Ong and Georg Schmalhofer for proof reading. Both made many style suggestions and corrected numerous errors.

Thanks to all the people who continued to keep in touch with me in spite of the poor effort on my part, all those who believed in me from the start, and all those who were interested in my research. I especially acknowledge my parents, brothers and sisters, who have provided all sorts of support in the last three and a half years.

Last, but of course not least, I thank my girlfriend Inge Scheffing for what she is and has done for me. I thank her for enduring the large distance that separates us, the scarce amount of time that we have shared, and for always believing in me.

Abstract

In normal everyday viewing, we perform large eye movements (saccades) and miniature or fixational eye movements. Most of our visual perception occurs while we are fixating. However, our eyes are perpetually in motion. Properties of these fixational eye movements, which are partly controlled by the brainstem, change depending on the task and the visual conditions. Currently, fixational eye movements are poorly understood because they serve the two contradictory functions of gaze stabilization and counteraction of retinal fatigue.

In this dissertation, we investigate the spatial and temporal properties of time series of eye position acquired from participants staring at a tiny fixation dot or at a completely dark screen (with the instruction to fixate a remembered stimulus); these time series were acquired with high spatial and temporal resolution.

First, we suggest an advanced algorithm to separate the slow phases (named drift) and fast phases (named microsaccades) of these movements, which are considered to play different roles in perception. On the basis of this identification, we investigate and compare the temporal scaling properties of the complete time series and those time series where the microsaccades are removed. For the time series obtained during fixations on a stimulus, we were able to show that they deviate from Brownian motion. On short time scales, eye movements are governed by persistent behavior and on a longer time scales, by anti-persistent behavior. The crossover point between these two regimes remains unchanged by the removal of microsaccades but is different in the horizontal and the vertical components of the eyes. Other analyses target the properties of the microsaccades, e.g., the rate and amplitude distributions, and we investigate, whether microsaccades are triggered dynamically, as a result of earlier events in the drift, or completely randomly. The results obtained from using a simple box-count measure contradict the hypothesis of a purely random generation of microsaccades (Poisson process).

Second, we set up a model for the slow part of the fixational eye movements. The model is based on a delayed random walk approach within the velocity related equation, which allows us to use the data to determine control loop durations; these durations appear to be different for the vertical and horizontal components of the eye movements. The model is also motivated by the known physiological representation of saccade generation; the difference between horizontal and vertical components concurs with the spatially separated representation of saccade generating regions. Furthermore, the control loop durations in the model suggest an external feedback loop for the horizontal but not for the vertical component, which is consistent with the fact that an internal feedback loop in the neurophysiology has only been identified for the vertical component. Finally, we confirmed the scaling properties of the model by semi-analytical calculations.

In conclusion, we were able to identify several properties of the different parts of

fixational eye movements and propose a model approach that is in accordance with the described neurophysiology and described limitations of fixational eye movement control.

Zusammenfassung

Während des alltäglichen Sehens führen wir große (Sakkaden) und Miniatur- oder fixationale Augenbewegungen durch. Die visuelle Wahrnehmung unserer Umwelt geschieht jedoch maßgeblich während des sogenannten Fixierens, obwohl das Auge auch in dieser Zeit ständig in Bewegung ist. Es ist bekannt, dass die fixationalen Augenbewegungen durch die gestellten Aufgaben und die Sichtbedingungen verändert werden. Trotzdem sind die Fixationsbewegungen noch sehr schlecht verstanden, besonders auch wegen ihrer zwei konträren Hauptfunktionen: Das stabilisieren des Bildes und das Vermeiden der Ermüdung retinaler Rezeptoren.

In der vorliegenden Dissertation untersuchen wir die zeitlichen und räumlichen Eigenschaften der Fixationsbewegungen, die mit hoher zeitlicher und räumlicher Präzision aufgezeichnet wurden, während die Versuchspersonen entweder einen sichtbaren Punkt oder aber den Ort eines verschwundenen Punktes in völliger Dunkelheit fixieren sollten.

Zunächst führen wir einen verbesserten Algorithmus ein, der die Aufspaltung in schnelle (Mikrosakkaden) und langsame (Drift) Fixationsbewegungen ermöglicht. Den beiden Typen von Fixationsbewegungen werden unterschiedliche Beiträge zur Wahrnehmung zugeschrieben. Anschließend wird für die Zeitreihen mit und ohne Mikrosakkaden das zeitliche Skalenverhalten untersucht. Für die Fixationsbewegung während des Fixierens auf den Punkt konnten wir feststellen, dass diese sich nicht durch Brownsche Molekularbewegung beschreiben lässt. Stattdessen fanden wir persistentes Verhalten auf den kurzen und antipersistentes Verhalten auf den längeren Zeitskalen. Während die Position des Übergangspunktes für Zeitreihen mit oder ohne Mikrosakkaden gleich ist, unterscheidet sie sich generell zwischen horizontaler und vertikaler Komponente der Augen. Weitere Analysen zielen auf Eigenschaften der Mikrosakkadenrate und -amplitude, sowie Auslösemechanismen von Mikrosakkaden durch bestimmte Eigenschaften der vorhergehenden Drift ab. Mittels eines Kästchenzählalgorithmus konnten wir die zufällige Generierung (Poisson Prozess) ausschließen.

Des weiteren setzten wir ein Modell auf der Grundlage einer Zufallsbewegung mit zeitverzögerter Rückkopplung für den langsamen Teil der Augenbewegung auf. Dies erlaubt uns durch den Vergleich mit den erhobenen Daten die Dauer des Kontrollkreislaufes zu bestimmen. Interessanterweise unterscheiden sich die Dauern für vertikale und horizontale Augenbewegungen, was sich jedoch dadurch erklären lässt, dass das Modell auch durch die bekannte Neurophysiologie der Sakkadengenerierung, die sich räumlich wie auch strukturell zwischen vertikaler und horizontaler Komponente unterscheiden, motiviert ist. Die erhaltenen Dauern legen für die horizontale Komponente einen externen und für die vertikale Komponente einen internen Kontrollkreislauf dar. Ein interner Kontrollkreislauf ist nur für die vertikale Kompoente bekannt. Schließlich wird das Skalenverhalten des Modells noch semianalytisch

bestätigt.

Zusammenfassend waren wir in der Lage, unterschiedliche Eigenschaften von Teilen der Fixationsbewegung zu identifizieren und ein Modell zu entwerfen, welches auf der bekannten Neurophysiologie aufbaut und bekannte Einschränkungen der Kontrolle der Fixationsbewegung beinhaltet.

Contents

Chapter 1

Introduction to fixational eye movements

1.1 Introduction

If we compare a human and a frog, several major physiological and behavioral differences are immediately obvious. In this dissertation, we focus on one small difference, which is not visible to the naked eye. We focus on differences in eye movements, but not the large eye movements, i.e. saccades, which can be seen in humans and frogs. Instead, we focus on the difference in the movements during the, at first glance, motionless periods between saccades. While for frogs, the eyes indeed are not moving [Lettvin et al., 1959], measurements with high spatial and temporal resolution reveal that the human eye moves perpetually and involuntarily during these periods. The existence of both possibilities suggests that they both have their advantages in different situations, and shows that tiny eye movements are avoidable. For frogs, it seems to be sufficient to perceive the static environment only during its own movements. It also seems to be advantageous if everything except the moving fly or stork fades from vision. For humans, who often use parts of the static environment, it seems beneficial to perceive it in detail - even at rest. The following dissertation will solely focus on humans.

The investigation of fixational eye movements supplies valuable results for several scientific disciplines, e.g. psychology, neuroscience and physics [e.g. Engbert, 2006]. From a psychological perspective, fixational eye movements can be seen as a minimal cognitive process. Evidence for this point of view comes from experiments that reveal interactions between focusing on a certain task, like performing a saccade to an appearing stimulus and the occurrence of microsaccades. In neuroscience, fixational eye movements allow deeper insight into control mechanisms and the interaction of motoric behavior and visual perception. This is due to the extremely

fast reaction of the oculomotor system to changes of visual stimuli. Furthermore, the idea of active vision [Findlay and Gilchrist, 2003], the alteration of visual performance by movements of the eye, allows conclusions to be drawn about the neurophysiological setup. For the field of physics, especially nonlinear dynamics, fixational eye movements supply dynamically controlled time series that can be described by a random walk. Furthermore, they server as a source of information about possible realizations of control processes on the basis of noisy input. The investigation of fixational eye movements can further deliver deeper insights into the information processing of spatio-temporal fields. In paticular, studies on the retina of salamanders and rabbits [Ölveczky et al., 2003] revealed that already at the level of the retina object motion is separated from background motion.

In this dissertation, the dynamical properties of fixational eye movements under different conditions are investigated. We apply several analyses to reveal mechanisms like dynamical triggering of microsaccades or the scaling behavior of fixational eye movements. Finally, we construct a dynamical model consisting of a stochastic delayed difference equation.

Vision has evolved as an exceptionally precise sense organ to perceive accurate locations and velocities of approaching predators and fleeing prey. Furthermore, it supplies good feedback about our own position within a diversified environment, which is mainly important while we are moving. These functional ideas about vision lead to the assumption that motion detection is one of the most important components in vision. However, after the first step of seeing a moving object, it is important to recognize it, and thus a high spatial resolution and the perception of color are beneficial. All these demands seem to be taken into account looking at the design of the human eye and the variety of eye movements the human eyes perform. A short description of the anatomy of the eye can partially explain the different types of eye movements observed in humans (Figure 1.1A). The exterior of the eye provides structural stability; it is made up of the transparent cornea, found anteriorly, which allows light into the inside of the eye, and the opaque sclera. If we follow the path of the light through the eye after it is refracted through the cornea, we find the lens, which allows variable focusing, the vitreous body, and the retina, which contains the photoreceptors and corresponding neural connections to the brain. The highest density of cone photoreceptors is at the centrally located fovea, which corresponds to the part of the retina with the highest spatial resolution and color discrimination; this area has an extent of approximately 1° of visual angle. As one moves further into the retinal periphery, one finds a decreasing number of cones and an increasing number of rods [Curcio et al., 1990], which are the photoreceptors more adapted to low light levels; one also finds that the size of the receptive field increases, which allows better motion detection.

Large eye movements are designed to bring the most interesting stimulus onto the fovea. To achieve this movement of the visual axis, the eyes are rotated within

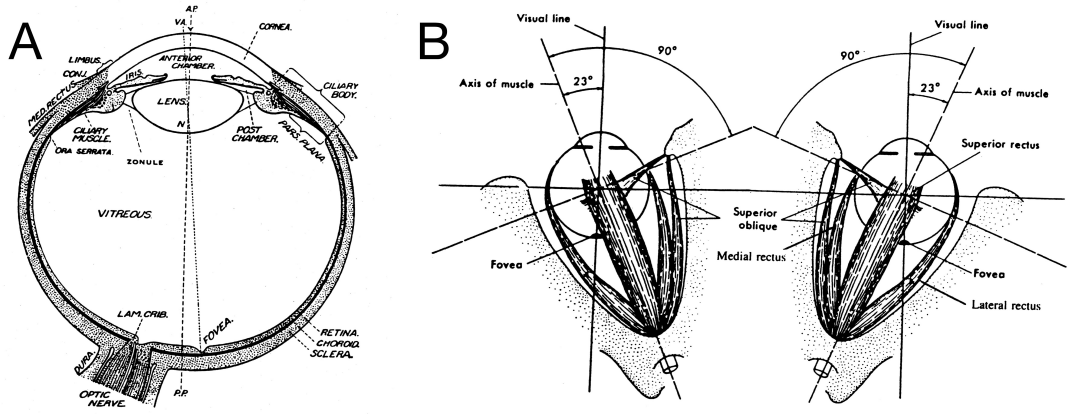

Figure 1.1: (A) Anatomy of the eye. (B) Placement of the eyes in the head and orientation of the muscles. Images from [Hung, 2001]

the eye socket by six extraocular muscles (Figure 1.1B); two of these are responsible for rotations along a horizontal axis, while the other four produce combined vertical and torsional rotations. A pulley allows one of these muscles to exert its force in such a direction that accurate rotation is possible [Angelaki and Hess, 2004]. All six muscles are equiped with mechanoreceptors which supply proprioceptive input; if the signal is used in eye movemente control is still discussed [Donaldson, 2000]. The extraocular muscles are controlled directly or indirectly by motoneurons, tonic neurons (to maintain the current eye position), burst neurons (to accelerate the eye), omnipause neurons (to suppress the bursting and stop saccades), and several other brain stem regions like the superior colliculus, the cerebellum and the cortex [Moschovakis et al., 1996].

Functionally, the larger eye movements can be separated into vergence and version [Hung, 2001]. During vergence, the left and right eyes rotate in opposite directions, to move from a centrally presented object far away to a near object, or vice versa. During version, the eyes move in the same direction but usually with different velocities. In normal viewing, the two movements are superimposed. A different classification of eye movements is the separation into saccades and smooth pursuit; these two movements are separated by their velocity. While smooth pursuit is a continuous motion usually driven by locking the gaze to moving objects, saccades are jumps within the natural scene or to locations of very fast moving objects. Brockmann and Geisel [2000] investigated the trajectory generated by saccades within a natural scene. They showed that the saccade amplitudes and directions are much better described by a Cauchy process (Levy process with $\mu = 1$ [Applebaum, 2004; Bouchaud and Georges, 1990]) than by a Gaussian process.

While the larger types of eye movements can easily be seen by looking at another person's eyes,a third type is usually neglected—the small eye movements during

fixations called fixational eye movements. Interestingly, by looking at some optical illusions we can percieve them (Figure 1.2 see also hompage by: Kitaoka) There are several reasons to take a closer look at fixational eye movements. Firstly, the eyes normally fixate about 80% of the time. Secondly, the processing of the visual surroundings is mostly performed during fixations, although the development of eyes to detect changes and movements in the environment required fast decaying responses in the photoreceptors to stationary stimuli. To counteract the perceptual fading of stationary objects, their image on the retina has to be moved across several photoreceptors. Although our eyes constantly perform these involuntary miniature movements, we normally do not perceive them. Instead, an image that is completely stabilized on the retina rapidly vanishes and cannot be perceived afterwards. Like the larger eye movements, the fixational eye movements can be separated into a low velocity component called drift and a high velocity component called microsaccades. A tiny oscillation can be found superimposed on the drift, which is called the micro tremor.

1.2 General overview of fixational eye movements

Several researchers have been investigating why humans perform small fixational eye movements and what the impact of these movements is on our capability to perceive the environment. More than 200 years ago, Robert Darwin [1786] suggested small perpetual movements of the eye as reason for the lucid edge around centrally fixated dark objects on a bright background. He stated that these small movements move fatigued and unfatigued photoreceptors across the boundaries. The unfatigued photoreceptors perceive the bright background brighter than the fatigued ones generating the corona. Helmholtz [1867] suggested that the small eye movements counteract retinal fatigue and that they also may be useful in the resolution of fine spatial gratings. By the mid 20th century, the eye movement recording techniques had improved and quantitative analyses of eye movements and fixational eye movements were applied. As early as 1934, the three different types of fixational eye movements were described by Adler and Fliegelman [1934]. However, the size of the movements is given more accurately in [Ratliff and Riggs, 1950]; they described fast jerky movements occurring one to two times per second called microsaccades, a slower random walk like motion called drift and a tiny oscillatory movement superimposed onto the drifting movement called tremor. For a recent review, see [Martinez-Conde et al., 2004].

1.2.1 Drift and tremor

The smaller components of the fixational eye movements are called tremor and drift.

Tremor is the name of a tiny oscillatory eye movement pattern with amplitudes of less than 30″ visual angle and frequencies of 30–100 Hz. The first measurements that led to values around the given ones were made by [Adler and Fliegelman, 1934] with values recalculated in [Ratliff and Riggs, 1950]. Ratliff and Riggs [1950] also reported similar amplitudes in own measurements. Later on, there were several more measurements that confirmed these values, summarized in [Martinez-Conde et al., 2004]. To measure tremor, one needs to use techniques with extremely high spatial resolution; this has meant that most of the measurements of tremor are made with piezoelectric devices that are in direct contact with the eye. However, tremor can be measured without contact by the use of double Purkinje eye trackers or by laser interferometry. Tremor has been measured under several conditions like fixation on a stimulus, instructed ceasing to fixate, fixations at an eccentric position, while sitting and lying down, in darkness and with added inertia [Bengi and Thomas, 1973]. It has been found that the spectral power at several frequencies is higher in fixations compared to the ceasing condition, that the power is more widely spread over frequencies for eccentric fixation positions, that increased inertia reduced the frequencies, that lying down reduced the power in the horizontal component while increasing it in the vertical component and that in darkness the spectral maxima are narrower. Another large investigation of the tremor was performed by Michalik [1987], who compared the tremor of 61 healthy subjects with 79 patients with diagnosed brain herniation. In his study, the well pronounced spectral maxima around 80 Hz vanish for small herniations and the more severe the herniations were, the more the frequencies tended to lower values. Both of these studies suggested that the origin of tremor is located within the brain stem; explicitly, the reticular pontine formation is suspected as the origin. Using a detailed analysis of the obtained power spectrum for intervals of drift and tremor between microsaccades, Eizenman et al. [1985] identified two frequency components; the data were collected with a non-contact technique. For lower frequencies (0–40 Hz), the power declines with frequency as $1/f^2$, suggesting an underlying Poisson process damped by friction and inertia of the eye ball in the socket. For the second component (40–100 Hz), a clock-like firing of motoneurons was proposed as origin. The clock-like firing could also explain the spreading of power to neighboring frequencies in eccentric fixation tasks. The question if tremor is conjugate in both eyes is still being discussed: Spauschuss et al. [1999] show evidence for small correlations between the eyes in the high frequency components.

Tremor is superimposed on the slow component called drift, which resembles a random walk. In addition to tremor and microsaccades drift was investigated in several studies [Helmholtz, 1867; Adler and Fliegelman, 1934]. The temporal behavior was initially described as a completely random process generated by instabilities in the tonic behavior of extraocular muscles. This was motivated by a coarse-grained analysis of the drift by Cornsweet [1956]. The author took intervals of 0.5 s approximately every 2 s from recordings of 45 s, discarded intervals with obvious

microsaccades, and used the difference between initial and final position as measure for the amount of drift. He further stated that drift changes its direction seldom enough that almost all intervals were without direction change. On the basis of this measure, he concluded that the disappearance of visual stimuli does not influence drift and that drift is typically not corrective to displacements and therefore "that drift ins not under direct visual control" (p. 991). However, Ditchburn and Ginsborg [1953] and Nachmias [1961, 1959] pointed out that drift is not completely random in direction. Nachmias further wrote that drift is substantially greater during fixations in darkness, and that the median direction of drift, computed as the difference in position between onset and offset of intervals of 0.2 s, changes between fixations on stimulus and in darkness for most participants; in this experiment, all fixations had a length of 3 s. Especially, the findings of Boyce [1967] and St.Cyr and Fender [1969] strongly emphasize control processes acting within the drift movement. St.Cyr and Fender [1969] showed that drift and microsaccades are comparable in their ability to correct for errors; but while drift mainly corrects vergence errors, microsaccades seem to have a stronger version correcting function. Recently, Møller et al. [2006] confirmed that 30 % of microsaccade end points were closer to the center of the most frequently used retinal area during fixation and 53 % of the drift interval end points were closer to the fixation center. The study by Steinman et al. [1967] revealed a difference between the two instructions "hold eyes still" and "fixate" on the same stimulus in the rate of microsaccades while the fixation error was approximately the same. This already suggests the existence of a slow control system. Collewijn and van der Mark [1972] investigated fixations in rabbits, which do not perform microsaccades but are able to maintain fixations by slow control while visual input feedback is supplied.

Further evidence for control mechanisms acting within the drift came from Steinman et al. [1973], who instructed their two participants to suppress microsaccades as effectively as possible. They reported that after 3 minutes of training with feedback about the number of microsaccades made, both participants were extremely good in maintaining their fixation position for 15 s without performing microsaccades. One of the participants showed a slight tendency to drift to the right. As a result, the authors suggested that some people correct errors in eye position resulting from an unintended directed drift with microsaccades. Generally, the ability to maintain a prior fixation position is strongly reduce in darkness [Skavenski, 1972; Goltz et al., 1997].

The first analyses that looked at the drift, investigating its resemblance to Brownian motion, were performed by Matin et al. [1970]. They investigated the distributions of the distances the drift progresses within certain time intervals. In this way, they were able to investigate systematic displacements and the deviation from a normal distribution. Since the random walking of the eyes is one of the cornerstones of this dissertation, we describe the analyses made by Engbert and

Kliegl [2003], which were motivated by the analysis of postural control data by Collins and De Luca [1993], in more detail in the analysis section.

1.2.2 Microsaccades

The fast components of the fixational eye movements are called microsaccades, since they resemble their larger counterparts, the saccades. Again, first measurements on their size were made by Adler and Fliegelman [1934]. In the numerous articles published since, the amplitude of microsaccades varies in the range of 1–120 minutes of arc, but the mean of the amplitude is mostly in the range of 6–20 minutes of arc. The large range occurs because the detection of a microsaccade strongly depends on velocity criteria and microsaccades in the early articles were detected by eye and marked by hand. The frequency of microsaccades is more consistently reported, and is mostly in the range of 1–2 Hz. Most of the literature is summarized by Martinez-Conde et al. [2004]. Microsaccades are reported to be, like saccades, occurring closely linked in time in both eyes, with similar amplitude and direction [Møller et al., 2002, 2006; Schulz, 1984].

The discussion rages on about the role of microsaccades. Some suggest that microsaccades reset the gaze point to the intended fixation position after error-producing periods of drift, while others argue that they move a stimulus from one fatigued region of photoreceptors to an unfatigued one. It has also been suggested that at least two types of microsaccades exist [Boyce, 1967]: larger ones that move a stimulus onto a new local region of receptors, and smaller ones that occur within the local regions. For the smaller ones they reported that they are directed toward the center of the small regions but not the center of the whole fixation. They further reported that microsaccades are most likely horizontally or vertically oriented. In 1980, Kowler and Steinman [1980] strongly argued against a functional role of microsaccades. Their leading argument was the ability to maintain fixation at a intended location while suppressing microsaccades. They further added arguments that microsaccades are a laboratory artifact due to exceptionally long fixations with a restrained head. On the other hand, Ditchburn [1980] argued that drift and tremor display mainly random behavior and that microsaccades are the major error correcting movement of the eye. Up to now, the importance or microsaccades in the process of image stabilization is unclear. Especially, as slow control processes in the drift is corrective by itself [Nachmias, 1959; Boyce, 1967; Møller et al., 2006]. Nevertheless, effects of attention on the rate and direction of microsaccades have been found [Kohama and Usui, 2002; Engbert and Kliegl, 2003; Laubrock et al., 2005; Betta and Turatto, 2006; Hafed and Clark, 2002], which suggesting a functional role of microsaccades to visual perception.

When we look at the two-dimensional eye movement trajectories of microsaccades, they seem to resemble Levy flights [Applebaum, 2004; Bouchaud and Georges, 1990;

Shlesinger et al., 1995], but in [Engbert, 2006], it was shown that they have a power law tail with too large an exponent. We reinvestigate this behavior by looking at the scaling properties of the amplitude distributions.

1.3 Functional role of fixational eye movements

Ever since the discovery of the fixational eye movements, their functional roles have been the theme of numerous publications and many heated exchanges. The two major roles attributed to fixational eye movements are the prevention of retinal fatigue and the enhancement of perceptual acuity. To investigate their functions, Riggs and Ratliff [1952]; Riggs et al. [1953] and Ditchburn and Ginsborg [1952] stabilized stimuli on the retina by attaching a small suction device to the eyeball, which moved the seen image to compensate for eye movements. Thus, the image always remained on the same photoreceptors. In these studies, they found out that stabilized images fade and cannot be perceived any more afterwards. In detail the effects of the three types of fixational eye movements on visibility were investigated by Ditchburn et al. [1959]. They concluded that large amplitude tremor, drift and microsaccades all are necessary to counteract retinal fading. The fading in these early studies took several seconds, but later, using a less invasive technique, where the eye is tracked and the stimulus is moved by the measured eye movement, [Rucci and Desbordes, 2003] found that the fading occurs within several hundred milliseconds. This discrepancy can be explained by slippage of the contact lenses [Barlow, 1963], thus validating the smaller values. The fading of entoptic images [Coppola and Purves, 1996] is even faster and occurs within 80 ms. The first function, the prevention of retinal fatigue, is widely accepted; while the second function, the better resolution of fine gratings, is still hotly debated.

As early as 1867, Helmholtz [1867] suggested fixational eye movement as a source for hyperacuity, the capability to resolve gratings that are smaller than the projected size of the photoreceptors. Investigations on hyperacuity were also performed by Riggs and Ratliff [1952]. They found out, using exceptionally short presentation times of 70 ms, that acuity is higher if the eyes perform a small, but not a large, amount of movement. Another hypothesis explaining hyperacuity uses spatial pooling over several receptors. To investigate this hypothesis, Tulunay-Keesey [1960] built an experiment presenting vernier offsets, single fine lines and oriented gratings for time intervals between 0.02 s and 1.28 s while stabilizing the image. In his experiment, he did not find differences between stabilized and unstabilized images, though he found a large effect of the presentation time, leading to his conclusion that spatial pooling better explains hyperacuity. Later on, a comparison of different stabilization techniques [Kelly, 1979] suggested that his stabilization was imperfect and that better stabilization strongly decreases acuity. Non-contact stabilization techniques have

been recently improved to allow stabilization along one dimension [Rucci et al., 2007]; use of these improved techniques have shown that the capability to recognize the orientation of gratings with a high spatial frequency, and consequently resolve them, is strongly reduced if fixational eye movements perpendicular to the orientation of the grating are suppressed by stabilization. Interestingly, this effect did not take place for gratings with low spatial frequencies.

During the 1970s, the question arose, how much the fixational eye movements under laboratory conditions differ from fixational eye movements under natural conditions. Laboratory conditions included strongly restraining heads by using bite boards or forehead and chin rests, and using heavy contact lenses. The main argument fueling the discussion was that head movement could suffice to counteract retinal adaption, and that during head movements, the eye movements have to have a head movement correcting component [Skavenski et al., 1979]. Investigations of fixations while the head can be moved strongly depend on the vestibulo-ocular reflex, and therefore include the performance and measurement of the vestibular system. Additionally, [Steinman et al., 1973], who conducted experiments where microsaccades were voluntarily suppressed, questioned their role in perception and gaze stabilization, and rather emphasized that drift plays a major role. In [Steinman et al., 2003], it has been shown that the accuracy of the fixation, in this case measured as the gaze error (the angle between the gaze vector for a given eye and the vector from the sighting center of the eye to the target), is significantly lower if the task demands accurate fixations on a distant target than if the fixations are on a near target that has the same physical extent. Currently, it is still unclear how much fixational eye movements are changed during fixations, where head and body movements have to be compensated.

1.4 Control of fixational eye movements

Going along with the question about the purpose of the fixational eye movements, the question arises, how are the fixational eye movements controlled; or are they controlled at all? Again, contradicting hypotheses have been suggested. On the one hand, there is the hypothesis that fixational eye movements are generated by random flexing of the extraocular muscles. In this hypothesis, flexing of the whole muscle generates drift and microsaccades, while actions of single muscle fibers generate the tremor component [Eizenman et al., 1985]. On the other hand, there is the hypothesis that drift and microsaccades are controlled by cortex and cerebellum or at least by brain stem areas [Spauschuss et al., 1999]. The control of fixational eye movements then needs to be separated in the slow drift/tremor component and the fast microsaccade component. While there is currently almost no literature on tremor control except the discussion of brain stem control in general [Michalik, 1987],

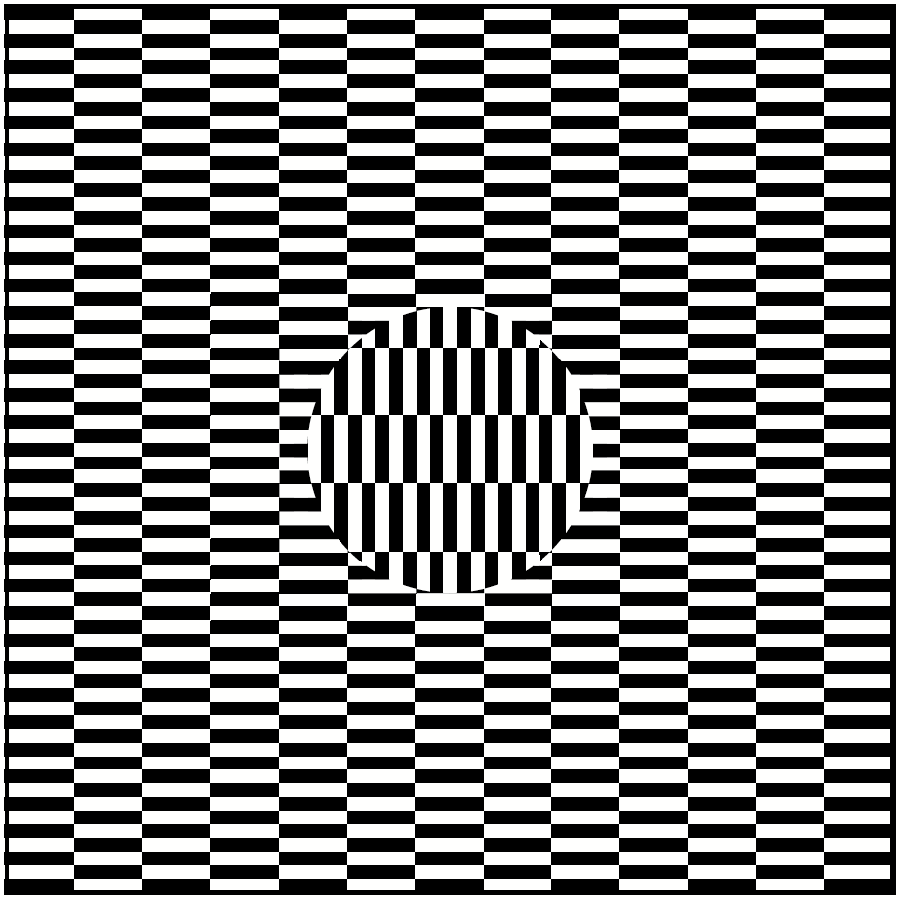

Figure 1.2: When looking at the center the inner disc seems to jitter on top of the background. This is an effect of the mainly horizontally oriented microsaccades. Figure composed by Ouchi [1977] and taken from [Ölveczky et al., 2003]

other fixational eye movements generate more interest. However, up to now, most of the control mechanisms for fixational eye movements are motivated by models for larger eye movements: The control of microsaccades is derived from the control of saccades, and drift control might be explained as smooth pursuit control with a target of zero velocity. As the control mechanisms have motivated our model, the possible control hubs are explained in more detail in Chapter 4.

In this context, the investigation of the control of fixational eye movements appears to be a missing link in eye movement control and qualifies as an interesting research field. The investigation of the control mechanisms is therefore chosen as the major research topic for this dissertation. Time series analyses are applied to reveal dynamical properties and a model for fixational eye movement control, based on the obtained properties, is suggested.

Chapter 2

Experiments

The basis for the following analyses and the model building are fixational eye movement data sets acquired with the EyeLink-II video based eye tracker (SR-Research, Osgoode, ON, Canada). The setup of the eye tracker is shown in Figure 2.1. There are three cameras sensitive to infrared light. One camera designated to detect the head movements, is directed towards the stimulus presentation screen, measuring displacements against the position of four fixed infrared markers (880 nm infrared) at the corners of the stimulus presentation computer screen. Two cameras are mounted on arms below the eyes. On the same arms, there are two types of infrared diodes illuminating the eyes: 925 nm infrared diodes for pupil detection and 880 nm infrared diodes for corneal reflex detection. Within the recorded videos, the pupils, as they appear much darker than their surrounding, are detected using a reflection threshold adjusted to the individual level necessary for each participant. The center of the darker area in the horizontal and vertical directions then represents the center of the pupil. Dilation and contraction of the pupil, e.g. pupillary fluctuations (hippus) [Beatty and Lucero-Wagoner, 2000] could only marginally effect the position meassurement, as dilation and contraction occur mainly with a radial symmetry and on much slower time scales than displacements, e.g. hippus occur with a frequency lower than 0.04 Hz. The corneal reflex can be used additionally to obtain better absolute position of the fixations. But the noise level is doubled for combined measurements. In the pupil only mode, the one used for the measurements, the EyeLink-II system measures with 500 Hz and a spatial resolution better than 0.01° visual angle. During the recording process, a heuristic filter was applied, which is based on [Stampe, 1993] and filters for random outliers. It can be used in a lower stage filtering for outliers that are one sample long (stage 1) and a higher stage which additionally reduced the data by outliers two samples long (stage 2).

The direction of the gaze corresponding to a certain position of the pupil was calibrated by presentation of a nine point grid, four points close to the corners, four points half the distance between these points along the edges, and one in the center

of the screen. Except for the center point, which was presented at the beginning and the end of the calibration routine, the points were presented in random order. For each point within an interval of 1 s, a fixation of at least 300 ms was expected. As soon as a fixation of 300 ms was found, the last 100 ms were used to average the pupil position and to match it to the gaze position at the center of the calibration stimulus. Saccades of at least 2.5° visual angle had to be performed between fixations. After the calibration was completed, its accuracy was checked by a validation routine, performed in the same way as the calibration. The calibration was considered to be sufficiently good for the measurements if the sum of squared error distances for the nine points of the validation was below 1° visual angle.

The experimental software performing the stimulus presentation was run in MATLAB (Version 6.5 for Apple Macintosh, Mathworks Natick, Massachusetts, USA) and based on the Psychophysics [Brainard, 1997; Pelli, 1997] and the EyeLink [Cornelissen et al., 2002] toolboxes. The participants were seated at a distance of 50 cm from the screen (Iiyama Vision Master Pro 514, 40 × 30 cm, 100 Hz, 1024 × 768 pixels) with their head resting on a chin rest. The height of the table could be adjusted to allow a comfortable seating position.

All participants in the experiments had normal or corrected to normal eye sight. In case of corrected to normal sight the participants were wearing their own glasses but not contact lenses.

2.1 Experiment 1: Simple fixation task

In the first experiment, a naive group of participants were asked to perform exceptionally long fixations (20 s) on a black fixation dot (2 × 2 pixels, equivalent to 0.09°) on a white background. Further, a check for blinks, which the EyeLink represents as missing data samples, was implemented to reduce the loss of data. As soon as the participants performed a blink the trials were restarted. Prior to the measurement period, a fixation check (lasting 0.5 s within a box of 1° × 1°) was performed on a fixation cross (composed of two rectangles, 10 × 2 pixels and 2 × 10 pixels wide) centered at the same location as the later fixation point. After the 20 s of fixation, the participants were presented a photograph of a natural scenes for 10 s, and were instructed that they should relax and blink. All participants performed 30 successful trials and were received either 7 Euro or 1.5 hours of study credit. The heuristic filter was at stage 1.

We measured 24 naive participants in this experiment. 23 were between 19 and 26 years with a mean of 22 years and one participant was 51 years old. Some of the participants had frequently participated in different types of eye tracking experiments within the same laboratory. In Figure 2.2 a typical trajectory is shown.

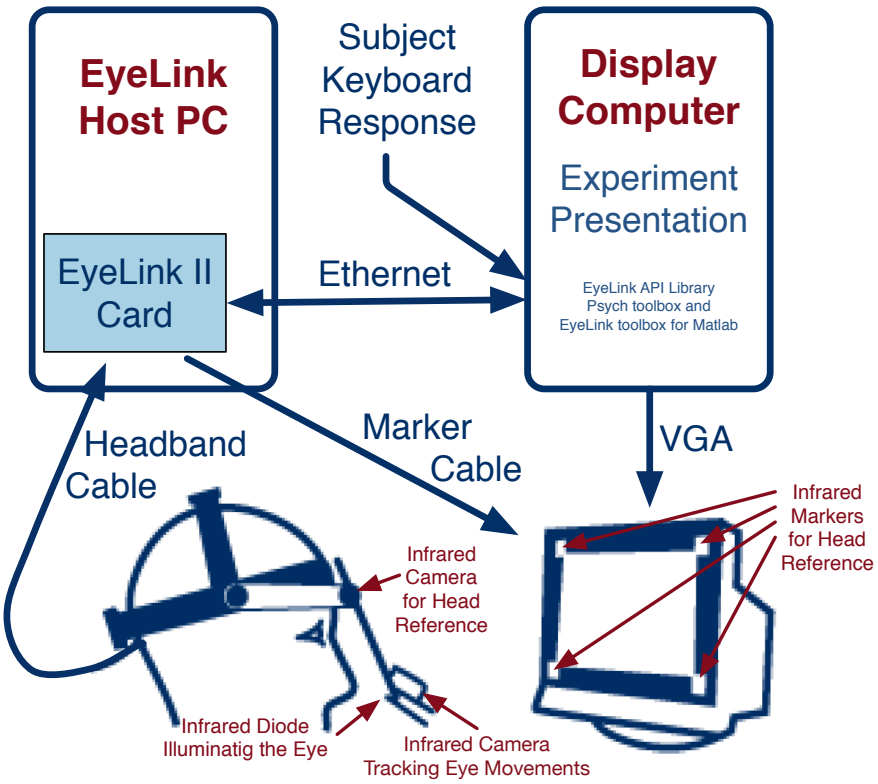

Figure 2.1: Setup of the EyeLink2 system, Image adapted from EyeLink2 Manual

2.2 Experiment 2: Simple fixations and fixations in darkness

The second experiment was based on the first one and again consisted of fixations of 20 s, Again a fixation check was performed and after the fixation duration, a natural scene was shown. In this experiment, we had two conditions. One was again a fixation at a fixation dot of the same size as in the first experiment, but now with inverted colors, i.e., a white dot on a dark background. In the second condition, the participants saw the fixation cross, but after a successful fixation check, the screen became completely dark. The participants were instructed to stay fixated on the memorized position of the fixation cross. Again, a total of 30 trials was performed, 15 in each condition. They were grouped into groups of 5 and half of the participants started with trials of the darkness condition, while the other half started with trials of the stimulus condition. During the entire experiment, a box was placed around the screen and the participant to exclude external light sources. The screen was

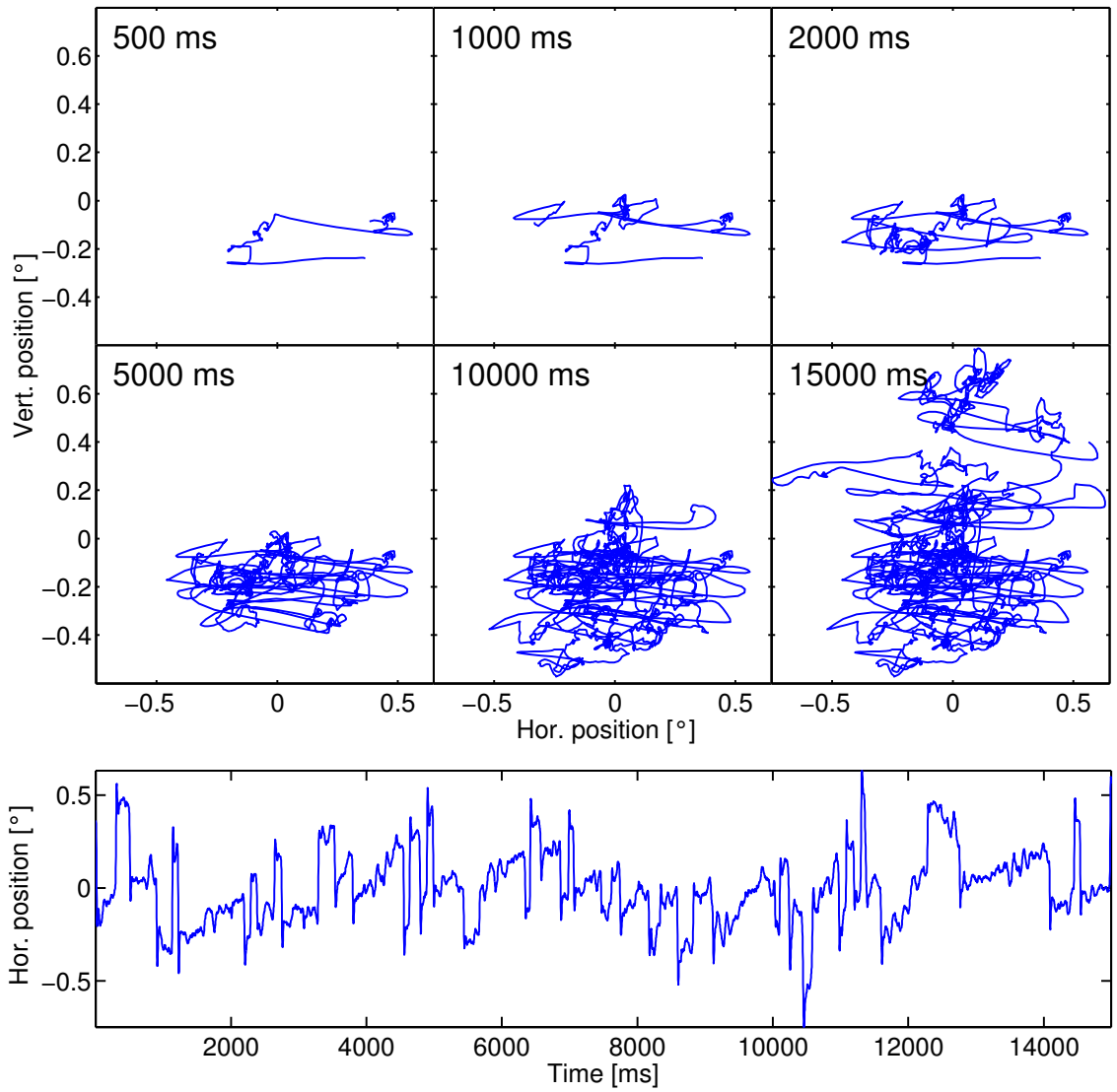

Figure 2.2: (upper) Six graphs depicting the 2d-trajectory within 500, 1000, 2000, 5000, 10000, 15000 ms. (lower) horizontal component of the same data set

invisible in the darkness condition. The rest of the setup was the same as in the first experiment.

In this experiment, we measured 20 experienced participants, most of them who had already taken part in fixational eye movement experiments. They were between 20 and 30 years old with a mean of 24.4 years. Ten were measured with the heuristic filter at stage 1 (participant 1 and 12-20) and ten were measured with the heuristic filter at stage 2 (participant 2-11).

Chapter 3

Time series analysis

In this chapter, we perform several analyses on the time series acquired from measurements of fixational eye movements. Part of the analyses investigate the local scaling of the entire eye movement data, while the rest look at parts of the trajectories separated by a microsaccade detection algorithm. The first analysis described in Section 3.1 is the detection of microsaccades, which is based on finding eye movements that surpass a velocity threshold. In Section 3.2, the analyses of the temporal local scaling of fixational eye movements are performed. They were used on the full time series and on time series where the microsaccades are removed. The analyses of the microsaccades, like the determination of microsaccade rate and amplitude are described in Section 3.3 and Section 3.4 respectively. Finally, interactions between drift prior to a microsaccade and the occurrence of the microsaccade (Section 3.5) and microsaccade amplitude (Section 3.6) are investigated. The central results discussed in Section 3.1, Section 3.3, and Section 3.4 are presented in [Mergenthaler and Engbert, subm]. Results from Section 3.2 are published in [Mergenthaler and Engbert, 2007]. Results from Section 3.5 are published in [Engbert and Mergenthaler, 2006].

3.1 Detection of microsaccades

Microsaccades are classified as fast directed events during fixations. In the early articles [e.g. Adler and Fliegelman, 1934; Ratliff and Riggs, 1950; Nachmias, 1959], microsaccades were detected by looking at the data and marking apparently fast directed events. Later, microsaccades were detected by various automated procedures. As one of the first authors using automated detection, [Boyce, 1967] used a three stage threshold algorithm: The first stage is the detection of velocities above 1°/s visual angle; then, a saccade onset is detected if the velocity within the next two samples exceeds 2°/s visual angle; finally, a saccade is stopped if two successive samples are

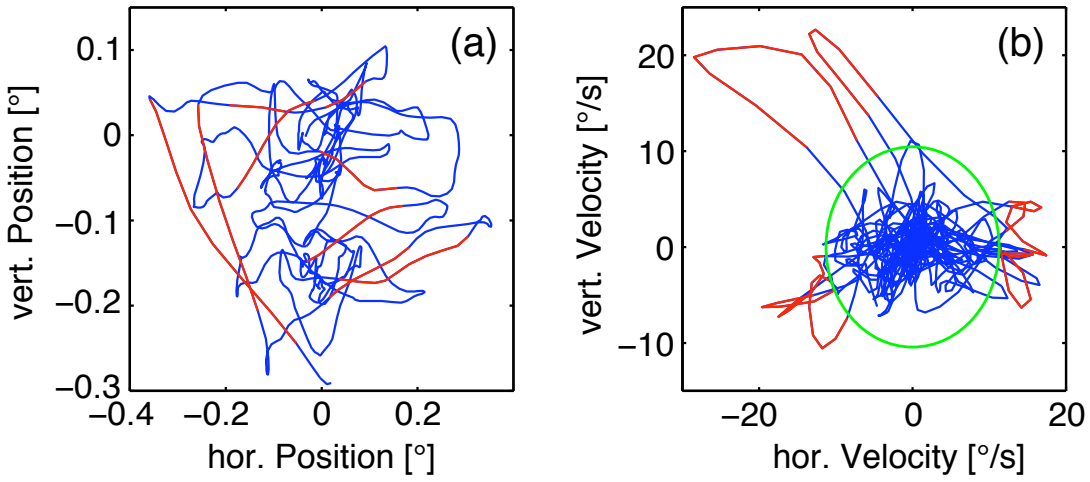

Figure 3.1: Illustration of the microsaccades and the microsaccade detection algorithm. (a) The microsaccades (red) as part of the fixational eye movement trajectory. (b) Velocity of the eye movement. The randomness of the direction of the movement centers it around zero. The green ellipse illustrates the detection threshold ($\lambda = 5.5$). The detected microsaccades are marked in red.

below 1°/s visual angle again. Another method is described in [Martinez-Conde et al., 2000], which is again based on the velocity but in this case in polar coordinates. In this method, two different measures are checked to determine the existence of a microsaccade: Velocity samples belong to a microsaccade as long as their "amplitude" value is above 3°/s visual angle and the angular value does not change more than 15° between consecutive samples. Widespread are also algorithms using thresholds within velocity and acceleration [e.g. Møller et al., 2002; Kohama and Usui, 2002]. One disadvantage of these methods is the use of rigid thresholds, independent of the participant, although different participants have different drift and microsaccade velocity ranges. To counteract this disadvantage, Engbert and Kliegl [2003] suggested an algorithm that takes the mean velocity of the trial into account. That algorithm is the basis for the following method to detect microsaccades.

The microsaccade detection algorithm consists of several steps. The first step is the generation of a smoothed two-dimensional velocity signal $\vec{v}$ from the fixation data $\vec{x}$ to suppress noise via,

$$\vec{v}_i = \frac{\vec{x}_{i+2} + \vec{x}_{i+1} - \vec{x}_{i-1} - \vec{x}_{n-2}}{6\Delta t} \,, \tag{3.1}$$

with $\Delta t = 2$ ms (sampling rate: 500 Hz). The random orientation of the fixation data samples leads to a mean value that is effectively zero (Figure 3.1b). As the microsaccades are events with high velocity, they consist of the data samples with the largest distance to the origin. In the second step, the median squared distance

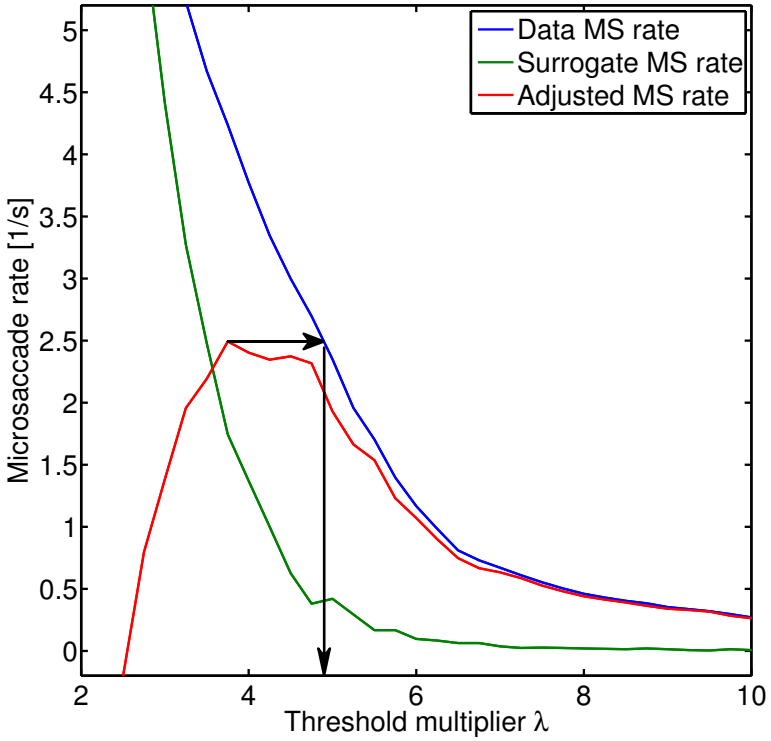

Figure 3.2: Illustrates the procedure leading to the optimal choice of the threshold multiplier. We used participant 1 of Experiment 2 in Condition 1 (visual fixation). The maximum of the rate difference at $\lambda = 3.75$ leads to an optimal threshold of $\lambda = 5$ for the participant by selecting the λ which yields a microsaccade rate in the original data that equaled the corrected microsaccade rate.

from the median,

$$\sigma_{0.5} = \sqrt{((v - (v)_{0.5})^2)_{0.5}}\ , \tag{3.2}$$

which is close to zero, is computed, for both velocity components v_h (horizontal) and v_v (vertical) independently; here, $(.)_{0.5}$ denotes the median estimator. In the next step, a threshold multiplier λ, chosen to be the same for both coordinates, determines the threshold which has to be exceeded,

$$\theta = \lambda\sigma_{0.5}\ . \tag{3.3}$$

We can choose one fixed value for λ by intuition for all participants as in [Engbert and Kliegl, 2003], or use a theoretically motivated approach on the basis of [Engbert and Mergenthaler, 2006] as described in the next section. Either way, the choice of λ substantially affects the number of detected microsaccades (Figure 3.2, blue line): As λ increases, the number of detected microsaccades decreases. In the next step of the algorithm, events are detected that surpasses the threshold ellipse (Figure 3.1, green ellipse) for at least three consecutive samples:

$$\left(\frac{v_h(i)}{\theta_h}\right)^2 + \left(\frac{v_v(i)}{\theta_v}\right)^2 > 1\ ; \tag{3.4}$$

here, the i denotes the index of the current sample and the indices v and h denote the vertical and horizontal components, respectively. θ is obtained from Eqn. (3.3). In

Figure 3.1b the detection of microsaccades due to the high velocities surpassing the threshold is illustrated; in Figure 3.1a the microsaccades are superimposed (red) on the eye position data. Finally, we considered microsaccades to be binocular events, similar to Ciuffreda and Tannen [1995]; Schulz [1984]; Møller et al. [2002, 2006]. This means that we kept only those candidate microsaccade epochs that are observed binocularly with a temporal overlap of at least one data sample.

3.1.1 Choice of threshold multiplier

There are two reasons for the increase in the amount of detected microsaccades when we diminish the threshold multiplier λ. One reason is that we can detect slower and therefore smaller (see: main sequence in [Engbert, 2006]) microsaccades if we reduce the threshold multiplier λ; this result is desired. The other reason is that the number of false alarms—fast drift events that surpass the threshold by chance—increases, which is obviously undesired. Therefore, it is necessary to choose the threshold multiplier in a way that we achieve an optimal balance between correct and falsely detected microsaccades. Furthermore, a data driven choice of the threshold multiplier λ allows us to take individual microsaccade shapes and relations between drift and microsaccade amplitudes into account [Mergenthaler and Engbert, subm].

The algorithm we used to determine the optimal threshold multiplier λ is based on the idea that the correct rate of microsaccades can be calculated from the actual rate of microsaccades detected for a chosen threshold multiplier λ by subtracting the number of wrongly detected microsaccades for the same λ. Therefore, we search for a way to generate surrogate data that maintains the drift properties but distorts the microsaccades. Thus we aim at the rejection of the null hypothesis that high-velocity epochs of fixational eye movements (possible microsaccads) occur by chance due to autocorrelations in the drift uncorrelated between eyes; if we cannot reject the null hypothesis, microsaccades do not exist.

A first idea is to randomly permute all the velocity samples of our data and then, to generate a position time series by $x_i = \sum_{k=1}^{i} v_k + x_1$, where k is the new index of the shuffled time series (Figure 3.3c) and x_1 the initial position of the eye. This maintains the original distribution of the velocity samples while completely destroying the existing temporal correlations within the data. As can be seen by comparison of Figure 3.3a and Figure 3.3c this heavily affects the drift, because fixational eye movements are characterized by temporal correlations [Engbert and Kliegl, 2004; Engbert, 2006; Mergenthaler and Engbert, 2007]. Furthermore, this kind of surrogate data is inappropriate for the rejection of the formerly stated null hypothesis. To reject the null hypothesis at least the autocorrelation function within each eye should be approximated. The phase-randomized amplitude-adjusted surrogate data generation suggested in [Theiler et al., 1992; Prichard and Theiler, 1994] tries to approximate the autocorrelation function, and therefore mimic the

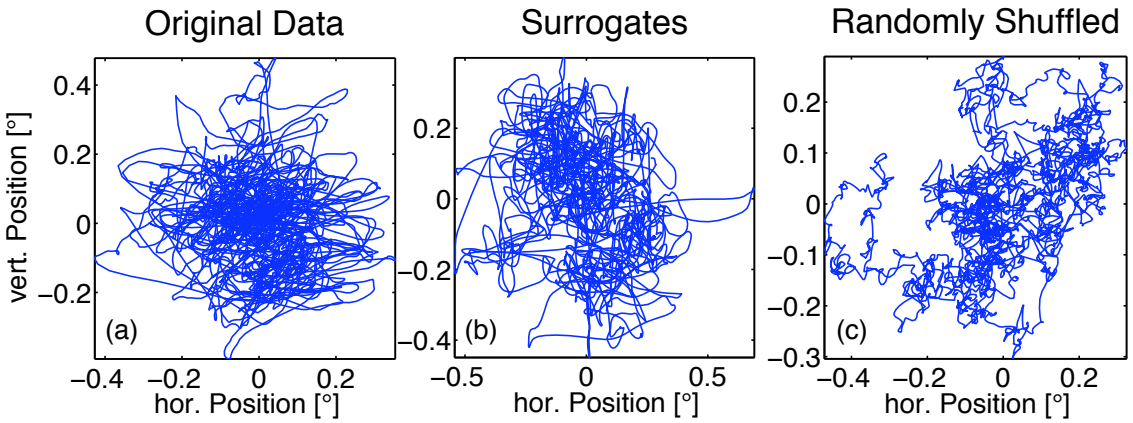

Figure 3.3: Effects of the surrogate data generation algorithms on data. (a) The original data set. (b) The amplitude-adjusted phase-randomized surrogates [Theiler et al., 1992] of (a) on the basis of the velocity are shown. (c) An illustration of an inappropriate surrogate data algorithm: random shuffling of the velocity samples.

temporal correlations, while shuffling the velocity samples[1]. It consists of several steps:

1. Two vectors v_s and i_v are generated from the velocity time series v, which must have an odd length N. v_s contains the samples of v ordered according to their size, and the vector i_v contains the rank of the data samples of v. Thus, $v_s(i_v) = v$.

2. Generate a vector g of uncorrelated normal distributed random numbers with the same length as the velocity time series v.

3. Sort the Gaussian vector g_s as in the first step.

4. Rearrange the sorted normal distributed random numbers g_s using the ranking vector i_v: $g_r = g_s(i_v)$. In this way, we generate a time series g_r that is a rescaled time series of v with the property that the amplitudes of the samples belong to a normal distribution.

5. Perform the discrete Fourier transform $f_g = \mathcal{F}(g_r)$. The vector f_g contains complex numbers and their complex conjugates which are symmetrically placed right and left of the zero frequency component at $(N + 1)/2$.

[1]The chosen type of surrogate data neglects possible non-linear dependencies within the data sets. Nevertheless, as we aim to separate microsaccades and drift, the possible separation by only their linear properties is sufficient.

6. Generate a random phase vector. This is done by generating a vector $\phi_0(k)$ with $k \in 1, \ldots, (N-1)/2$ filled with uniformly distributed random numbers within the range $-\pi \leq \phi_0(k) \leq \pi$. Using this vector, a full phase vector ϕ is constructed so that $\phi(k) = \phi_0(k)$ and $\phi(N-k+1) = -\phi_0(k)$ for $k \in 1, \ldots, (N-1)/2$ and $\phi(k) = 0$ for $k = (N+1)/2$. This routine is used to ensure that in the next step the values right of the 0 Hz frequency are the complex conjugate values of the values to the left. The complex conjugate values are necessary to obtain surrogate data consisting of real values.

7. The phase of the Fourier transformed Gaussian samples is randomized: $f_{gr} = f_g e^{i\phi}$.

8. The inverse Fourier transform returns a shuffled version of the Gaussian time series: $g_f = \mathcal{F}^{-1}(f_{gr})$.

9. The shuffled Gaussian time series g_f is sorted according to the size of the samples and a ranking vector i_g of g_f is achieved.

10. Finally, the sorted original time series v_s is rearranged using the ranking vector i_g: $v_r = v_s(i_g)$.

The vector v_r contains the surrogate data that is built from the original data samples that have been shuffled by random phase shifts of their Fourier transform. This has the effect that the distribution function of the original data is maintained and the autocorrelation function is slightly changed by fringe effects due to finite data size. Therefore, these surrogates were termed amplitude-adjusted phase-randomized (AAFT) surrogate data. The similarity between Figure 3.3a and Figure 3.3b corroborate our belief that this is an appropriate surrogate data method. Note that the surrogates cannot contain microsaccades by construction, but can exhibit fluctuations of velocity resembling microsaccades due to their non-vanishing autocorrelations.

With the AAFT surrogate data now available, we are able to compute the rate of microsaccades for the original data $r_{\mathrm{O}}(\lambda)$ and the rate of false alarms for the surrogate data $r_{\mathrm{AAFT}}(\lambda)$ and investigate the effect of the chosen threshold multiplier to both rates. In both time series the number of detected microsaccades increase with decreasing λ. However, the speed of the increase differs. We can then compute the rate of detectable proper microsaccades $r_{\mathrm{C}}(\lambda)$ (Figure 3.2, red line) by subtracting the rate of false alarms from the rate of events in the original data, $r_{\mathrm{C}}(\lambda) = r_{\mathrm{O}}(\lambda) - r_{\mathrm{AAFT}}(\lambda)$. In the following, we will refer to $r_{\mathrm{C}}(\lambda)$ as the corrected microsaccade rate. The maximum in the corrected rate $r_{\mathrm{C}}(\lambda)$ at λ_{max} gives the maximal number of detectable proper microsaccades. While λ_{max} is the point where the maximal number of proper microsaccades can be identified, it is not the point where only proper microsaccades are found, i.e., $r_{\mathrm{AAFT}}(\lambda_{max})$ can be large. Taking

this into account the optimal threshold multiplier (λ_0) is the threshold multiplier λ where the rate in the original data corresponds to the maximum of the corrected rate, $r_O(\lambda_0) = r_C(\lambda_{max})$ (denoted in Figure 3.2 by the arrows targeting the x-axis). Thus, λ_0 is always larger than λ_{max}. The maximum corrected rate $r_C(\lambda_{max})$ and the optimal threshold multiplier (λ_0) are determined for each participant separately within a range of $2 \leq \lambda \leq 12$. The high variety of the optimal threshold multipliers λ_0 (see arrows in Figure 3.2) is caused by varying relationships between drift and microsaccade velocity. The larger values of λ_0 observed in some participants derive from microsaccades that have a very high speed compared to the participants drift velocity. Later on, if we talk about a data set where the microsaccades are removed, the microsaccades used are those detected at the optimal threshold multiplier λ_0. Effects of experimental condition, individual differences and the absolute values of the rate are discussed in Section 3.3.

3.2 Temporal local scaling of fixational eye movements

To better understand the apparently erratic movement of the eye, we investigate its temporal local scaling, since temporal scaling classifies the type of random walk. For classical Brownian motion [Einstein, 1905], the mean square displacement $\langle x(t)^2 \rangle$, where $\langle . \rangle$ in this case denotes the ensemble mean, increases proportionally to t:

$$\langle x(t)^2 \rangle = 2Dt \ . \tag{3.5}$$

For ergodic processes, the sample mean is equivalent to the temporal mean. An analytical generalization of the classical Brownian motion was supplied by Mandelbrot and van Ness [1968], which was motivated by the work of Hurst [1951] on the outflow of large reservoirs like the lake Alberta which feeds the Nile river. The generalization allows scaling proportional to t within a range of $0 < H \leq 1$ leading to:

$$\langle x(t)^2 \rangle \propto t^{2H} \ . \tag{3.6}$$

This so-called Hurst exponent describes tree types of random behavior characterized by the dependence of single time points on earlier points in time. The random walk is either a classical Brownian motion $H = 0.5$ or a fractional random walk for $H \neq 0.5$. Fractional random walks can further be separated in sub-diffusive $H < 0.5$ and super-diffusive $H > 0.5$ processes. The major difference between classical Brownian motion and fractional Brownian motion is the correlation between increments. For classical Brownian motion, consecutive increments are uncorrelated while for fractional Brownian motion, the correlation function C is described by [Feder, 1988]:

$$C = 2(2^{2H-1} - 1) \ . \tag{3.7}$$

For $H = 0.5$, Eqn. (3.6) is the same as Eqn. (3.5) and $C = 0$. For $0 < H < 0.5$, the signal is anti-persistent, which means negative correlations ($C < 0$) between consecutive increments or the current and following data points. For $0.5 < H < 1$ the signal is persistent, which means positive correlations ($C > 0$) between consecutive increments or the current and following data points. Thus, random walks of these types have the tendency to move against ($0 < H < 0.5$), independently of ($H = 0.5$), or in ($0.5 < H < 1$) the direction of the current movement. An investigation of the local scaling behavior of data sets can be performed with several analyses, summarized in [Scafetta and Grigolini, 2002]. The first was suggested by Hurst [1951]; Hurst et al. [1965] and is called *rescaled range analysis*. The second, called *standard deviation analysis* (SDA), is even more directly connected to the variance of the underlying signal and was used in a two-dimensional version for the investigation of the center of pressure trajectory in [Collins and De Luca, 1993, 1994; Delignières et al., 2003]. A third possibility, developed by Peng et al. [1994] with the emphasis on the analysis of non-stationary time series, is *detrended fluctuation analysis* (DFA). A fourth way to obtain the local scaling behavior of a given time series is *spectral wavelet analysis*. It decomposes the time series variance on a scale-by scale level [Percival and Walden, 2000]. There are several other local scaling exponent analyses, e.g., *diffusion entropy analysis* [Scafetta and Grigolini, 2002].

For theoretical models of fractional Brownian motion, the scaling can be found independently of the absolute scale chosen, as they are fully scale invariant. This does not hold for most biological systems, which commonly show scaling within a range of scales, but also can show different local scaling behaviors within different local scaling regimes [Liebovitch and Yang, 1997]. The transitions between local scaling regions are commonly called crossovers and have been found for several biological systems, e.g., center-of-pressure trajectories [Collins and De Luca, 1993, 1994], voltage difference across the cell membrane of human T-lymphocyte cell lines [Churilla et al., 1996], and fixational eye movements [Engbert and Kliegl, 2004; Mergenthaler and Engbert, 2007]. All these biological systems share the property that the transition occurs from persistent behavior at small scales to anti-persistent behavior at large scales. We apply two of the scaling analyses to the data acquired from the experiments.

3.2.1 Rescaled range analysis

In this analysis, the time series x_t of length N is divided into non-overlapping time intervals of length n. For each interval, the deviations from the mean $\langle x \rangle_n = \frac{1}{n} \sum_{t=1}^{n} x(t)$ are summed up:

$$X(n, \tau) = \sum_{t=1}^{\tau} (x_t - \langle x \rangle_n) \; . \tag{3.8}$$

Then, the range $R(n)$ is computed as the difference between the maximum and minimum of the summed series:

$$R(n) = \max_{1\leq\tau\leq n} X(n,\tau) - \min_{1\leq\tau\leq n} X(n,\tau) \ . \tag{3.9}$$

To normalize the acquired values, they are divided by the standard deviation within the time intervals $S(n) = \sqrt{1/n \sum_{t=1}^{n}(x_t - \langle x\rangle_n)^2}$. Hurst [1951]; Hurst et al. [1965] showed that the water storage of the Nile river followed the scaling behavior described by the scaling relation:

$$\frac{R(n)}{S(n)} \propto t^H \ . \tag{3.10}$$

Thus, the scaling exponent can be acquired from a linear fit to the log-log plot of $R(n)/S(n)$ vs. n.

3.2.2 Standard deviation analysis

With this method we are following the example of Collins and De Luca [1993, 1994], who also investigated erratic physiological data. Their research was performed on the trajectories of center-of-pressure data of humans during quiet standing. The method is directly based on the computation of the diffusion constant on the basis of the mean displacement within a given time interval. However, biological systems show crossover phenomena between different scales, so it is not possible to talk about a diffusion constant, which would be independent of the chosen scale. To obtain the Hurst exponent at a certain scale, we compute the lagged standard deviation given by the expression:

$$D^2(l) = \frac{1}{2(N-1)} \sum_{i=0}^{N-l} \left[x(i-l) - x(i) - \overline{x}(l)\right]^2 \ , \tag{3.11}$$

where $x(i)$ denotes the ith data point of the time series. The mean value for the distance is denoted by $\overline{x}(l) = 1/N \sum_i^N x(i-l) - x(i)$. x could also denote a two dimensional data set as in [Collins and De Luca, 1993, 1994; Delignières et al., 2003]; which is illustrated in Figure 3.4. To investigate power-law behavior of the form $D^2(l) \propto l^{2\alpha}$, we analyze log-log plots of $D(l)$ vs. l (Figure 3.5a) and the slope of $D(l)$ (Figure 3.5b). The local slope is computed by fitting a linear function to five consecutive points of $\log(D(l))$ vs. $\log(l)$; this corresponds to a running average. Thus, we can read off the local scaling exponent at the chosen scale directly from Figure 3.5b. As i can be every single point within 0 and $N-l$, the windows overlap, and thus, the trajectory parts are not totally independent. Another possibility would be the choice of non-overlapping windows by dividing the original trajectory into parts and perform the analysis within these windows. The disadvantage of this

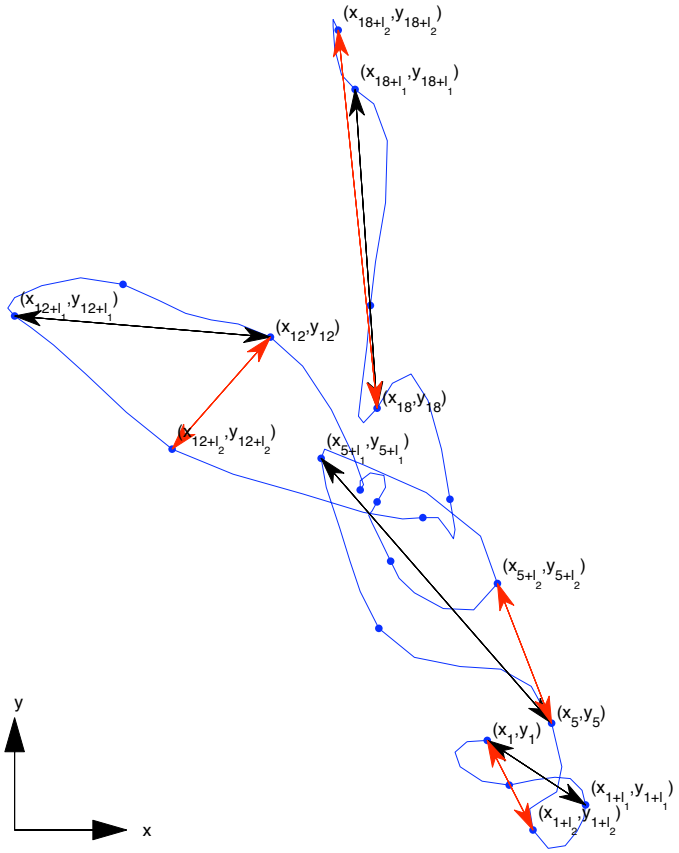

Figure 3.4: Illustration of the two-dimensional standard deviation analysis. The black arrows show the displacements during a time interval l_1 from the start positions $i = 1, 5, 12, 18$. Their mean gives us the mean displacement within a time interval l_1. The red arrows show the displacements during a larger interval l_2.

approach is that only a few intervals remain and the statistical power is strongly diminished. The two-dimensional version is used for the investigation of the center of pressure trajectory in [Collins and De Luca, 1993, 1994; Delignières et al., 2003]. This two-dimensional version $D^2(l)$ is not reduced by the mean $\overline{x}(l)$ as in Eqn. (3.11).

3.2.3 Detrended fluctuation analysis

Detrended fluctuation analysis (DFA) was introduced by Peng et al. [1994], and was primarily developed to investigate local scaling properties in DNA nucleotides, which contain coding and non-coding regions. With this method, they were able

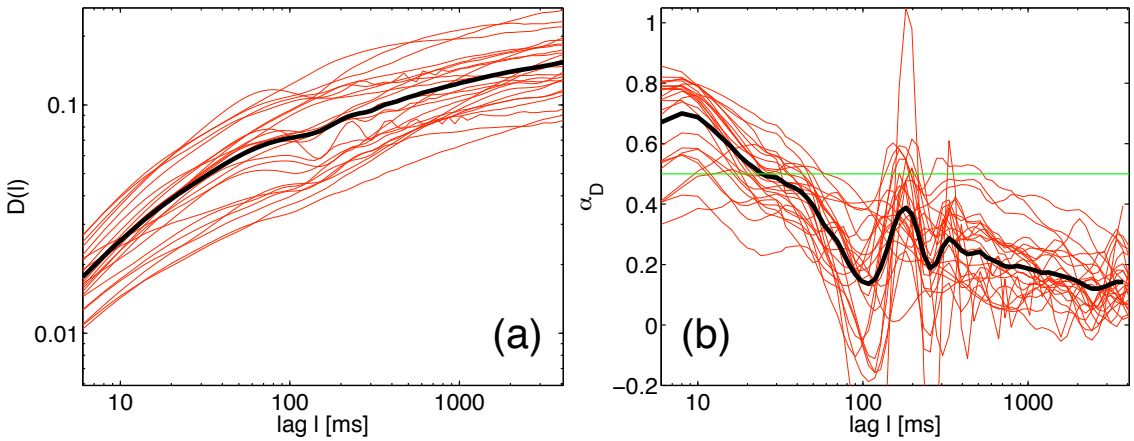

Figure 3.5: (a) $D(l)$ computed via SDA is plotted in a log-log plot. The black line denotes the mean over all participants and the red lines denote the within participant means for horizontal fixational eye movements. (b) The slope of the functions in (a) is plotted. The green horizontal line at 0.5 separates persistent and anti-persistent behavior.

to show that the patchiness (mixed coding and non-coding regions) of the DNA by itself cannot account for long-range power law correlations found in DNA dominated by non-coding regions. Later, they applied the method to heartbeat data [Peng et al., 1995], which is highly non-stationary. It was unclear if the non-stationarity arises from external environmental changes or if the changes arise from an underlying complex nonlinear system. With this method, they were able to distinguish a healthy subject from one with congestive heart failure. DFA was further applied to fixational eye movement data [Liang et al., 2005; Mergenthaler and Engbert, 2007]. The major difference to the earlier methods is the assumption that the data is not uniquely governed by stochastic forces but additionally is influenced by local trends. These local trends, as long as they are polynomial, can be removed by using DFA. DFA-p is capable of removing polynomial trends of order $p-1$. An illustration of DFA can be found in Figure 3.6. To compare the results of DFA with those from SDA, DFA is performed on the velocity $v(i) = T_s(x(i+1) - x(i))$ of the eye movement data; $T_s = 500$ Hz denotes the sampling frequency. DFA consists of five steps:

1. Perform a cumulative sum of the investigated data. Instead of performing this first step, we could also use the direct position data instead of the velocities.

2. The time series, with length N, is cut in $N_l = \lfloor N/l \rfloor$ segments ν of length l. In DFA, l is the parameter that determines the scale that the scaling exponent analysis works on. For DFA, reliable results can be obtained within the range $2p+1 \leq l \leq N/10$. The lower boundary arises from the fitting criterion for polynomials, that at least $2p+1$ points are necessary for a polynomial trend of order p. The upper boundary is a bit more flexible, arising from the fact

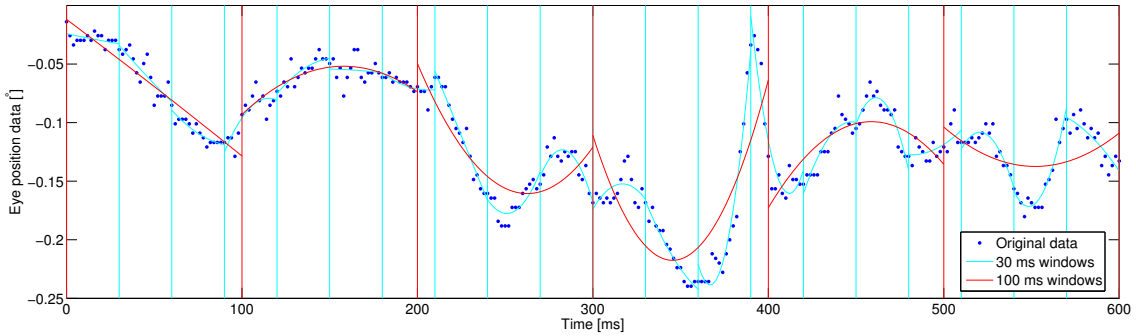

Figure 3.6: In DFA, the mean of the squared distance from the polynomial trend within a chosen window is computed. In the illustration, this translates to the squared distance of the blue dot from the polynomial trends within the windows, i.e. from the blue curve for 30 ms windows.

that the larger the intervals are, the less values are available to compute their mean.

3. In each of the segments ν, the polynomial trend y_ν of order p is determined using linear least-squares.

4. The mean of the mean squared deviation of the data with the trends removed is computed:

$$F^2(l) = \frac{1}{N_l} \sum_{\nu=1}^{N_l} \frac{1}{l} \sum_{i=1}^{l} [v((\nu-1)l+i) - y_\nu]^2 \ . \tag{3.12}$$

5. In the last step, the local scaling exponent can be determined as the slope of the log-log plot of $F(l)$. The local slope is computed as in the description of SDA as the slope of five consecutive data points.

There are two important points concerning the application of DFA to eye movement data, one concerning the time series with microsaccades, and the other relating to the time series with the microsaccades removed. In the two cases, we have nonstationarities of different types. For the data containing microsaccades, which are regions within the drift data with different local scaling properties, the entire signal is composed of regions with different local scaling behavior. In the case where the microsaccades are removed, we have nonstationarities due to the removal of time intervals. Both types of nonstationarities influence the local scaling of the entire data [Chen et al., 2002]. Cutting segments from the data does not affect persistent behavior but strongly affects anti-persistent behavior. This cutting results in a crossover separating the short timescales, which is still anti-correlated, from the large timescales where the local scaling yields an uncorrelated process. For the

data containing the microsaccades, we have to take their effects on different scales into account. For systems with a scale-independent scaling exponent and injected intervals with a different scaling, a superposition rule is supplied [Chen et al., 2002; Hu et al., 2001] that contains the scaling properties of the two processes, as well as effects generated by the number, the distance and the length of the injected intervals.

3.2.4 Spectral wavelet analysis

Spectral wavelet analysis (SWA) [Percival and Walden, 2000; Scafetta and Grigolini, 2002] is another method for the determination of the local scaling. In SWA, the separation of scales is performed via a wavelet transform, which uses wavelets $\psi_{\tau,t}(u)$ that are localized in time and frequency. The parameters of the wavelet are: τ, the chosen width of the wavelet determining further its frequency; t, the position in time of the wavelet; and u, the time variable. To determine the local scaling properties, we perform several steps:

1. Compute the wavelet transform of the data set $x(u)$ via:

$$W(\tau, t) = \int_{-\infty}^{\infty} \psi_{\tau,t}(u) x(u) du \; . \tag{3.13}$$

2. Compute the wavelet spectral density function $S_w(\tau)$, which returns how much energy is contributed at timescale τ via:

$$S_w(\tau) = \frac{1}{C_\psi \tau^2} \int_{-\infty}^{\infty} W^2(\tau, t) dt \; ; \tag{3.14}$$

   here, C_ψ is a wavelet-dependent constant. Equation (3.14) is a result of the wavelet equivalent of Parceval's theorem in Fourier analysis.

3. For the wavelet spectral density function $S_w(\tau)$ for the given data set, we obtain the scaling law:

$$S_w(\tau) \propto \tau^{2H-1} \; . \tag{3.15}$$

3.2.5 Application to fixational eye movement data

SDA applied to the data–method

The SDA is applied to several data sets obtained from the left eye in the two experiments. We apply the method to horizontal (Figure 3.5 and Figure 3.7a, b), vertical (Figure 3.7c, d) and two-dimensional (Figure 3.7e, f) eye movements. While Figure 3.5 shows the means of single participants (red) and the mean over all (black) for the horizontal component, Figure 3.7 shows the means over all participants for

all investigated data sets. In addition, we investigate the influence of microsaccades on the local scaling behavior. This is done by removing microsaccades detected with the optimal threshold (Section 3.1); as a control condition, we removed random intervals[2]from the original data. Microsaccades and random intervals were removed from the difference of consecutive data points $v(i) = x(i+1) - x(i)$, afterwards the cumulative sum was computed: $x_{MSrem.}(k) = \sum_1^k v(i)$. For all three types of data: full data (black, gray), microsaccades removed (blue, light blue) and random intervals removed (red, orange), the mean of the slopes of all participants is plotted. The last separation can be only made for Experiment 2 as it is the separation between fixations with a stimulus and fixations in darkness.

The local scaling behavior is investigated for lags within the range $2 < l < N/4$, where N denotes the length of the data; instead of choosing every possible lag, the lags are scaled by 1.09^k with $k \in \mathbb{N}$ in such a way that $l < \lfloor N/4 \rfloor$, where $\lfloor . \rfloor$ denotes the resulting of rounding down to the nearest integer. The choice of 1.09 supplies high resolution at the short time scale and a comparable resolution at the long time scale, as the obtained plots are in logarithmic units. Furthermore, it strongly reduces the computation time without affecting the results of the analyses.

SDA applied to the data–results

We start out by describing the results obtained for the fixations on the stimulus; with this condition, we can expect visual control to be present. During fixations on a stimulus (Experiment 1 and Condition 1 in Experiment 2), the slope of the log-log plots for horizontal (Figure 3.7a, b), vertical (Figure 3.7c, d)), and two-dimensional (Figure 3.7e, f) SDA show persistent behavior for short timescales up to 30 ms. The removal of the microsaccades from the horizontal component allows us to deduce that microsaccades generate persistent behavior on the shortest timescales of up to 15 ms, but between 15–40 ms, the main contribution to persistent behavior is due to drift. For the vertical component, the influence of microsaccade removal is small, which is in accordance to the observation that microsaccades are mainly horizontal, and therefore apply their influence mainly to the horizontal component.

At intermediate timescales (40–150 ms, 30–100 ms, and 30–150 ms for the horizontal, vertical and two-dimensional analyses respectively), we find a trough in the local scaling behavior. The minimum of the trough is located at a lag of 100 ms

[2]The random intervals are determined in the following way. Let $x(i)$ be the data points of a fixation with their indices $i = 1, \cdots, N$ where N is the length of the data. Further say that r microsaccades of individual length $l_1, l_2, \cdots, l_r$ were detected at the indices $j_1, j_1+1, \cdots, j_1+l_1; j_2, \cdots, j_2+l_2; \cdots; j_r, \cdots, j_r+l_r$. While during microsaccade removal the data points $v(j_1, \cdots, j_r+l_r)$ are excluded. During the removal of random intervals the values at: $N-j_1, L-(j_1+1) \cdots, N-(j_1+l_1), \cdots$ are discarded. Thus the choice of the "random" intervals maintains the inter-microsaccade intervals and the length of microsaccades; but removed different trajectory parts—most likely drift.

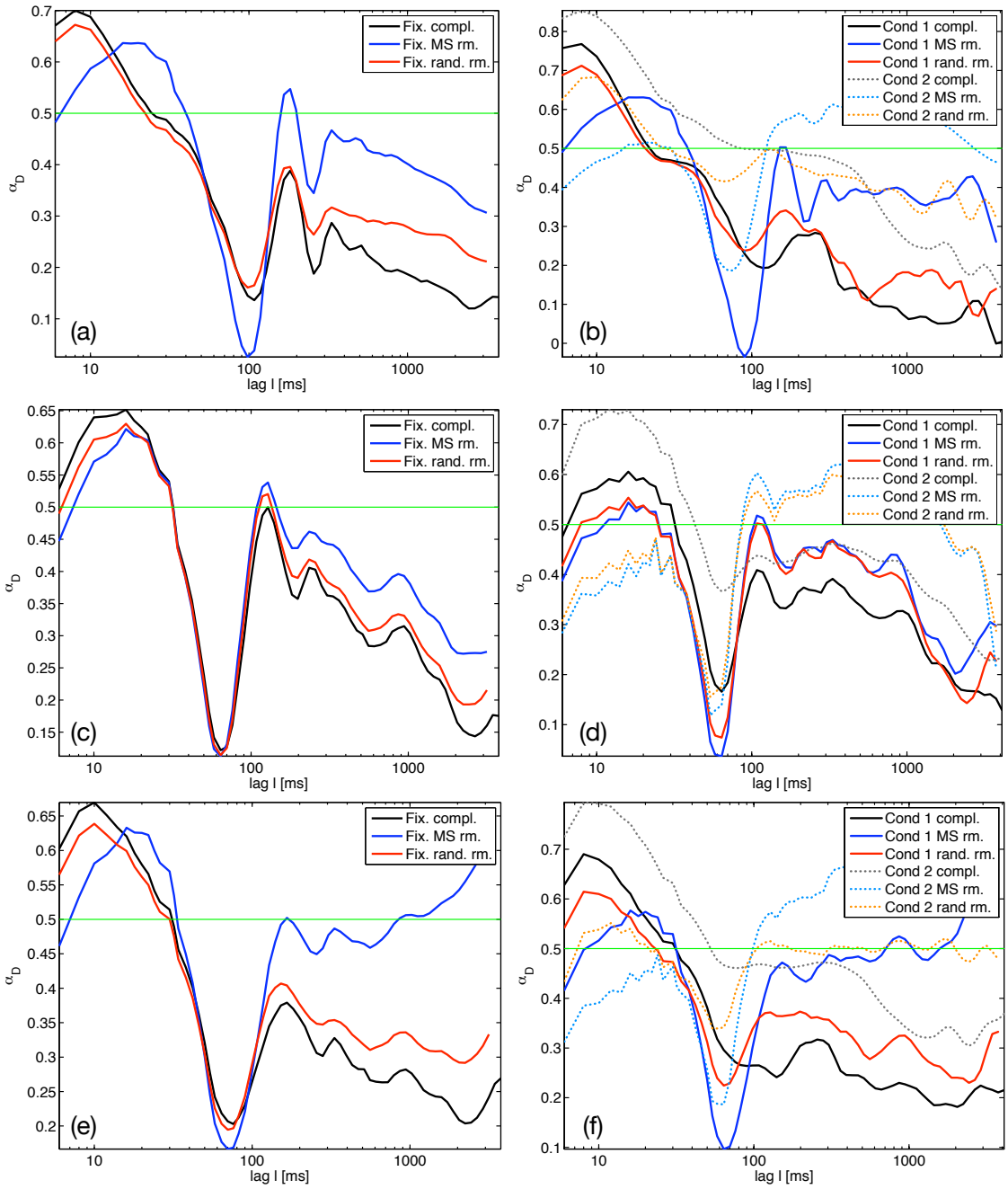

Figure 3.7: All the figures show the mean over all participants of the slope obtained via SDA for different data sets: (a), (b) the horizontal, (c), (d) the vertical and (e), (f) the two-dimensional slope. Visual fixation data are marked by bold lines (left: Experiment 1, right: Experiment 2, Condition 1). Fixations in darkness (Experiment 2, Condition 2) were marked with dotted lines .

for the horizontal component, and at a lag of 60 ms for the vertical component; for the combined signal, the trough is between these values at around 80 ms. At the trough the local scaling exponent goes down to $\alpha_D < 0.2$. When microsaccades are removed the trough is even deeper. Unlike the depth, the position of the trough remains unchanged. We exploit the location of the trough to adjust of the delay parameter in our model in Chapter 4.

At long timescales, for both, the horizontal and the two-dimensional analysis, we find a large influence of the microsaccades on the local scaling. A removal of the microsaccades strongly reduces the correlations in the process: The analyses show that the local scaling exponent for the full data and the data with random intervals removed is $\alpha_D \approx 0.25$, while for the data where the microsaccades are removed, $\alpha_D \approx 0.4$ (horizontal) or $\alpha_D \approx 0.5$ (two-dimensional). Here, it is important to note that the combined signal of microsaccades and drift, and also the introduction of nonstationarities due to the microsaccade removal, influence the long timescale suggesting that the values from DFA (Subsection 3.2.3) are more reliable.

The removal of random intervals, from the data obtained during fixations on a stimulus, only slightly affects the local scaling properties, while the removal of microsaccades reveal a strong impact of microsaccades on the local scaling properties.

A quite different picture is obtained in the darkness condition. The major difference is the lack of the trough in horizontal and two-dimensional analyses on the complete data set. When we remove the microsaccades, the trough reappears. However, the removal of the microsaccades in darkness also leads to a disappearance of the persistent short timescale, and α_D drops to approximately 0.5. For long timescales, the complete data set shows an anti-persistent behavior, while the data set without microsaccades shows a persistent behavior. The full data set of the vertical component in darkness reveals a strong persistence at short timescales followed by a long timescale with a local scaling exponent of $\alpha_D \approx 0.4$. As soon as microsaccades are removed the behavior is changed: The persistence at short timescales vanishes and is replaced by anti-persistence, the trough at the intermediate scale reappears and persistent behavior is also found at long timescales. An unexpected result is observed, when random intervals are removed from data sets collected in darkness. The removals has a much stronger effect than in the stimulus condition. For the horizontal component the removal of random intervals has the effect of a general reduction of correlations on all time scales. For the two-dimensional analysis the effect is even stronger leading to an almost fully uncorrelated process. For the vertical component the effect of random interval removal is as if microsaccades were removed.

DFA applied to the data

The description of the results when we apply DFA to eye movement data closely resembles the description after SDA. The biggest difference is that we did not use a

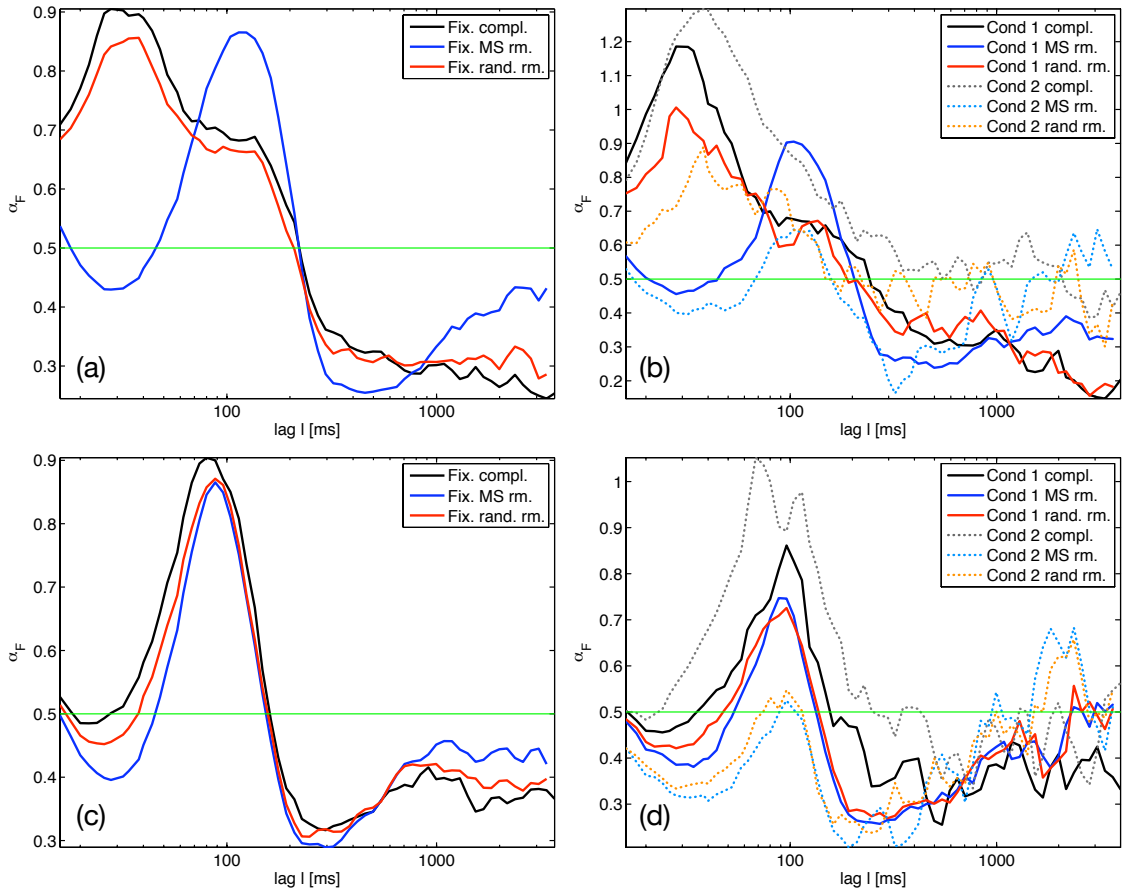

Figure 3.8: DFA for the two experiments. (a), (c) are from Experiment 1 and show the horizontal and vertical eye movements, respectively. (b), (d) are from Experiment 2, and again, the upper is for horizontal eye movements, while the lower one is for vertical eye movements.

two-dimensional version of DFA. At the level of the data, we again investigate the influence of microsaccades and experimental condition (fixation on stimulus and in darkness) on the vertical and horizontal components (Figure 3.8).

For fixations on a stimulus in the horizontal component, we again find that on short timescales up to 200 ms, the eye movements are persistent and that for timescales up to 60 ms, the microsaccades generate the persistence. For time lags between 60 ms and 200 ms, the persistent behavior is caused by drift. For the horizontal component a crossover point to anti-persistent behavior is found at 210 ms. The crossover point is not shifted when intervals, microsaccades or random intervals are removed. The observed shift of the crossover point towards larger values in the DFA with respect to the SDA is a well-known effect of the DFA [Kantelhardt et al., 2001]. On long timescales of above 300 ms, we again find anti-persistent behavior ($\alpha_F \approx 0.3$). The anti-persistent behavior between 300 ms and 900 ms mainly derive

from the drift. For lags larger than 900 ms the anti-persistence weakens when microsaccades are removed, which suggests a strong influence of microsaccades at time scales larger than 900 ms.

The vertical component during fixations on a stimulus shows again that microsaccades do not influence the vertical local scaling behavior. The vertical local scaling behavior shows a region with $\alpha_F \approx 0.5$ up to lags of 40 ms, which is followed for larger lags by a peak of strong persistent behavior up to lags of 160 ms. For higher lags, the local scaling exponent remains around $\alpha_F \approx 0.4$.

In the darkness condition, the results of DFA on the horizontal component resemble the results of the fixations on stimulus condition. However, the persistence on short timescales is stronger, while on longer timescales, the data does not show anti-persistent behavior, but rather uncorrelated behavior. Furthermore, the effect of interval removal is stronger. For data sets with removed microsaccades, the local scaling behavior is very similar to the one of the fixations on stimulus data with microsaccades removed; the only difference is the shallower peak around 100 ms. For the vertical component in darkness the effect of interval removal is extremely strong. A strong persistent behavior on short time scales in the full data set vanishes and the uncorrelated or slightly anti-persistent behavior on long timescales is replaced by a strong anti-correlation up to 1000 ms.

3.3 Microsaccade Rate

While the analyses on the local scaling behavior use the entire time series, the following analyses only look at the small intervals called microsaccades. As described in Section 3.1, the corrected microsaccade rate is computed separately for every participant of Experiment 1 (only fixations on stimulus) (Figure 3.9, Table 3.1) and within the two experimental conditions in Experiment 2 (fixations on stimulus and in darkness) (Figure 3.10, Table 3.2). The different positions of the maxima within

	S1	**S2**	**S3**	**S4**	**S5**	**S6**	**S7**	**S8**	**S9**	**S10**	**S11**	**S12**
λ_0	5.50	7.00	4.50	3.75	4.50	5.75	5.50	5.75	4.00	4.00	9.00	4.50
rate	1.91	2.64	3.39	1.80	1.19	2.21	2.81	2.61	1.10	4.07	0.91	2.57
	S13	**S14**	**S15**	**S16**	**S17**	**S18**	**S20**	**S21**	**S22**	**S23**	**S24**	**S25**
λ_0	4.00	4.75	5.50	5.00	4.00	11.50	8.50	8.50	4.00	9.75	6.25	9.75
rate	1.04	1.70	2.10	2.06	2.91	1.81	2.33	1.90	0.92	1.62	1.91	1.41

Table 3.1: Listed are all participants in Experiment 1 with their individual optimal threshold multiplier λ_0 and the rate of microsaccades.

the corrected rates (Figure 3.9, Figure 3.10) show the necessity to determine the optimal threshold multiplier λ_0 individually for each participant and experimental

condition. In Experiment 2, we have the stage of the heuristic filter as an additional change, as participant 1 and 12 to 20 were measured with the heuristic filter at stage 1 and 2 to 11 with the heuristic filter at stage 2 . It significantly changes the rate of detected microsaccades according to a two way analysis of variance with repeated measures for every subject.

In Experiment 1, we find a mean rate of microsaccades of 2.0 ± 0.8 Hz over all participants.

	S1	**S2**	**S3**	**S4**	**S5**	**S6**	**S7**	**S8**	**S9**	**S10**
Cond. 1: λ_0	4.50	9.25	3.50	3.75	7.75	6.75	3.75	6.75	5.00	4.25
Visual rate	1.91	1.91	3.34	2.41	1.90	1.34	2.26	1.87	2.44	1.63
Cond. 2: λ_0	6.50	9.50	3.50	3.75	17.00	4.50	3.75	18.25	5.50	3.75
Dark rate	0.93	2.12	2.80	1.79	1.26	1.86	1.40	1.07	1.23	2.40
	S11	**S12**	**S13**	**S14**	**S15**	**S16**	**S17**	**S18**	**S19**	**S20**
Cond. 1: λ_0	5.00	4.50	8.00	6.50	5.00	20.00	4.25	7.75	5.00	7.50
Visual rate	1.92	1.40	1.80	1.57	1.94	0.44	1.28	1.75	1.61	1.59
Cond. 2: λ_0	4.00	7.50	18.25	8.25	16.25	3.50	18.75	28.50	15.75	5.00
Dark rate	2.65	0.62	1.14	1.22	0.87	1.27	0.54	0.86	0.46	1.04

Table 3.2: Listed are all participants in Experiment 2 with their individual optimal threshold multiplier λ_0 and the rate of microsaccades.

3.3.1 Difference between experimental conditions

As early as 1955, the influence of visual condition on fixational eye movements, especially on the rate of microsaccades, was being discussed [Ditchburn, 1955; Cornsweet, 1956]. This discussion was fueled by the proposed mechanisms of microsaccade control and the questioned necessity of visual feedback. It was unclear which properties of visual input, e.g., luminance, are relevant. If, for example, the superior colliculus (see: Section 4.1) plays an important role for microsaccade as well as saccade generation, there should be a delayed effect of color changes on microsaccades, since the retinotectal pathway to the superior colliculus is supposed to be color-blind [Schiller and Stryker, 1972], and information carried by color is only available to the superior colliculus at a later point in time [McPeek and Keller, 2002; Rolfs et al., 2008]. In fact it has been found that effects on the microsaccade rate in complex tasks are delayed for isoluminant stimuli [Valsecchi and Turatto, 2007]. In the two early articles [Ditchburn, 1955; Cornsweet, 1956] visual feedback for the control of eye movements was reduced by stabilizing the image via a mirror placed on a contact lens that was attached by suction to the cornea. In [Cornsweet, 1956], peripheral information was still available. Nevertheless, they found a strongly reduced rate of microsaccades in the stabilized condition compared to normal viewing; this

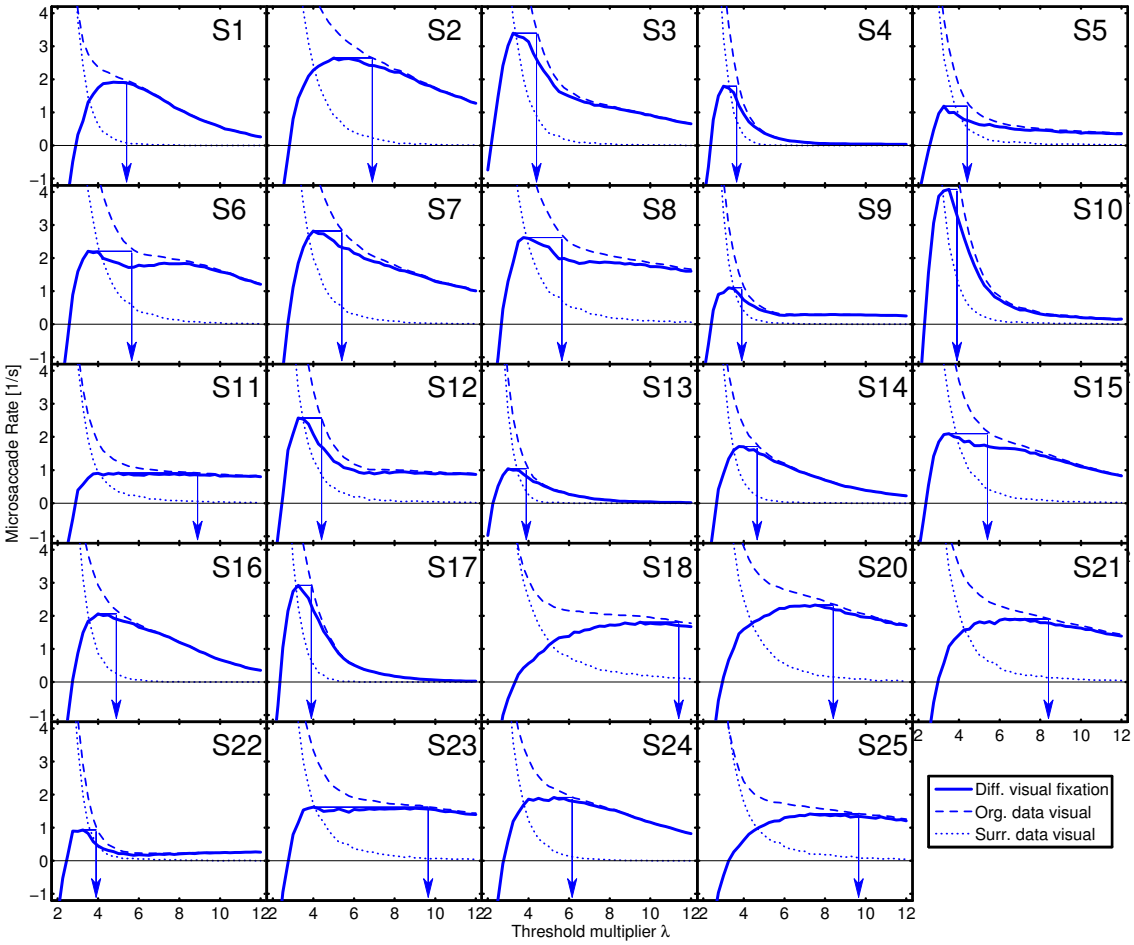

Figure 3.9: For every participant, the threshold multiplier λ dependent rate is computed. Using the maxima the optimal threshold multipliers λ_0 (denoted by the arrows targeting the x-axis) are computed as illustrated in Figure 3.2.

contradicted the results in [Ditchburn, 1955], where in stabilized viewing, the eye movements were unchanged. Later, in [Skavenski and Steinman, 1970; Nachmias, 1961; Fiorentini and Ercole, 1966], the rate of microsaccades in darkness compared to microsaccades during fixations was investigated. While [Nachmias, 1961] reported a reduced rate of microsaccades in darkness, [Fiorentini and Ercole, 1966] found exactly the opposite, an increased rate in darkness. Already in [Skavenski and Steinman, 1970], as one of their two subjects showed a behavior in accordance with [Nachmias, 1961] and the other with [Fiorentini and Ercole, 1966] it was suggested that the change in the rate of microsaccades can strongly differ between participants. All three studies had the drawback of using only two participants. The results presented for 20 participants in Table 3.2 and Figure 3.10 are consistent with this view that

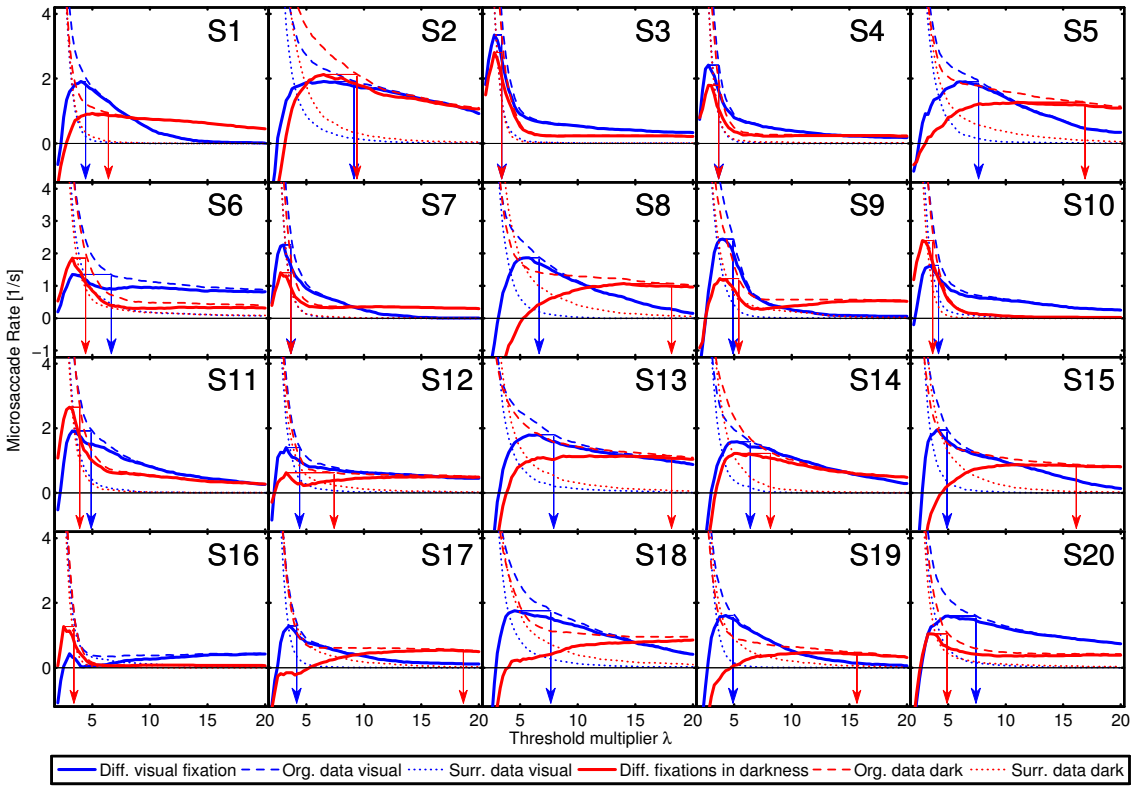

Figure 3.10: The maximal rate and the optimal threshold multipliers λ_0 (denoted by arrows targeting the x-axis) are chosen individually for each participant within both conditions.

changes in the microsaccade rate happen at the level of the individual and can differ in their directionality. For the 20 participants, we obtain a mean microsaccade rate of 1.8 ± 0.6 Hz for the visual fixation condition and a rate of 1.4 ± 0.7 Hz for the darkness condition. The rate between the two experimental conditions do significantly ($p < 0.01$) differ in a two-way repeated measures analysis of variance. This clearly shows that the properties of the visual input strongly influence the microsaccade rate. Nevertheless, 5 out of 20 participants showed an inverse effect: The rate of microsaccades increased when visual input was absent. Which states that the reduction of the microsaccade rate without visual input is not systematic. Along with the significant effect of the visual condition the stage of the heuristic filter affects the rate of detected microsaccades significantly (stage 1: 1.2 Hz and stage 2: 2.0 Hz).

The total number of detected microsaccades for all participants in each experiment are as follows: In Experiment 1, we found 25620 microsaccades; in Experiment 2 with visual fixation (Condition 1), we found 6687 microsaccades; and in Experiment 2 in darkness (Condition 2), we found 4923 microsaccades. Analyses on microsaccade

amplitude (Section 3.4) and local box count (Section 3.5) were applied to these microsaccades.

3.4 Microsaccade Amplitude

One of the properties that the microsaccades have in common with large directly visible saccades is the so-called main sequence [Zuber et al., 1965; Bahill et al., 1975; Harris and Wolpert, 2006; Engbert, 2006]. It describes the linear dependence that saccades and microsaccades have between the maximal velocity of the saccade and its amplitude for small saccades, and the saturation of velocity for saccades larger than 10° visual angle. This relation is also present in our data, which can be seen when combining the results shown in the upper and lower graphs of Figure 3.11.

3.4.1 Difference between experimental conditions

Alongside the investigations of the rate of microsaccades under different visual conditions, we investigated changes in the amplitude and maximum velocity of microsaccades. The really interesting finding was that, unlike the well-known unimodal distribution of the microsaccades during visual fixations, we found a bimodal distribution for the microsaccades in darkness (Figure 3.11 lower). The maximum of the unimodal distribution is centered around 0.15° of visual angle. The same maximum can be found as one of the peaks of the bimodal distribution in the darkness condition, although it is slightly shifted to smaller values around 0.08° of visual angle. The second maximum, which was unexpected and has an unclear functional role, is centered around 1° visual angle. In the peak velocity we find again one maximum for the visual condition and two maxima for the darkness condition. (Figure 3.11 upper). We initially checked if the bimodality is an effect of aggregating participants that have a single maximum at one of the two peaks. This investigation revealed that this is not the case as even single participants show the bimodality within their microsaccade amplitudes in darkness. We also checked statistically if the distribution is really bimodal by using the dip test, a non-parametric test for multimodality [Hartigan and Hartigan, 1985; Hartigan, 1985], on the logarithm of the microsaccade amplitude. The dip test looks for a difference between the empirical distribution function given by the data and the unimodal distribution function that minimizes the maximum difference between these two distributions. For unimodal distributions, the dip test asymptotically reaches zero, while for bimodal distributions, it asymptotically reaches a positive value. This positive value shows that the distribution has more modes than one. The significance of the test depends on the number of data points used. We obtained a value of 0.0129 for 5821 microsaccades, which is significant ($p < 10^{-5}$) as it is larger than 0.0121, which is the minimal value for the

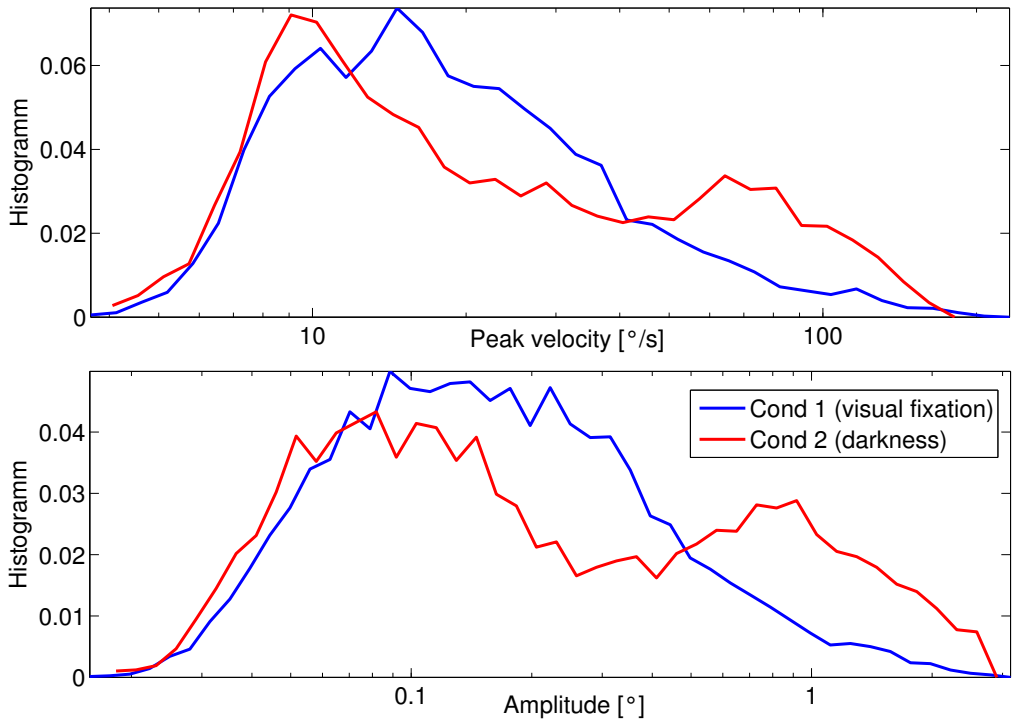

Figure 3.11: Normalized histograms of the logarithms of the peak velocity and the amplitude of the microsaccades. Upper panel: Microsaccade peak velocity, which is connected via the main sequence to the amplitude of the microsaccades. Lower panel: Microsaccade amplitude: It can be clearly seen that the distribution for the darkness condition is bimodal (peaks around 0.1° and 1° visual angle) while the microsaccades during fixation are not (peak around 0.2°).

used significance level. With our finding of larger microsaccades in darkness, we are in accordance with the results of [Ditchburn, 1955]. For the microsaccades obtained during fixations on a stimulus, we did not find any significant bimodality.

3.4.2 Large amplitude tail of the microsaccades

Another analysis that we perform on the amplitudes is to investigate the tail of the microsaccade amplitude distribution for a power law scaling. Firstly, we followed the approach suggested in [Viswanathan et al., 1996] which searches for linear trends in the log-log plots of the large amplitude tail within the histogram of the microsaccade amplitudes. These values are then compared to the later suggested, more theoretically driven approach described in [Edwards et al., 2007]; in this approach, log-likelihoods $\log[L_i(.)]$ for two models f_i of the tail, a power-law tail

$$f_1(x) = (\mu - 1)a^{\mu-1}x^{-\mu} \quad \text{for} \quad x > a \,, \tag{3.16}$$

and an exponential tail

$$f_2(x) = \lambda e^{-\lambda(x-a)} \quad \text{for} \quad x > a \,, \tag{3.17}$$

are computed. For the power-law tail the log-likelihood is determined by

$$\log[L_1(\mu|\vec{x})] = n\log(\mu-1) + n(\mu-1)\log a - \mu\sum_{j=1}^{n}\log x_j \,, \tag{3.18}$$

and for an exponential tail by

$$\log[L_2(\lambda|\vec{x})] = n\log\lambda + n\lambda a - \lambda\sum_{j=1}^{n} x_j \,, \tag{3.19}$$

where $\vec{x} = (x_1, x_2, \cdots, x_n)$ is the long tail data set, and a is the value at which the tail starts. The maximum likelihood estimators Newman [2005] for the two unknown parameters μ and λ are given for the power law tail by:

$$\hat{\mu} = 1 - \frac{n}{n\log a - \sum_{j=1}^{n} x_j} \,, \tag{3.20}$$

and for the exponential tail by:

$$\hat{\lambda} = \frac{1}{\frac{1}{n}\sum_{j=1}^{n} x_j - a} \,. \tag{3.21}$$

Additionally, an Akaike's information criterion (AIC_i) and Akaike weights (w_i) are supplied in Edwards et al. [2007]. AIC_i is found to be

$$AIC_i = -2\log[L_i(\hat{\theta}|\vec{x})] + 2 \tag{3.22}$$

for both models, with $i = 1, 2$ and $\hat{\theta} = \hat{\mu}$ for the power law trend and $\hat{\theta} = \hat{\lambda}$ for the exponential trend. The Akaike weights (w_i) are relative likelihoods of the two models and based on the difference of the models AIC ($\Delta_i = AIC_i - AIC_{min}$) from the best model ($AIC_{min}$):

$$w_i = \frac{e^{-\frac{\Delta_i}{2}}}{e^{-\frac{\Delta_1}{2}} + e^{-\frac{\Delta_2}{2}}} \,. \tag{3.23}$$

For the microsaccades in Experiment 1 and the microsaccades during visual fixations (Condition 1) in Experiment 2, the Akaike weights favor power law tails ($w_1 = 1$, $w_2 = 0$) with exponents of $\hat{\mu} = 3.4$ for Experiment 1 and $\hat{\mu} = 2.5$ for Condition 1, Experiment 2. The values are smaller than the value $\mu = 4.4$ computed for microsaccades in [Engbert, 2006] although the tails started around the same amplitude

$a = 10^{-0.5}$ degrees of visual angle. The values $\hat{\mu}$ observed in the tails of the microsaccade amplitudes of Experiment 1 ($\hat{\mu} = 3.4$) and Condition 1 of Experiment 2 ($\hat{\mu} = 2.5$) are quite different. While the value for Experiment 1 lies outside the range of possible Levy-flights ($1 \leq \mu \leq 3$) [Shlesinger et al., 1995; Metzler and Klafter, 2004; Shlesinger, 2006], we cannot exclude, that microsaccades in Condition 1 of Experiment 2 derive from a Levy-walk. For the microsaccade amplitudes in darkness, it is difficult to talk about power law scaling in the tail; even if we started the tail at the secondary maximum, the tail would not cover one order of magnitude, which is extremely short for the investigation of power laws. For completeness, however, for amplitudes larger than $a = 10^0$ degrees of visual angle, $\hat{\mu} = 2.7$ and the Akaike weights are in favor of power law scaling ($w_1 = 0.999$, $w_2 = 0.001$). As soon as we consider longer tails, though, the Akaike weights suggest more and more that the tail is better described by an exponential tail in darkness.

3.5 Local box count

Based upon the investigations of Hartline [1940] on information transmission in the visual pathways, Ditchburn [1955] discussed the influence of fixational eye movements on the images perceived by the retina. It is argued there that in the nerve fibers transmitting visual information, responses are much stronger if rapid changes occur for the receptive fields of cones than if low changing stimuli or steady inputs were applied. It is further argued that even the tremor movements increase our ability to perceive boundaries between dark and bright regions; this was confirmed by Ditchburn et al. [1959]. Recently, another successful experiment following this idea has been performed by Rucci et al. [2007], who were able to show the influence of fixational eye movements on the ability to detect the direction of blurry high frequency Gabor-patches[3]. The functional role of micro-movements of perception enhancement led us to the question: Contains the drift movement preceeding a microsaccade information, which could serve as a triggering signal for the microsaccade? Therefore, in [Engbert and Mergenthaler, 2006], we proposed a simple box-count measure that should estimate the number of cone receptive fields stimulated during small time intervals. As described in Engbert and Mergenthaler [2006] variation of ϵ yields a powerlaw for the box-count $N_b(\epsilon) \propto \epsilon^{-f_D}$ [Mandelbrot, 1967] with a range from $f_D = 1.35$ to $f_D = 1.65$ for different participants. The box-count measure is simple to calculate; the method is illustrated in Figure 3.12a. One only has to count the boxes N_b of a chosen size ϵ in a chosen time window τ; as the cone receptive field is approximately 0.01° of visual angle in diameter [Ölveczky et al., 2003], we choose boxes with a vertical and horizontal extent of $\epsilon = 0.01°$. The time window has a fixed

[3]Gabor patches are: Patches consisting of a combination of a two-dimensional Gaussian brightness distribution, with a superimposed sinusoid along one direction.

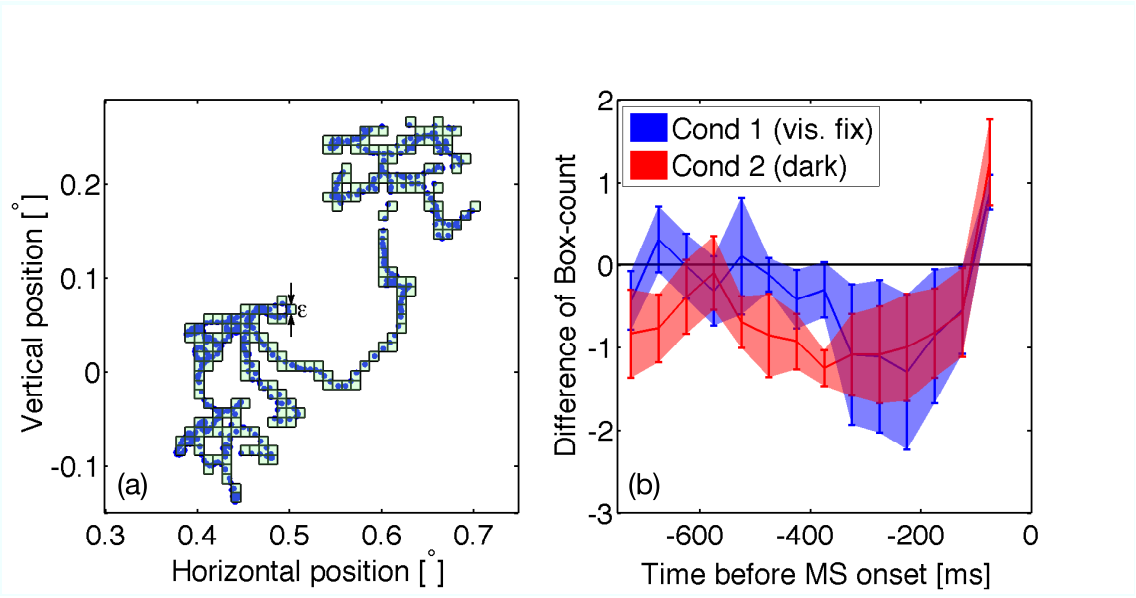

Figure 3.12: (a) Illustration of the box-counting. The number of boxes used to cover the trajectory of 50 ms length is counted. (b) Difference between the box count for the control condition (randomly chosen intervals) and box count locked to a microsaccade. Box-count is reduced independent of visual condition.

length of 50 ms (or 25 data points) and is non-overlapping. Further, the windows are locked to the microsaccade onset with lags between −750 ms and −100 ms in steps of 50 ms, following the idea that microsaccades might be triggered visually to counteract retinal fatigue due to slow retinal image slip. We further ensured that no further microsaccades occurred within the the box-count window and between the box-count window and the following microsaccade. To compare the box count preceding a microsaccade with the general box count during the drift, we chose random points in time, at which we locked box-count window with the chosen lag (control condition). The random points had to be within inter-microsaccade intervals that were at least 250 ms longer than the time span composed of time window and lag. Additionally, they had to be chosen to be located at least 250 ms away from the following microsaccade. Furthermore, we made sure that none of the random intervals contains microsaccades. We computed the local box count preceding the microsaccades for Experiment 1 [Engbert and Mergenthaler, 2006] and Experiment 2 [Mergenthaler and Engbert, subm]. Due to the result that the local box count is significantly reduced in the time span from −400 ms to −150 ms the first analyses for Experiment 1 suggested that microsaccades are triggered by low retinal image slip via visual feedback. The same analyses were performed on Experiment 2 for both conditions independently. For Condition 1 (visual fixation) we find as we expected a reduction in box count for lags between −400 ms and −150 ms prior

to microsaccade onset (Figure 3.12b). The suggestion that the reduction in retinal image slip is based on visual feedback control is difficult to support due to the astounding finding that the local box count prior to microsaccades in Condition 2 (in darkness) is also reduced. Thus, visual input is not the origin of the feedback leading to microsaccade triggering after reduced prior box count. The reduced box count prior to microsaccades could be explained by internal representations of position, e.g. through path integration or an efference copy. Otherwise, it could also mean that microsaccade and saccade preparation generates the reduced box count at an earlier point in time.

3.6 Triggering of microsaccades

The observation of the reduced box-count prior to a microsaccade offers the chance to investigate if the number of boxes preceding a microsaccade is linked to its amplitude. To investigate this, we plot the mean of the box count preceding a microsaccade with lags between -400 ms and -200 ms against the logarithm of the microsaccade amplitude (Figure 3.13) for both conditions (Condition 1, fixations on stimulus; Condition 2, fixations in darkness). For Experiment 1, where we only have Condition 1, the result is the same as for Condition 1 in Experiment 2. Interestingly, we find that when we use quantile regression to separate influences of different parts of the clouds of dots that for the microsaccades in darkness, two populations with different behavior exist. A first indicator for the existence of two types of microsaccades is the bimodality in the amplitude distribution. It concurs with the observations of different types of microsaccades by Boyce [1967]; Møller et al. [2002].An additional finding is that in darkness, small microsaccades with amplitude up to 0.3° increase with an increasing prior box count, while larger microsaccades with amplitude larger than 0.3° are unaffected by prior number of crossed boxes. For the microsaccades from Condition 1, we find a similar division into large and small microsaccades, but in this case, there is no less populated region in-between.

3.7 Summary of results

The advanced microsaccade detection algorithm, which determines the optimal threshold (see: Section 3.1) on the basis of the median squared distance from the median of the eye velocity and amplitude-adjusted phase-randomized surrogates, allows the comparison of individual microsaccade properties within differently shaped micro eye movements. This allows better comparability between different participants and between the two conditions in Experiment 2. The detected microsaccades were then used to determine microsaccade properties, both independently and in interaction

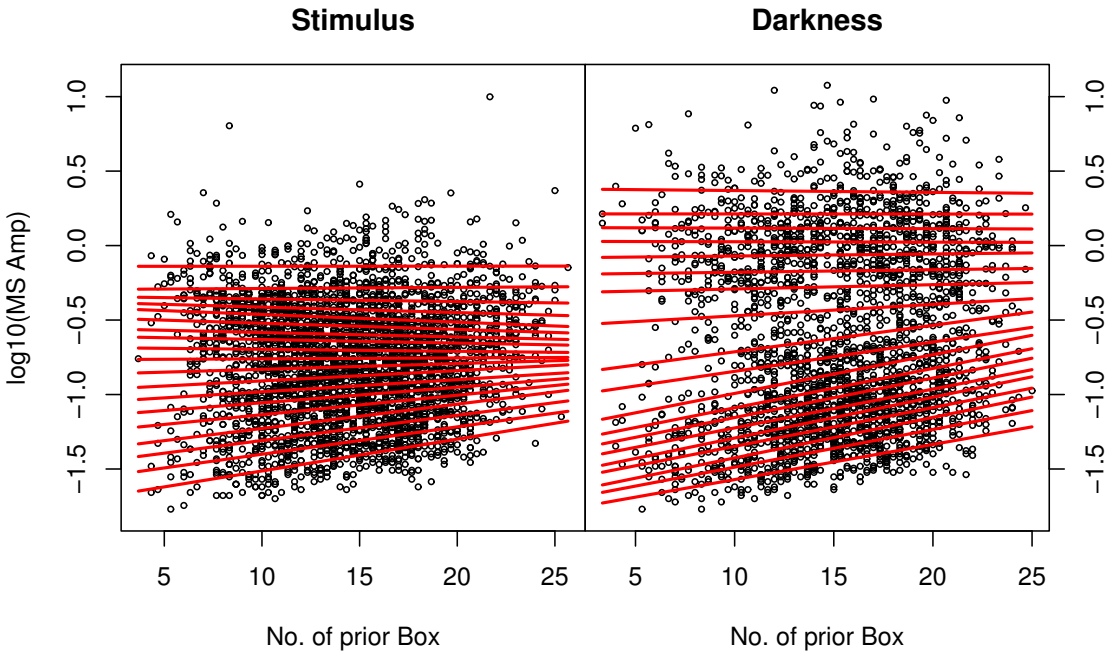

Figure 3.13: Scatterplot of the logarithm of the microsaccade amplitude vs. the box count preceding the same microsaccade between −400 ms and −200 ms. The red lines are quantile regression lines. In the darkness condition, the separation into two populations is verified by the lines. The lower population appear to be affected by the prior box count while the upper one is not.

with drift. The temporal local scaling analyses performed on the complete data set and on the data remaining after microsaccade removal revealed that the horizontal component of the eyes is governed by persistent local scaling on short timescales and anti-persistence on long timescales. Between the short and long timescales, at a lag of 100 ms, there is a trough in the SDA with a local scaling exponent around $\alpha \approx 0.2$. This trough will be exploited along with the local scaling exponents for the drift model in the next chapter. We found that the microsaccade rate is around 2 Hz during visual fixations and that during darkness, the rate of microsaccades is significantly reduced. Nevertheless, the reduction is not systematic for all participants as 5 of 20 participants showed a higher microsaccade rate in darkness. Under all conditions, the microsaccade amplitude distribution has a maximum at 0.1° visual angle, and gains a secondary maximum at 1° visual angle in darkness. The last analysis, namely the box count, revealed that −400 to −200 ms before microsaccade onset, the number of cones crossed by the stimulus is significantly reduced under all experimental conditions; this suggests either an internal representation of fixational eye movements or a pre-motor activity. Further, we found that the amplitude of small microsaccades in darkness increases with an increasing prior box count, the amplitude of large microsaccades remains unchanged.

Chapter 4

Toward a theoretical model of fixational eye movements

In general, dynamical models are built to improve our understanding of the underlying mechanisms, as dynamical models allow us to make strong and specific predictions. A model should naturally be consistent with the data that the model is based upon, but should also allow predictions that go beyond the data. The testability of dynamical models can help to classify the type of control mechanisms and to investigate the functions of fixational eye movements.

In neuroscience, two modeling approaches are in use. One approach is based on the neurophysiological structure. The modeling occurs at different scales. At the lowest level, single complex neurons or even single synapses are modeled. These are then combined into microcircuits consisting of several neurons. At the next level up are models of large networks, usually composed of simpler models of the single neurons within brain areas. The highest level consists of networks made of connected areas, each of which could then be networks of connected neurons or dynamical systems motivated by the dynamical behavior of the area. This approach is motivated by the question of how an observed behavior can be generated by a neuronal structure, and what the underlying neuronal mechanisms are.

In the other approach, modeling is not started at the lowest level, the neurons or ion channels, but at the highest level, the observed behavior. At this level, we are interested in why the behavior has evolved in this way? Modeling observed behavior has to be constrained by assumptions, like minimal effort or minimal energy to maximize the benefit [Harris and Wolpert, 2006]. This approach is usually further motivated by evolution, as the fittest survive within the constraints of their inhabited niche. This leads to the assumption that the observed behavior is purposeful and beneficial.

The purpose and benefits of fixational eye movements have already been mentioned in the introduction. Summarized, fixational eye movements allow the constant

perception of an unchanging environment with a sensory organ that has the detection of changes and movements as their primary purpose. Another function is the maintenance of a steady fixation position on a selected position. One benefit of fixational eye movements is a resolution that is higher than the spatial resolution of the sense.

Our approach to model of fixational eye movements is motivated by the explanation of observed behavior on the basis of a minimal control loop within the known neurophysiology. Thus, we use the information acquired in the previous chapter about fixational eye movements to implement a model for fixational eye movements [Mergenthaler and Engbert, 2007]. The model is based on the neurophysiology but does not trying to take all the possible sources, which will be shortly described in Section 4.1, into account. Instead, it tries to reproduce the observations found within the data while using only a small amount of neurophysiology, especially since it would have been unlikely that all the existing pathways would contribute to the simple tasks that the participants had to perform.

4.1 Physiological background

The knowledge about the physiological background of fixational eye movements is quite sparse as the signals are weak compared to signals that are generating saccades. Most of the physiological background is adapted from the knowledge about large saccades. For microsaccades, there is already strong evidence that they are generated by the same generation process as saccades. For the smaller movements composed of drift and tremor, the common origin with saccades has not been proven, but some evidence suggests that it is not unlikely. In general, many separated regions, mainly in the brain stem, contribute to the generation of saccades. Another possibility that has to be taken into account is the common generation of drift and smooth pursuit.

4.1.1 Saccades

The neurological basis for the generation of saccades is described in detail by Moschovakis et al. [1996] and summarized by Sparks [2002]. According to Moschovakis et al. [1996], several large brain areas have been identified that participate in the generation of saccades, including areas in the cerebral cortex, cerebellum, brain stem; those in the brain stem are found in the basal ganglia, thalamus, superior colliculus (SC), the paramedian pontine reticular formation (PPRF) the rostral interstitial nucleus of the median longitudinal fasciculus (riMLF), and the interstitial nucleus of Cajal (NIC); this list is however not exhaustive. While the cortex and cerebellum mainly affect the targeting of saccades [Girard and Berthoz, 2005; Lefévre et al., 1998] and the integration of complex visual stimuli, the brain stem supplies

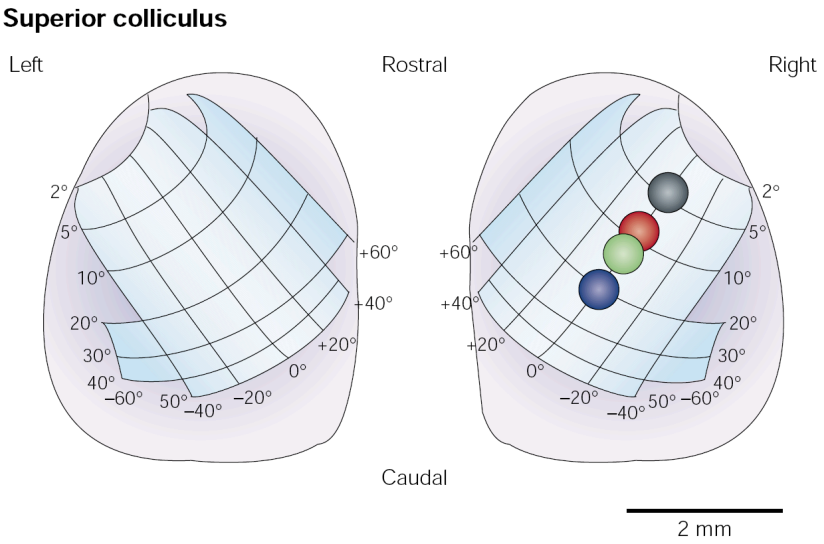

Figure 4.1: Topographic map of the two superior colliculi. The colored dots denote horizontal saccades of 5 to 20 degrees of visual angle. Taken from [Sparks, 2002]

low level integration of simple visual stimuli and the triggering of saccades. The brain stem further links reflexes, e.g., the vestibulo-ocular or cervico-ocular reflex, to eye movements.

The superior colliculi contribute most to the saccade generation, although lesion studies have shown that saccades can be performed with nonfunctional or even removed superior colliculi [Aizawa and Wurtz, 1998; Quaia et al., 1998; Schiller et al., 1980]. The superior colliculi are spatially organized according to function. Horizontal saccades are initiated in the contralateral superior colliculus, and small saccades are triggered when the peak activation is close to the rostral pole (see: Figure 4.1). When the distance of the peak activation to the rostral pole is increased, the amplitude of the saccade becomes larger. Oblique and vertical saccades are expressed very similarly, while the deviation from the rostral-caudal mid-line codes the vertical component. At the rostral pole, so-called fixation neurons Bergeron and Guitton [2000] are found. These fixation neurons cannot be distinguished, e.g., by their discharge pattern, from neurons that cause the smallest saccades.

The common origin of microsaccades and saccades is still under discussion, although there is much evidence for at least a large share of common neurophysiology [Zuber et al., 1965; Martinez-Conde et al., 2004; Bergeron and Guitton, 2000]. An extensive chart of connections within the brain stem is given in Appendix A. In [Girard and Berthoz, 2005], most of the existing saccadic burst generator models are compared. Further, criteria are given there, which at least should be fulfilled by models of saccadic burst generators: Saccadic burst generator models should be able to produce saccades that belong to the main sequence (peak velocity amplitude relation), generate straight oblique saccades, resume the execution of a saccades

after interruption by omnipause neurons, generate staircase saccades in the case of continuous input simulation SC stimulation, generate small bursts within the antagonistic burst generators at the end of the saccade (counteracting the overshoot), and coactivate horizontal and vertical saccadic burst generators during purely vertical or horizontal saccades.

4.1.2 Horizontal and vertical saccadic control mechanisms

Although the movements our eyes perform vertically and horizontally do not seem to differ, they are affected by separated nuclei within the brain stem [Moschovakis et al., 1996]. While the cortex, cerebellum and superior colliculus supply saccadic control for both vertical and horizontal saccades, several lower areas in the brain stem can be assigned to either horizontal or vertical saccades, but not both. This dichotomy provides an explanation for the displaced trough in the SDA and the crossover point in the DFA obtained in Section 3.2.

Horizontal saccadic control in the brain stem (Figure 4.2) is mediated by the SC, which directly projects excitatory connections to the PPRF, the nucleus paragigantocellularis dorsalis (PGD) and the nucleus raphé interpositus (RIP). The PPRF houses the excitatory burst neurons for the horizontal component of saccades. These propagate directly to the motoneurons in the abducence nucleus (VI N), to horizontal neural integrator neurons in the nucleus prepositus hypoglossi (PH), to the inhibitory burst neurons in the PGD, and back to the RIP. The inhibitory burst neurons inhibit the areas on the contralateral side.

The vertical saccadic control centers in the brain stem (Figure 4.3) again receive inputs from higher brain areas, but interestingly, these neurons involved can be divided into two separate groups, one lot producing upward movement and the others producing downward movement. The excitatory burst neurons for vertical eye movements are located in the riMLF and can be separated into inhibitory and excitatory burst neurons. As well as projecting to the oculomotor complex, they project to upward and downward integrator neurons in the interstitial nucleus of Cajal (NIC), to the downward inhibitory feedback neurons in the NIC, and upward resettable integrator neurons in the contralateral nucleus posterior commissure (nPC). The last two connections close short range negative feedback circuits.

In patients with cerebellar ataxia, there is an increase in the amplitude of fixational eye movements [Hotson, 1982]. For four patients of the patients, this increase was especially pronounced for microsaccades. One of the patients mentioned that his subjective perception during fixations was unstable. The author suggested that the cerebellum has a suppressive influence on saccade generation.

The most important information that we carry across from the neurophysiology to the model building are the transmission delays between the participating areas. The transmission delays have been measured in rhesus monkeys and cats, but we expect

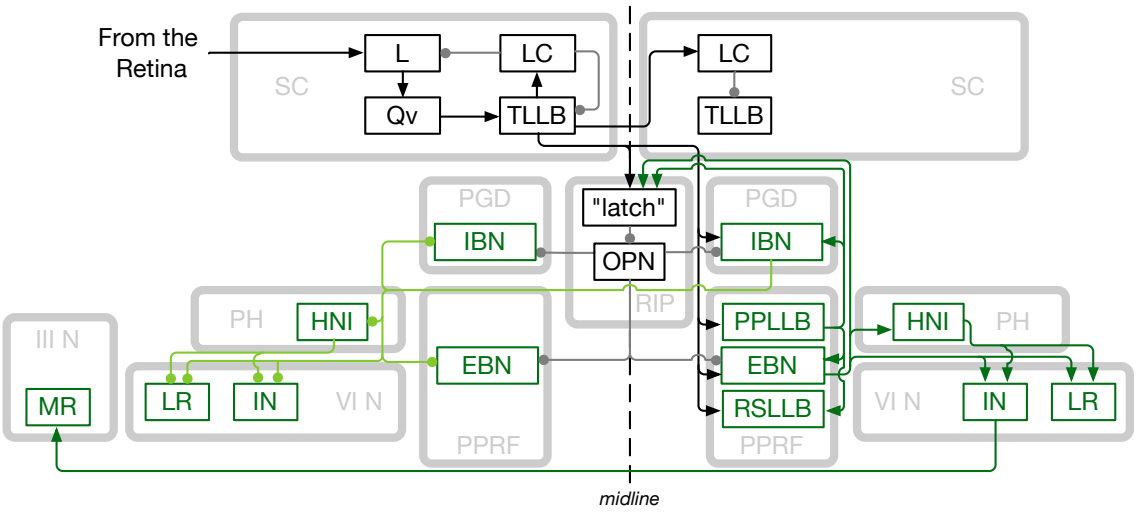

Figure 4.2: Horizontal saccadic control loops. In alphabetical order, the abbreviations are: III N: oculomotor nucleus; VI N: abducens nucleus; EBN: excitatory burst neuron; HNI: Horizontal neural integrator; IBN: inhibitory burst neuron; IN: internuclear neuron; L: lateral neurons of the Superior colliculus (SC); LC: local circuit neuron of the SC; LR: lateral rectus; MR: medial rectus; OPN: omnipause neuron; PGD: nucleus paragigantocellularis dorsalis; PH: nucleus prepositus hypoglossi; PPLLB: pontopontine long lead burst neurons; PPRF: paramedian pontine reticular formation; Qv: Quasivisual neurons; RIP: nucleus raphé interpositus; RSLLB: reticulospinal long lead burst neurons; TLLB: thalamic long lead burst neurons.

that the values for humans are in approximately the same range. The delay between stimulus onset and reactive saccade has been measured in behavioral experiments and is around 180–220 ms; however, express saccades with latencies around 130 ms and down to 80 ms have also been reported. A rough indication of the path distance between the thalamus and the burst generators (see Appendix A) is provided by the observation that the latency of saccades evoked from the thalamus (60–80 ms) is longer than the latency of saccades evoked in response to the electrical stimulation of other saccade related areas [Moschovakis et al., 1996]. For electrically evoked saccades in the frontal eye field (FEF), the latency is around 25 ms which is half the latency for stimulation in the supplementary eye field (SEF). Strong electrical stimulation of the posterior parietal cortex (PPC) leads to saccades with a latency of 120–140 ms. The cerebellum contributes a much shorter latency of 15–40 ms. Furthermore, stimulation of cells in the SC generates an eye movement around 20 ms later [Sparks, 1986]. Within the brain stem, the latencies are shorter. In general, LLB activity precedes EBN activity, which precede motoneuron (MN) activity, but the ranges of the latencies to saccade generation overlap (LLB: 10–14 ms; EBN: 8–12 ms but up to 32 ms; MN: 5–10 ms). Nevertheless, the LLBs precede the EBN by 3–20 ms. In general, the inhibitory neurons (IBN) discharge 13 ± 7 ms, but up to 35 ms before saccade onset. Latencies of IBN and EBN cannot be distinguished.

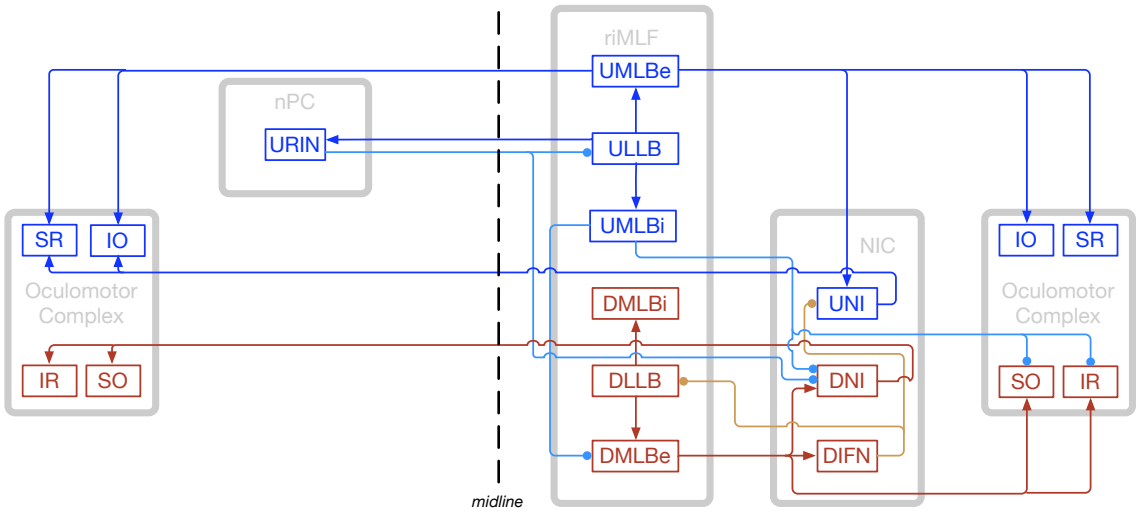

Figure 4.3: Vertical saccadic control feedback loops. In alphabetical order, the abbreviations are: DIFN: downward inhibitory feedback neuron; DLLB: downward long lead burst neuron; DMLBe: excitatory downward medium lead burst neuron; DMLBi: inhibitory downward medium lead burst neuron; DNI: downward neural integrator; IO: inferior oblique; IR: inferior rectus; NIC: interstitial nucleus of Cajal; nPC: nucleus of posterior commissure; OPN: omnipause neuron; riMLF: rostral interstitial nucleus of the median longitudinal fasciculus; SO: superior oblique; SR: superior rectus; ULLB: upward long lead burst neuron; UMLBe: excitatory upward medium lead burst neuron; UMLBi: inhibitory upward medium lead burst neuron; UNI: upward neural integrator; URIN: upward resettable integrator neuron.

For the vertical component, the execution of the saccade follows the activity of DLMBes with delays in the range of 4–16 ms with a mean of 5 ms. For the inhibitory feedback connections between the DLLBs and the DIFNs, as well as between the ULLBs and URINs, the delays are unknown.

For the feedback loop from the retina via the SC to the MN on the basis of visual information entering the retina, we further need the latency of visual input to the SC. This information is supplied in [Guitton, 1992] and is given with a value of around 40–50 ms. Therefore, a lower bound for a visually guided or external control loop is $\tau_{hor} = 60$ ms.

4.1.3 Smooth pursuit

Although the smooth pursuit and the saccadic systems have different latencies, there is more and more evidence of a common neurological pathway [Keller and Missal, 2003]. However, the higher brain regions like the frontal eye field (FEF) and the supplementary eye field (SEF) as parts of the premotor cortex and the cerebellum play a more important role in smooth pursuit generation than in saccadic generation. Additionally, the medial superior temporal (MST) region and the medial temporal

(MT) area contribute to smooth pursuit but not to saccadic generation. MST cells mainly process target motion as compared to background motion and are supplied with an efference copy of eye velocity during pursuit movements, while the MT contains cells that process the direction and speed of motion [Pack et al., 2001]. Neuronal activity close to the rostral pole in the SC is also suspected of playing an important role in smooth pursuit. This region sends signals to the omnipause neurons in the RIP. The common pathways of saccades and smooth pursuit within the brain stem suggest that it is not too far-fetched to assume that fixational eye movements are mediated by the same areas. Nachmias [1961]; Murphy et al. [1975]; de Bie and van den Brink [1986] suggested a common source of fixational eye movement control and smooth pursuit.

4.1.4 Drift

As already mentioned, fixational eye movements are small signals and therefore their neuronal correlates are weak, which makes localization of hubs difficult. There are regions in the brain that fire tonically during fixations [Bergeron and Guitton, 2000; Munoz and Wurtz, 1993a,b; Hanes et al., 1998]. One of the major regions with strong tonic activity is the rostral pole of the SC; the neurons there have been called the fixation neurons of the SC. They project mainly to the omnipause neurons (OPN) in the RIP, which, by itself, fires tonically. Unfortunately, the role of the tonic nodes and the way they interact is not understood [Bergeron and Guitton, 2000]. Furthermore, it is unclear how these regions interact with saccadic generation. Probably, variations within the tonic activity could be an origin of fixational eye movements—even the slower ones, like drift and tremor. The localization of fixational eye movement hubs can be done by relying on data for larger eye movements like smooth pursuits and saccades. This is supported by studies on patients with brain stem lesions who lack certain kinds of fixational eye movements.

For tremor, the maxima of the energy in the power spectrum are influenced by the oculomotor nuclei [Bengi and Thomas, 1973], suggesting brain stem control. Spauschuss et al. [1999] found further evidence for a central origin of ocular microtremor and drift: Specifically, they found correlations between the two eyes that remain after a sophisticated removal of components generated by head movements. Moreover, measurement of microtremor in patients with known brain stem damage or sedated but not paralyzed patients show a reduction in tremor frequency [Michalik, 1987]. However, it is still under discussion whether tremor is conjugate; the study by Spauschuss et al. [1999] suggests that only weak correlations can be found within the frequency band around 70 Hz, which has the most power. Likewise, the discussion continues about the combined control of drift in the two eyes. Two early studies [Ditchburn and Ginsborg, 1953; Riggs et al., 1954] proposed conjugacy between the eyes during drift, but in a later study [Krauskopf et al., 1960], no conjugate drift

movement could be found.

4.2 Position dependent model

Along with the investigation of the origin of fixational eye movements, arose the question how accurate is the eye position information for motor control. Several experiments, like fixations on targets with differences in target size and luminance [Rattle, 1969; Steinman, 1965], sequences of saccades performed in radom directions [Wyman and Steinman, 1973; Timberlake et al., 1972], maintained fixations during dark periods [Hansen and Skavenski, 1977], and hitting movements with a tool directed to the actual fixation position, were performed to quantify the accuracy . The result summarized by Hansen and Skavenski [1977] was that the spatial representation of eye position is highly accurate (below 0.1° visual angle) and that spatial memory of location is a lot poorer (1–2° visual angle).

In an almost completely unnoticed paper, Vasudevan et al. [1972] proposed a first quantitative model for the generation of fixational eye movements. It is mainly based on the description of fixational eye movements by Boyce [1967], who separated the fixational eye movements into movements within local areas composed of drift, and small microsaccades and slightly larger microsaccades which move the stimulus to new regions on the retina. All local areas were located within the fovea. In their model, they already described the fixational eye movements by a stochastic model, with a white noise tremor component and microsaccades generated by a Poisson process with an intensity λ. The model further took into account the findings of Boyce [1967] that long fixations can be separated into shorter fixation periods. During these, the eye remains within sometimes overlapping regions. The separation is caused by larger microsaccades that propagate the stimulus to a new local region with unfatigued receptors. The within-region motion is described by:

$$\dot{\theta}(t) = -\beta\theta(t) + G_1(t) + G_2(t)\,; \tag{4.1}$$

here, $G_1(t)$ is the driving force applied by the tremor and is modeled by white noise with $\langle G_1 \rangle = 0$ and $\langle G_1(t)G_1(t') \rangle = D\delta(t-t')$; and $G_2(t)$ describes the input of inter-region microsaccades, which are modeled by a stochastic point process composed of temporal triggering via a Poisson process and a size drawn from a bimodal probability density function of the form:

$$\phi(y) = \frac{\alpha^2}{2}\,|y|\,e^{-\alpha|y|}.$$

The parameter α for the microsaccade generation is obtained from experiments. In this model, drift represents a compensatory movement due to the position control

loop. Finally, they end up with a description of the first two moments of the movement θ:

$$\langle\theta(t)\rangle = 0 \qquad \langle\theta^2(t)\rangle = \frac{D}{2\beta}(1 - e^{-2\beta t}) + \frac{\lambda}{\beta}\frac{2}{\alpha^2}(1 - e^{-2\beta t})$$

Further, they added large microsaccades, which move the eye to a new location and separate short fixation periods.

Another fixation model that is also able to produce fixations is given in [Seung, 1996]. In this model, the main question is if a two-layer neuronal network, with one layer storing the eye position information and the other reading it out and projecting it to the oculomotor nuclei, is capable of generating a linear attractor. In the memory layer the position is governed by a line attractor, while the read out network is governed by a state space with a single fixed point. The model is further based on a linear superposition rule for the contribution of recurrent and feedforward connections. It gives the total synaptic current u_i in neuron i as:

$$\tau_s \frac{du_i}{dt} + u_i = \sum_{j=1}^{N} T_{ij}\nu_j + h_i \ , \tag{4.2}$$

where $\nu_j \approx g_j u_j + \nu_j^p$ is the firing rate; h_i, the feedforward term, is constant without head movements; ν_i^p is the spontaneous pacemaker activity; T_{ij} is the synaptic strength, and $\tau_s = 150$ ms. The fixed point equation for the firing rate ν_i has the form:

$$\nu_i = \sum_{j=1}^{N} W_{ij}\nu_j + f_i \ ,$$

where $W_{ij} = g_i T_{ij}$ is the synaptic weight matrix, and the rate of firing without input is $f_i = g_i h_i + v_i^p$. If W_{ij} is chosen to have one single unity eigenvalue and f_i is chosen to be orthogonal to the left eigenvector of the unity eigenvalue, the solutions lay on a straight line. The proper choice for the parameters is obtained by a learning rule, as describe by Seung [1996].

4.3 Velocity dependent model

The two described models are based on feedback control of eye position. The question of whether the control of fixational eye movements is performed at the level of position or velocity signals was investigated in detail by Epelboim and Kowler [1993]. They found that fixation control has to be implemented on the velocity to explain the results of their experiments. This contradicts the two earlier described models of fixational eye movement control. Thus, we suggest a model based on control of the velocity of the signal.

We formulated a delayed random-walk model for FEMs that is motivated by the delayed random-walk models for postural sway proposed by Ohira and Milton [1995] and Yao et al. [2001] and the assumption that the anti-persistent behavior for long time scales (see Section 3.2) arises from a neural control mechanism. For our model, we can exploit the fact that the activity of oculomotor neurons [Sparks, 2002; Moschovakis et al., 1996] is given as the sum of excitatory burst neurons (EBNs) and tonic units (HNIs) (see Figure 4.2 and Figure 4.3). The firing rate of the EBNs is related to active movements independent of eye position, and therefore, EBN activity determines eye velocity. The activity of the HNIs is proportional to the fixation position relative to the center of the visual field (eccentricity), which means that the HNIs serve a function in gaze-holding. During FEMs, however, changes in absolute eye position are negligible (i.e., less than 1°). As a consequence, we do not expect systematic variations in HNI activity. The contribution to our FEM model of HNI activity is given by an additional noise source added to eye position.

We implement our model as a discrete map. First, we use an autoregressive term for EBN activity $w_{i+1} = (1-\gamma)w_i$ to generate the persistent correlations on short time scales created by the inertia of the eye. The second term, a noise term ξ_i, represents EBN baseline activity, where ξ_i are uncorrelated Gaussian random numbers with $\langle \xi_i \rangle = 0$ and $\langle \xi_i \xi_j \rangle = \sigma^2 \delta_{ij}$ and σ is the standard deviation of the noise. A third term $-\lambda \tanh(\epsilon w_{i-\tau})$ introduces negative feedback (with a delay) in order to stabilize the FEMs and to generate anti-persistent behavior on long time scales [Yao et al., 2001]. The parameters are the physiological delay, τ; the feedback strength, λ; and a parameter to allow variation of the steepness of the control function, ϵ. The influence of the EBNs is added to the HNI activity as an additive noise term η_i, with $\langle \eta_i \rangle = 0$ and $\langle \eta_i \eta_j \rangle = \rho^2 \delta_{ij}$, where ρ is the standard deviation. Taking all these terms together, we can write our model as:

$$\begin{aligned} w_{i+1} &= (1-\gamma)w_i + \xi_i - \lambda \tanh\left(\epsilon w_{i-\tau}\right) \ , \\ x_{i+1} &= x_i + w_{i+1} + \eta_i \ . \end{aligned} \tag{4.3}$$

In this model, all eye positions x_i are stable because of the lack of a systematic variation of HNI activity with eccentricity (see above). It is important to note that all parameters of our model have a direct physiological interpretation.

4.3.1 Delayed random walk without oscillations

Systems with delayed negative feedback typically produce oscillatory behavior [Longtin et al., 1990; Ohira and Yamane, 2000; Ohira, 1997; Yao et al., 2001]. As we do not find persisting dominant periodicity in the slow fixational eye movement part, but only sometimes regions which show slight oscillations, we have to remain in a parameter range where oscillations are non-dominant. This region is also called the

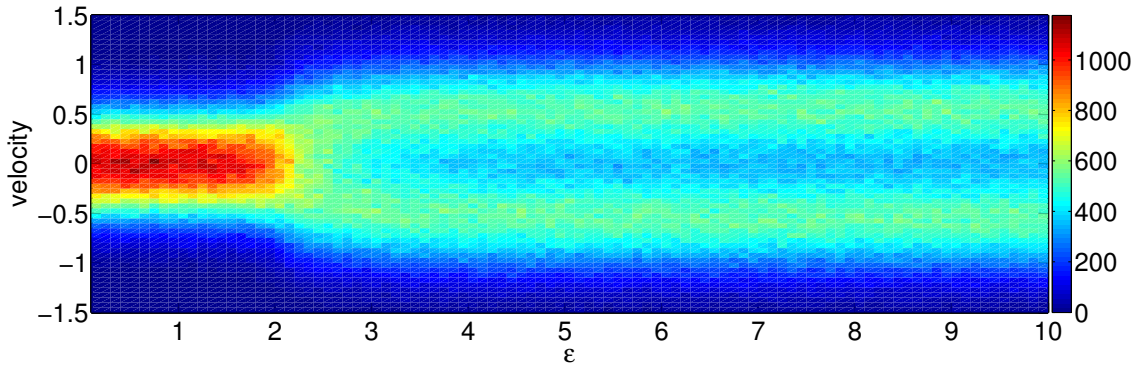

Figure 4.4: The histogram of the velocity simulated with fixed parameters $\gamma = 0.25$, $\lambda = 0.15$, $\sigma = 0.075$, $\rho = 0.35$, and $\tau = 70$ (see Subsection 4.3.2 while increasing ϵ. The bifurcation at $\epsilon \approx 2$ from a fixed point to a oscillatory solution is clearly visible.

low-gain regime [Eurich and Milton, 1996; Moreau and Sontag, 2003]. Nevertheless, it could be that the system enters the high gain regime under several conditions, e.g., nystagmus. Now, we investigate the behavior of the model while changing the parameter ϵ, searching numerically for transitions between regimes (Figure 4.4). If all other parameters are fixed to the values described in Subsection 4.3.2, we observe a bifurcation at $\epsilon \approx 2$. Different from postural sway data, we did not find a third time scale, where the local scaling exponent tends to zero. Such a time scale with a slope of zero is related to the high-gain regime, which we do not enter here.

4.3.2 Parameter estimation: horizontal

Naturally, we would like our model to reproduce the properties of real data. Therefore, we look for a parameter set which leads to the best agreement in the scaling exponent analyses between the model and the data. We simulated time series of length 200,000 in our numerical simulations (where one iteration step corresponds to 1 ms), and analyzed only the last 20,000 data points, to exclude potential transient effects. The SDA is computed directly on the basis of the position signal x_i. The DFA for the model is based on the velocity time series generated from the position x_i of (4.3) as described for the eye position data. A parameter set that is appropriate to reproduce the local scaling behavior of the FEM data is $\gamma = 0.25$, $\lambda = 0.15$, $\sigma = 0.075$, $\rho = 0.35$, and $\epsilon = 1.1$. For the horizontal component of the FEMs, a time delay of $\tau_{hor} = 70$ ms leads to the best match between the experimental data and the model simulations (Figure 4.5). This result is in good agreement with our current knowledge of the oculomotor circuitry (Subsection 4.1.2 and [Sparks, 2002; Moschovakis et al., 1996]) Visual information entering the retina needs $t_p = 40$ ms along the retinotectal pathway to reach the SC [Guitton, 1992], the top-level control

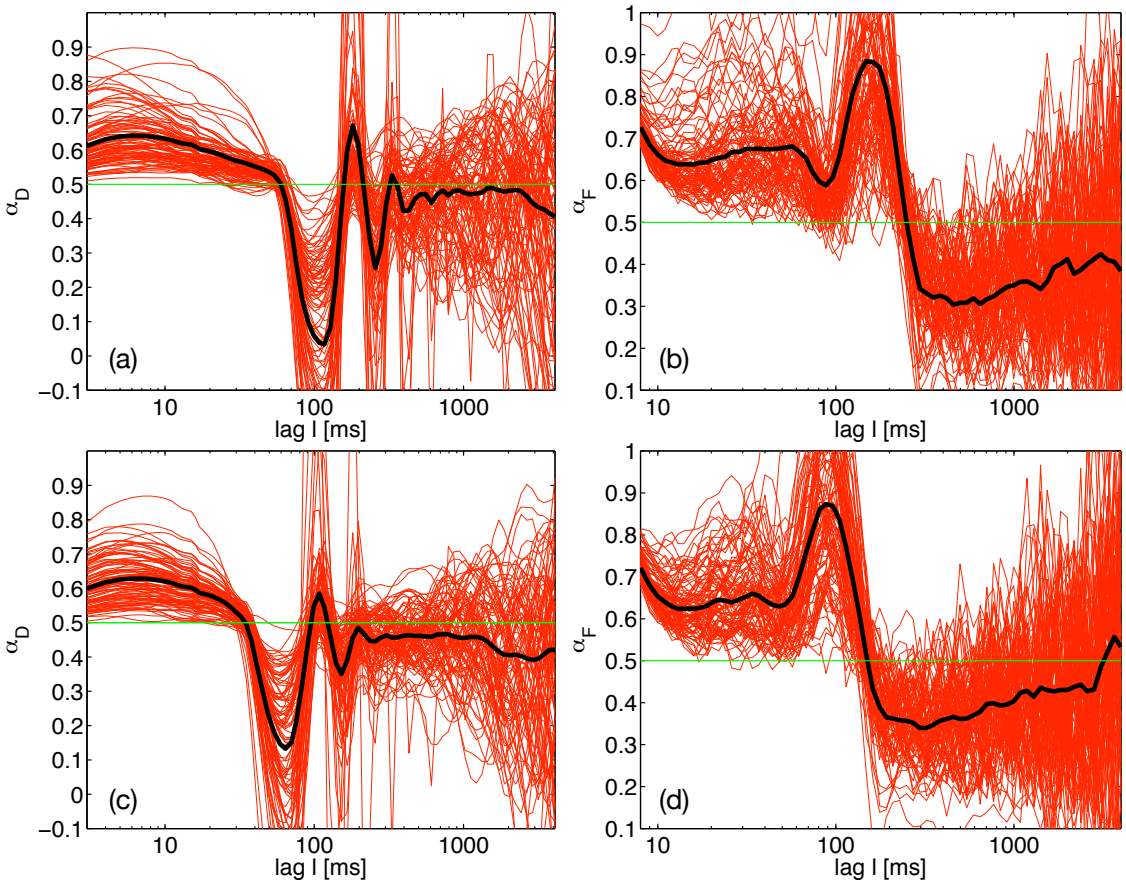

Figure 4.5: Scaling exponent analyses for the model with $\gamma = 0.25$, $\lambda = 0.15$, $\sigma = 0.075$, $\rho = 0.35$ and $\epsilon = 1.1$. To mimic individual variations we added normally distributed parameter variations with standard deviations of 0.1 for ρ and ϵ and standard deviations of 0.02 for σ, γ and λ. Black lines denote the mean of 100 model simulations. (a) The slope of the estimated local scaling behavior via SDA for the model of horizontal FEMs ($\tau \approx 70$ with deviations drawn from a binomial distribution with $p = 0.54$ and $N = 20$). (b) The slope of the local scaling estimated via DFA for the model of horizontal FEMs. (c) The slope of the estimated local scaling behavior via SDA for the model of vertical FEMs ($\tau \approx 40$, the rest of the parameters a as for horizontal FEMs). (d) The slope of the local scaling via DFA for the model of vertical FEMs.

structure for saccadic eye movements in the brainstem. Furthermore, stimulation of cells in the SC generates an eye movement $t_m = 20$ ms later [Sparks, 1986]. Therefore, a lower bound for the (visually guided or external) control loop is $\tau_{hor} = 60$ ms.

4.3.3 Parameter estimation: vertical

Additionally to the horizontal component, we investigated the vertical component of the eye movements (Figure 4.5). Again, we simulated model (4.3). The estimates

for the parameters, $\gamma = 0.25$, $\lambda = 0.15$, $\sigma = 0.075$, $\rho = 0.35$, and $\epsilon = 1.1$, are the same as for the horizontal component. Interestingly, though, we obtained a smaller delay of $\tau_{vert} = 40$ ms for vertical FEMs. This smaller numerical value is highly compatible with the existence of an internal (i.e., not visual) physiological control loop for vertical saccades (Subsection 4.1.2 and Moschovakis et al. [1996]) and suggests independence between the vertical and horizontal FEM components.

4.3.4 Semi-analytic local scaling investigation

Next, we present analytical approximations for the correlations on the short and long time scales. We assume that the local scaling exponent H is linear for the chosen range between lag t_1 and t_2.

$$2H = \frac{\log D^2(t_2) - \log D^2(t_1)}{\log t_2 - \log t_1}. \tag{4.4}$$

The estimation of the diffusion term $D^2(t_i)$ for a distinct lag t_i relies on the relation

$$D^2(t_i) = \langle (x_{k+t_i} - x_k)^2 \rangle \ . \tag{4.5}$$

For the short time scales, we estimate the local scaling behavior from the slope of the graph between lags 1 and 2, i.e.,

$$H_s = \frac{1}{2\log 2} \log \frac{D^2(2)}{D^2(1)} \ . \tag{4.6}$$

For the diffusion term with lag $t_i = 1$, we exploit the fact that the noise term η_k and velocities w_{k+1} are statistically independent, which gives

$$D^2(1) = \langle (x_{k+1} - x_k)^2 \rangle = \langle (w_{k+1} + \eta_k)^2 \rangle = \langle w_{k+1}^2 \rangle + \rho^2 \ . \tag{4.7}$$

For the calculation of $D^2(2)$, we iterate (4.3) and replace $\gamma' = 1 - \gamma$,

$$\begin{aligned} D^2(2) &= \langle (x_{k+2} - x_k)^2 \rangle = \langle (w_{k+2} + \eta_{k+1} + w_{k+1} + \eta_k)^2 \rangle \\ &= \langle [(1+\gamma')w_{k+1} + \xi_{k+1} - \lambda \tanh(\epsilon w_{k+1-\tau}) + \eta_k + \eta_{k+1}]^2 \rangle \\ &= (1+\gamma')^2 \langle w_{k+1}^2 \rangle + \lambda^2 \langle \tanh^2(\epsilon w_{k+1-\tau}) \rangle \\ &\quad -2(1+\gamma')\lambda \langle w_{k+1} \tanh(\epsilon w_{k+1-\tau}) \rangle + \sigma^2 + 2\rho^2 \ . \end{aligned}$$

As we would like to investigate the model behavior for different values of its parameters, we now introduce two approximations: (i) the linearization

$$\tanh(\epsilon w_k) \approx \epsilon w_k \ ,$$

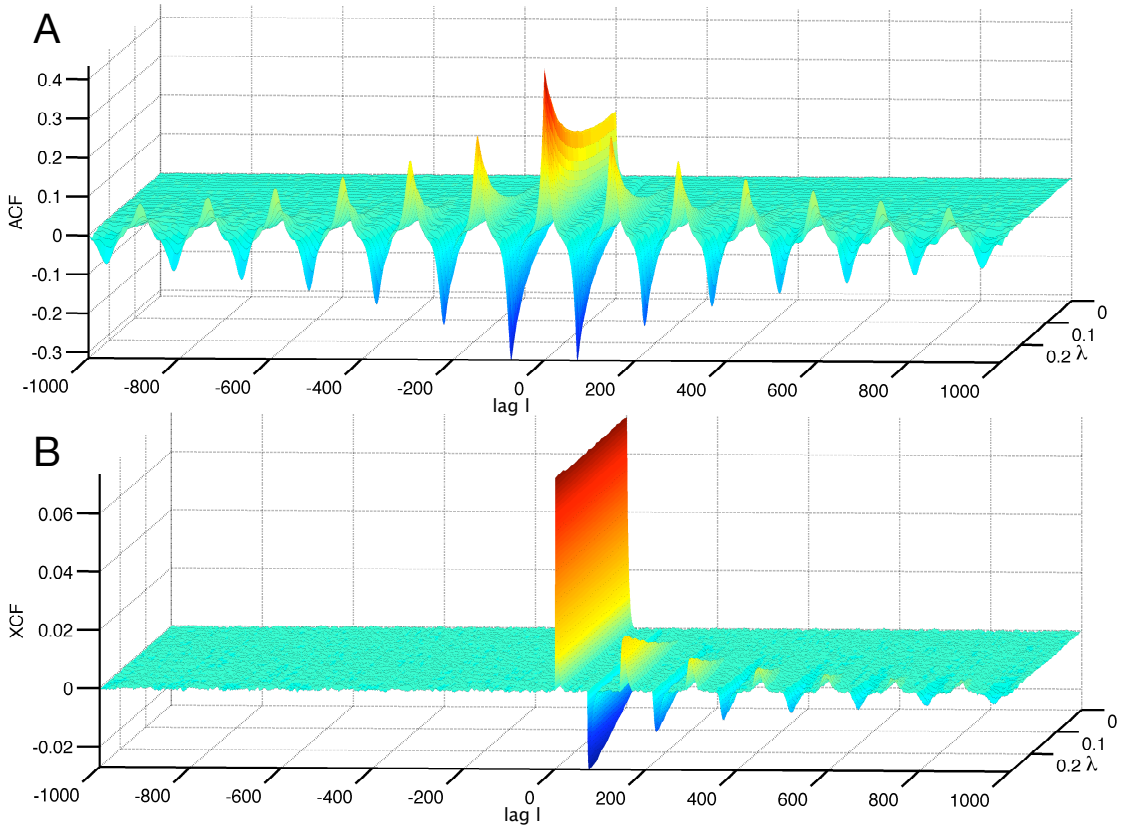

Figure 4.6: (A) The autocorrelation function of w_k with lags $-1000 \leq l \leq 1000$ and λ between $0 \leq \lambda \leq 0.28$. (B) The cross-correlation function $\langle \xi_k w_{k+\tau} \rangle$ between $w_k + l$ and ξ_k. Positive lags denote that $w_k + l$ is later than ξ_k.

and (ii) a relation within the autocorrelation function:

$$\langle w_k w_{k+\tau} \rangle \approx -2\lambda\epsilon \langle w_k^2 \rangle \ ,$$

which is obtained from numerical calculations around $l = 0, \tau, 2\tau, \cdots$ in the cross-correlation function (see Figure 4.6). The use of approximation (ii) also leads to another approximation: (iii) the relation between consecutive lags within the autocorrelation function:

$$\langle w_k w_{k+1} \rangle = \langle \gamma' w_k^2 + w_k \xi_k + \lambda w_k \tanh(\epsilon w_{k-\tau}) \rangle = (\gamma' + 2\lambda^2\epsilon^2) \langle w_k^2 \rangle \ .$$

For simplicity and due to stationarity we write: $\langle w_k^2 \rangle \equiv \langle w^2 \rangle$. Here, we see already one fact which will help us later on: The term $\langle w_k \xi_k \rangle$ with lag $l = 0$ does not contribute. When we now apply the approximations to $D^2(1)$ and $D^2(2)$, $D^2(1)$ remains unchanged but $D^2(2)$ ends up as:

$$D^2(2) = \left[(1+\gamma')^2 + \lambda^2\epsilon^2 + 4(1+\gamma')\lambda^2\epsilon^2 \right] \langle w^2 \rangle + \sigma^2 + 2\rho^2 \ . \tag{4.8}$$

Putting together Eqs. (4.6), (4.7) and (4.8), our approximation for short time scales can be written as

$$H_s = \frac{1}{2\log 2}\log\left(\frac{\left[(1+\gamma')^2+\lambda^2\epsilon^2+4(1+\gamma')\lambda^2\epsilon^2\right]\langle w^2\rangle+\sigma^2+2\rho^2}{\langle w^2\rangle+\rho^2}\right). \tag{4.9}$$

For long time scales, we consider additional effects of the delay term. Thus, we calculate the slope between lags τ and 2τ, i.e.,

$$2H_l = \frac{1}{\log(2\tau/\tau)}\log\frac{D^2(2\tau)}{D^2(\tau)}\ . \tag{4.10}$$

The choice of $t_1=\tau$ and $t_2=2\tau$ fulfills the requirement that $D^2(t_i)$ can be linearly approximated (see Figure 4.7); this would not be the case for, e.g., $t_1=\tau/2$ and $t_2=3\tau/2$. Generally, iteration of (4.3) within (4.5) gives

$$D^2(t_i) = \left\langle\left(\sum_{l=1}^{t_i}\gamma' w_{k+l}+\xi_{k+l}-\lambda\tanh(\epsilon w_{k+l-\tau})+\eta_{k+l}\right)^2\right\rangle. \tag{4.11}$$

In Figure 4.7, the dependence of $D^2(t_i)$ on t_i and λ is illustrated. While for $\lambda=0$, $D^2(t_i)$ is linearly increasing, as for simple diffusive processes, an increasing λ amplifies the diffusion on timescales up to τ, which generates a local maximum around $t_i=\tau$ in $D^2(t_i)$. For values of t_i around 2τ the influence of λ is inverse: it reduces the diffusion. We now expand Eqn. (4.11) by using stationarity $\langle w_k w_{k+j}\rangle = \langle w_0 w_{0+j}\rangle = \langle w w_j\rangle$ and removing all terms that do not contribute, e.g., $\langle w_0\xi_l\rangle = 0$ for all $l\geq 0$. This, and the approximation $\tanh(\epsilon w_k)\approx\epsilon w_k$, leads to

$$\begin{aligned} D^2(t_i) &= (\gamma'^2+\lambda^2\epsilon^2)\left[(t_i+1)\langle w^2\rangle+2\sum_{l=1}^{t_i}(t_i+1-l)\langle w w_l\rangle\right]+(t_i+1)\left(\sigma^2+\rho^2\right)\\ &\quad +2\gamma'\sum_{l=1}^{t_i}(t_i+1-l)\langle\xi_0 w_l\rangle-2\lambda\epsilon\sum_{l=\tau+1}^{t_i}(t_i+1-l)\langle\xi_0 w_{-\tau+l}\rangle\\ &\quad -2\lambda\epsilon\gamma'\left[\sum_{l=0}^{t_i}(t_i+1-l)\langle w w_{-\tau+j}\rangle+\sum_{j=1}^{t_i}(t_i+1-j)\langle w_{-\tau}w_l\rangle\right]. \end{aligned} \tag{4.12}$$

The major contribution to $D^2(t_i)$ of the auto- and cross-correlation functions arises from lags which are close to $n\tau$ with $n\in\mathbb{N}_0$. Thus, for the approximation, we restrict the analysis to terms with the lags $l=0,1,\tau,\tau+1,\tau+2,2\tau$. The restriction reduces $D(\tau)$ to:

$$\begin{aligned} D^2(\tau) &= (\gamma'^2+\lambda^2\epsilon^2)\left[(\tau+1)\langle w^2\rangle+2\tau\langle w w_1\rangle+2\langle w w_\tau\rangle\right]\\ &\quad +(\tau+1)\left(\sigma^2+\rho^2\right)+2\gamma'\tau\langle w_1\xi_0\rangle\\ &\quad -2\lambda\epsilon\gamma'\left[(\tau+1)\langle w w_{-\tau}\rangle+\tau\langle w w_{1-\tau}\rangle+\langle w^2\rangle+\tau\langle w_{-\tau}w_1\rangle+\langle w_{-\tau}w_{+\tau}\rangle\right]. \end{aligned} \tag{4.13}$$

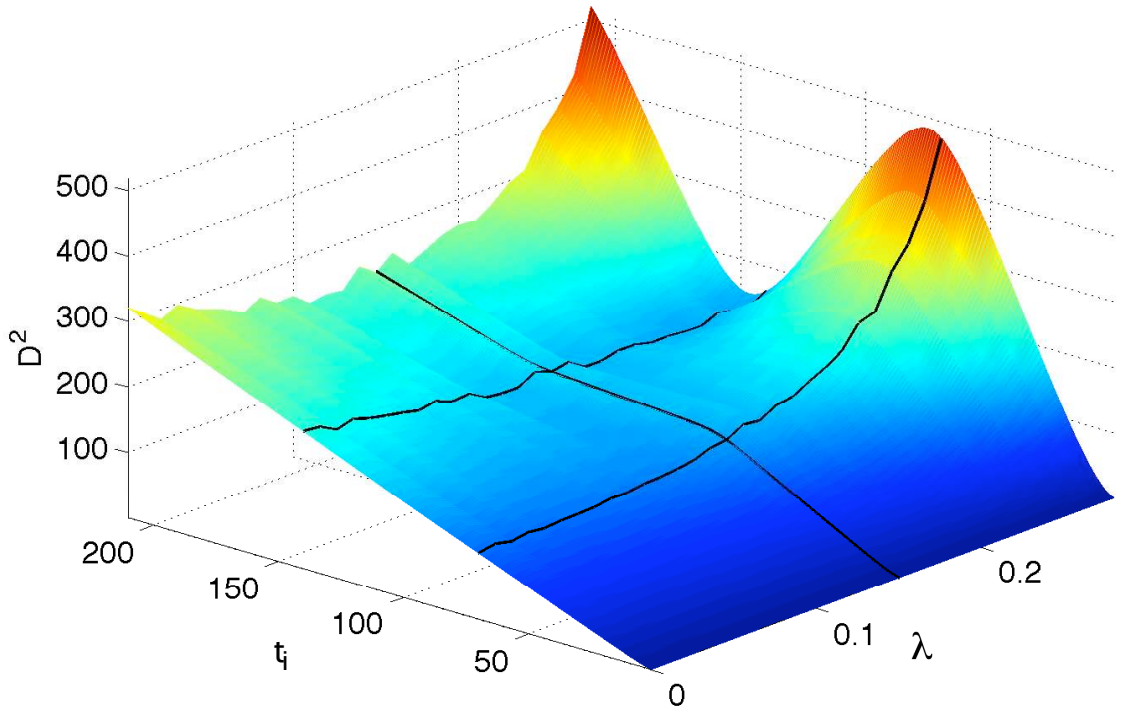

Figure 4.7: $D^2(t_i)$ for $t_i < 3\tau$ is shown; the third component illustrates the dependence of $D^2(t_i)$ on λ. The black lines denote, on the one hand, the choice of $\lambda = 0.15$ in accordance with the behavior found in the measured data, and on the other hand, the values $t_i = \tau$ and $t_i = 2\tau$ used in the approximation.

For $D(2\tau)$, additional terms remain and $D(2\tau)$ has the form:

$$\begin{aligned} D^2(2\tau) \;=\; & (\gamma'^2 + \lambda^2\epsilon^2)\left[(2\tau+1)\langle w^2\rangle + 4\tau\langle ww_1\rangle + 2(\tau+1)\langle ww_\tau\rangle\right] \\ & +(\gamma'^2 + \lambda^2\epsilon^2)\left[2\tau\langle ww_{1+\tau}\rangle + 2(\tau-1)\langle ww_{2+\tau}\rangle + 2\langle ww_{2\tau}\rangle\right] \\ & +2\gamma'\left[2\tau\langle w_1\xi_0\rangle + \tau\langle w_{\tau+1}\xi_0\rangle + (\tau-1)\langle w_{\tau+2}\xi_0\rangle\right] \\ & -2\lambda\epsilon\left[\tau\langle w_1\xi_0\rangle + (\tau-1)\langle w_2\xi_0\rangle\right] + (2\tau+1)\left(\sigma^2+\rho^2\right) \\ & -2\lambda\epsilon\gamma'\left[(2\tau+1)\langle ww_{-\tau}\rangle + 2\tau\langle ww_{1-\tau}\rangle + (\tau+1)\langle w^2\rangle\right] \\ & -2\lambda\epsilon\gamma'\left[\tau\langle ww_1\rangle + (\tau-1)\langle ww_2\rangle + \langle ww_\tau\rangle\right] \\ & -2\lambda\epsilon\gamma'\left[2\tau\langle w_{-\tau}w_1\rangle + (\tau+1)\langle w_{-\tau}w_\tau\rangle + \tau\langle w_{-\tau}w_{\tau+1}\rangle\right] \\ & -2\lambda\epsilon\gamma'\left[(\tau-1)\langle w_{-\tau}w_{\tau+2}\rangle + \langle w_{-\tau}w_{2\tau}\rangle\right] \;. \end{aligned} \tag{4.14}$$

Furthermore, the approximation that projects lags $l > 0$ of the auto-correlation function down to lag $l = 0$, $\langle ww_{-\tau}\rangle \approx -2\lambda\epsilon\langle w^2\rangle$, and the resulting dependence

$\langle ww_1\rangle \approx (\gamma' + 2\lambda^2\epsilon^2)\langle w^2\rangle$ were applied. Additionally, we use $\tau + 1 \approx \tau$ in (4.13),

$$\begin{aligned} D^2(\tau) &= \tau\left(\gamma'^2 + \lambda^2\epsilon^2 + 4\lambda^2\epsilon^2\gamma'\right)\left(1 + 2\gamma' + 4\lambda^2\epsilon^2\right)\langle w^2\rangle \\ &\quad -2\lambda\epsilon(\gamma' + 2\lambda^2\epsilon^2)(1 + 2\gamma')\langle w^2\rangle + \tau\left[(1 + 2\gamma')\sigma^2 + \rho^2\right] . \end{aligned} \tag{4.15}$$

For (4.14), we obtain:

$$\begin{aligned} D^2(2\tau) &= 2\tau\left(\gamma'^2 + \lambda^2\epsilon^2 + 4\lambda^2\epsilon^2\gamma'\right)\left(1 + 2\gamma' + 4\lambda^2\epsilon^2\right)\langle w^2\rangle \\ &\quad -2\tau\lambda\epsilon(\gamma' + 2\lambda^2\epsilon^2)(1 + 2\gamma')\left[1 + \gamma' + 2\lambda^2\epsilon^2 + (\gamma' + 2\lambda^2\epsilon^2)^2\right]\langle w^2\rangle \\ &\quad +4\lambda^2\epsilon^2(\gamma' + 2\lambda^2\epsilon^2)(1 + 2\gamma')\langle w^2\rangle \\ &\quad +2\tau\left[(1 + 2\gamma')\sigma^2 + \rho^2\right] - \tau\lambda\epsilon\left[2 + 2\gamma'\right]\sigma^2 . \end{aligned} \tag{4.16}$$

As τ is far larger than 1, the terms without τ are at least one order of magnitude smaller and can be neglected. Using the substitutions,

$$\begin{aligned} \Delta &= (\gamma'^2 + \lambda^2\epsilon^2 + 4\lambda^2\epsilon^2\gamma')(1 + 2\gamma' + 4\lambda^2\epsilon^2)\langle w^2\rangle + (1 + 2\gamma')\sigma^2 + \rho^2 , \\ \Lambda &= 2\lambda\epsilon(\gamma' + 2\lambda^2\epsilon^2)(1 + 2\gamma')\left[1 + \gamma' + 2\lambda^2\epsilon^2 + (\gamma' + 2\lambda^2\epsilon^2)^2\right]\langle w^2\rangle + 2\lambda\epsilon(1 + \gamma')\sigma^2 , \end{aligned}$$

we can write the mean square displacements in Eqns. (4.15) and (4.16) as $D^2(\tau) = \tau\Delta$ and $D^2(2\tau) = 2\tau\Delta - \tau\Lambda$, respectively. Finally, for Eqn. (4.10), we obtain:

$$H_l = \frac{1}{2\log 2}\log\left(\frac{2\tau\Delta - \tau\Lambda}{\tau\Delta}\right) \tag{4.17}$$

One last question remains: How can we find an approximation of the mean square of w_{k+1}? To answer this, as a first step, we assume stationarity. Then, for the mean square of the velocity-related process, we replace w_{k+1} according to the iteration rule in Eqn. (4.3):

$$\langle w_{k+1}^2\rangle = \langle w_{k+1}\left[\gamma' w_k + \xi_k - \lambda\tanh(\epsilon w_{k-\tau})\right]\rangle . \tag{4.18}$$

The next step is the approximation of the terms containing the $\tanh(w_{k-\tau})$ terms. Here, we again apply the approximations $\tanh(\epsilon w_k) \approx \epsilon w_k$, $\langle w_{k-\tau}w_k\rangle \approx -2\lambda\epsilon\langle w_k^2\rangle$ and $\langle w_{k+1}w_k\rangle = (\gamma' + 2\lambda^2\epsilon^2)\langle w_k^2\rangle$ to obtain

$$\begin{aligned} \langle w^2\rangle &= \gamma'\left(\gamma' + 2\lambda^2\epsilon^2\right)\langle w^2\rangle + \sigma^2 + 2\lambda^2\epsilon^2\left(\gamma' + 2\lambda^2\epsilon^2\right)\langle w^2\rangle , \\ &= (\gamma' + 2\lambda^2\epsilon^2)^2\langle w^2\rangle + \sigma^2 . \end{aligned}$$

Reordering the terms of this equation results in an approximation for the second moment of w, i.e.,

$$\langle w^2\rangle = \frac{\sigma^2}{1 - (\gamma' + 2\lambda^2\epsilon^2)^2} . \tag{4.19}$$

Equation (4.19) is used in the calculations of the local scaling exponents for the short H_s (4.19) and long time scale H_l (4.9) in dependence of λ and γ. The validity is checked by comparison with numerical simulations of Eqn. (4.3) for different λ and γ. In Figure 4.8A, we show the comparison of values of H_s for short time scales as a function of γ and in Figure 4.8C as a function of λ. Around the chosen values $\gamma = 0.25$ and $\lambda = 0.15$, the analytical approximation is in good agreement with the SDA. For the long time scales, we plot the dependence of H_l on γ (Figure 4.8B) and H_l on λ (Figure 4.8D). Here, the agreement between the analytic approximation and the DFA is better than with the SDA. Qualitatively, the analytical approximation and the numerical results agree, however, the analytical results are closer to the results obtained via DFA. Thus, the analytical calculations confirm the parameter dependence of the local scaling exponents observed in the numerical simulations.

4.4 Summary of the model

We are able to reproduce the local scaling behavior of fixational eye movements acquired in the analysis section with a model motivated by the known physiology. The model is set up to incorporate knowledge about the control mechanism: control of velocity, and feedback connections. Furthermore, the proposed model is closely associated with the motoneuron activity within the brain stem while reproducing the local scaling behavior, which is observed noninvasive by eye tracking.

The modeling approach on the basis of a delayed random walk proved to be very successful. One of the major successes of the model is that the delays obtained in the model through comparison of model simulations and real data lie in the range of physiological plausible delays. Additionally, the different delays observed for the horizontal and vertical components are in good agreement with the spatially separated physiological representations in the brain stem. We were able to suggest, by the comparison of known signal propagation times, the presence of an external feedback loop, which runs from the retina through the superior colliculus to the eye muscles for horizontal fixational eye movements. The delay obtained for the vertical component is smaller than this external feedback loop would account for, which suggests that the presence of internal feedback loops for fixation control in the vertical but not the horizontal component exists. Finally, we presented a semi-analytical investigation of local scaling. The investigation confirms the local scaling behavior for short and long time scales along two of the model parameters.

However, there are still many things which could be incorporated in the model. Currently, the model does not contain microsaccades; also, the reduction of the box count before microsaccades is not part of the model.

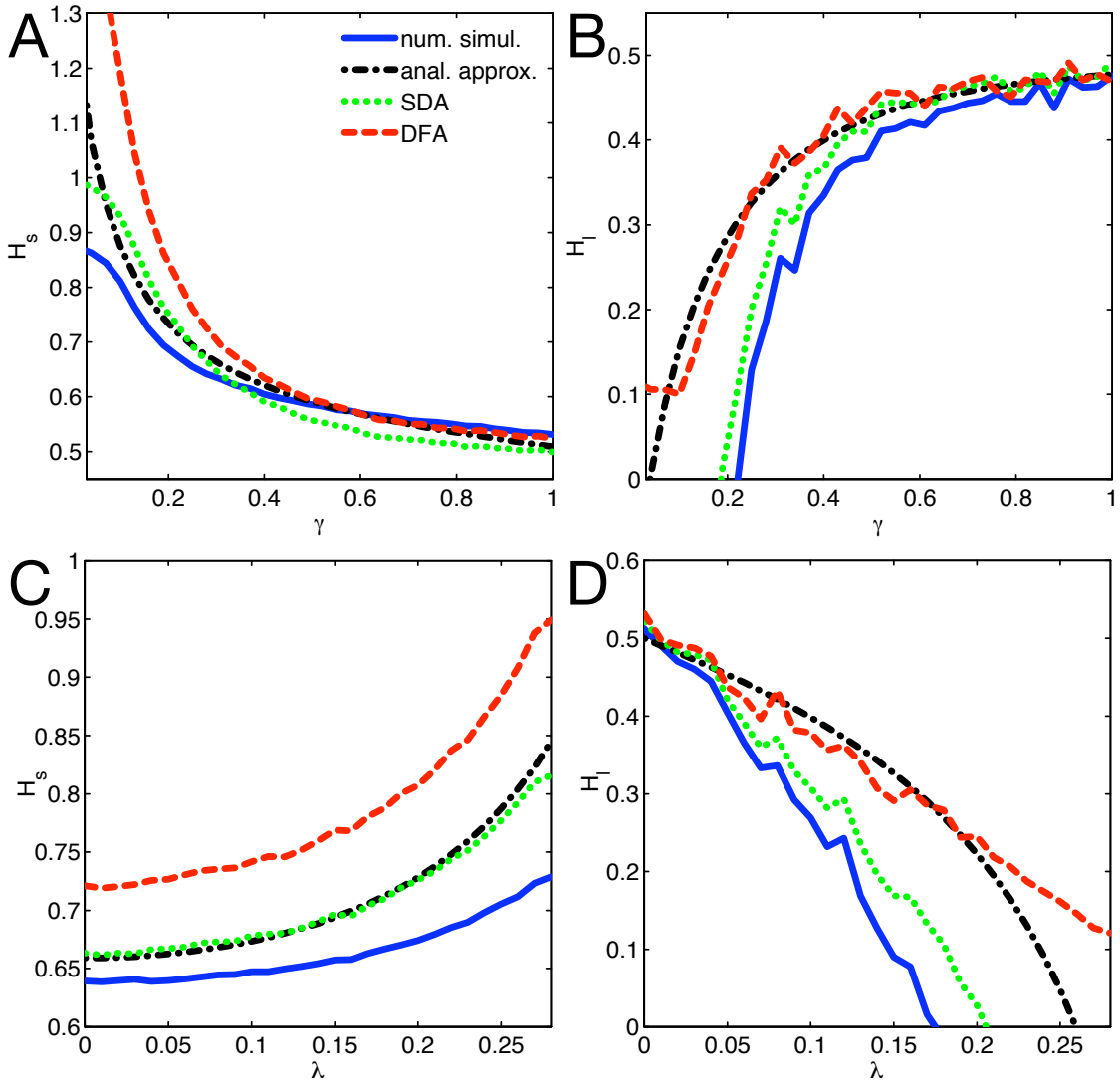

Figure 4.8: Comparison of analytical approximation (black dashed-dotted line) with numerical values (blue solid line), SDA (green dotted line), and DFA (red dashed line). (A): Short time scales: H_s vs. γ analytically from Eqn. (4.9), SDA for $l = 1$ to 20, and DFA for $l = 6$ to 100. (B): Long time scales: H_l vs. γ analytically from Eqn. (4.17), numerically from Eqn. (4.10), SDA for $l = 70$ to 210, and DFA for $l = 400$ to 2000. (C): Like (A), but H_s vs. λ. (D): Like (C), but H_l vs. λ

Chapter 5

Discussion

Fixational eye movements pose several challenging but promising questions in different scientific disciplines, i.e., psychology, neuroscience and physics. For psychologists, the link between attentional modulation of microsaccade rate and orientation [Laubrock et al., 2007; Engbert, 2006; Hafed and Clark, 2002] and effects of awareness on the same modalities [Betta and Turatto, 2006; Martinez-Conde and Macknik, 2007] make fixational eye movement a very interesting topic. Their interest is further boosted by possible explanations for numerous visual illusions, e.g., illusory motion of static patterns [Fermüller et al., 1997] ("Enigma" [Leviant, 1996; Kumar and Glaser, 2006; Martinez-Conde, 2006], Ouichi illusion Figure 1.2 [Ouchi, 1977], "Rotating Snakes" [Kitaoka and Ashida, 2003]), or brightness illusions (Hermann grid [Hermann, 1870]). Numerous illusions have been collected by Kitaoka. In neuroscience, fixational eye movements play a major role in the explanation of hyperacuity [Rucci et al., 2007] and visual discrimination of orientation of tiny bars [Pitkow et al., 2007]. Furthermore, it has been reported that microsaccades trigger visually evoked activity in visual cortex neurons [Martinez-Conde et al., 2000, 2002] and supply an explanation for Troxler fading (fading of a light blue annulus around a fixation dot) and reappearance [Martinez-Conde et al., 2006]. For physicists, fixational eye movements are generated by a dynamical system with feedback [Mergenthaler and Engbert, 2007] with distinct statistical properties. The tiny movements can also be used to go below the spatial optical acuity limits of CCD cameras by integrating temporal information [Wei et al., 2007]. In general, one could say that fixational eye movements are a research area which would greatly benefit from interdisciplinary work between cognitive neuroscience and nonlinear sciences.

The amount of research on fixational eye movements, especially on microsaccades, is currently growing strongly (Figure 5.1). At least three content related reasons for the growing interest should be mentioned. In the period before 1980, the amount of interest was increasing, but between 1980 and 2000, the number of publications remained roughly constant. The reason for the reduced interest is possibly due to

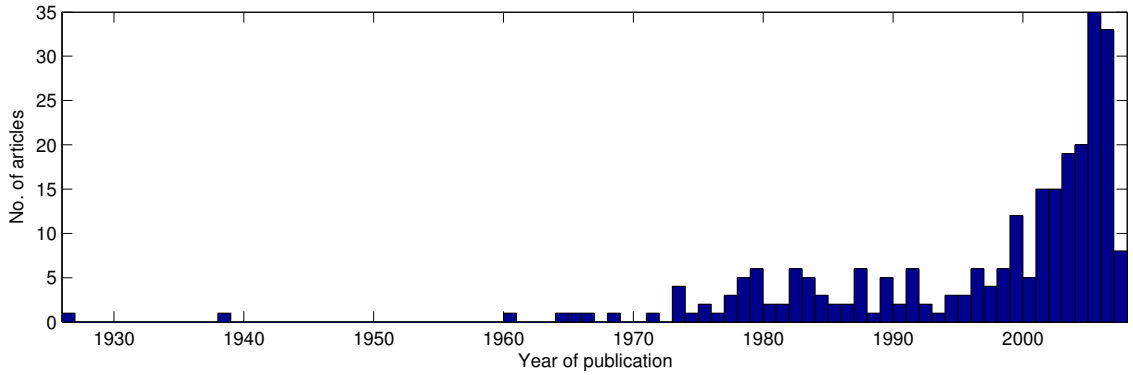

Figure 5.1: The number of publications found by a search of "microsaccad*" and "fixational eye" in ISI Web of Knowledge is strongly increasing.

the publication of two articles Kowler and Steinman [1979, 1980], which stated that microsaccades serve no useful purpose. The first reason for the resumed increase in interest starting around 2000 derives from the neurophysiological finding that microsaccades evoke activity in numerous areas of the cortex, e.g., striate cortex [Leopold and Logothetis, 1998; Martinez-Conde et al., 2000], lateral geniculate nucleus, and primary visual cortex [Martinez-Conde et al., 2002]. The second reason for the increase in publications arises from results published around 2002 that found a link between covert attention and microsaccades [Hafed and Clark, 2002; Kohama and Usui, 2002; Engbert and Kliegl, 2003]. The third, which is a current issue and will likely lead to several more publications, is that microsaccades evoke activity and generate ocular artifacts that are measurable by EEG [Yuval-Greenberg et al., 2008; Dimigen et al., subm]. In particular, the activity in the gamma-band Yuval-Greenberg et al. [2008] of the EEG can fuel new research as several earlier publications about gamma-band activity suffer from the problem that the effect of microsaccades was neglected, as usually the eyes are not tracked during EEG measurements. All three reasons are in contradiction to the statement that microsaccades serve no useful purpose, and thus led to revived interest in the field. Another, more technical, reason for the increase in publications is that video-based eye trackers allow much more convenient measurement than those setups where one needs to affix contact lenses by suction onto the cornea. Furthermore, the automatized detection of microsaccades and the ease of access to computer-based statistical packages that can handle large data sets, encourages the research on fixational eye movements.

5.1 Analyses on fixational eye movements

With improved analyses, much more information can be obtained, which will allow deeper insights into visual processing and motor behavior required for optimal visual

perception. Furthermore, questions about the interaction and organization of the two different and competing functions of fixational eye movements, i.e., the refreshing of fatigued receptors through movement and gaze stabilization during head movements, can be pursued by using the applied measures presented in this dissertation. Earlier analyses used for the characterization of fixational eye movements were rather primitive, e.g., the calculation of the direction of the eye movement caused by drift or microsaccades by comparison of start and end point of the intervals. While this measure of direction (sometimes used to classify if microsaccades and drift are corrective [Møller et al., 2006]) is useful for microsaccades, it poorly reflects the behavior of the drift. Therefore, the implementation of better measures characterizing the drift movement are necessary.

However, before the investigation of drift and microsaccade properties, it is crucial to classify whether a given sample of the eye movement trajectory belongs to a drift or microsaccade interval. Common microsaccade detection algorithms [Martinez-Conde et al., 2000, e.g., used in], do not take into account differences in the relationship between drift and microsaccade across participants and experimental conditions. We proposed an improved version of the two-dimensional velocity-based microsaccade detection algorithm (Section 3.1) [Mergenthaler and Engbert, subm] described by Engbert and Kliegl [2003]. The algorithm takes into account the individual differences that participants show. This also means that it allows the reinvestigation of results concerning changes in the rate of microsaccades between different visual conditions. Furthermore, the microsaccade rate within certain time windows is frequently investigated [Martinez-Conde et al., 2006; Valsecchi et al., 2007; Rolfs et al., 2006], but the rate is directly based on the detection of microsaccades and therefore directly affected by the detection algorithm.

Although fixational eye movements can now be separated in microsaccades and drift, it is unclear which role these different types of movements play. As a first approach to the separation of the function, we performed an experiment with two different visual conditions, fixations on a stimulus and in darkness, and we showed that microsaccade rate and amplitudes do change under different visual conditions. In darkness, the microsaccades became larger and less frequent, which is possibly related to the enhanced use of the peripheral part of the retina in low light conditions. These findings concur with the suggestion by Martinez-Conde [2006] that microsaccades and drift fulfill the role of retinal refresh for different receptive field sizes: drift for small receptive fields in the fovea and microsaccades for larger receptive fields in the periphery. They reported that the rate of microsaccades is reduced before Troxler fading [Martinez-Conde et al., 2006]) and increased before the reappearance of the peripheral stimulus. The effect of microsaccades was less strong when the annulus became smaller (tested diameters: 18°, 12°, and 6°).

After successful detection of the microsaccades, the local scaling behavior can be determined and compared to the behavior of the full time series. We tested for local

scaling properties by DFA and SDA and found persistent behavior on short timescales and anti-persistent behavior on long timescales [Mergenthaler and Engbert, 2007]. The trough on intermediate scales in the SDA suggests that fixational eye movements are controlled by a delayed feedback loop [Ohira, 1997], as the SDA is linked to the auto-correlation function. This strongly contradicts an earlier hypothesis that drift is a simple uncontrolled noise process.

Recently, Pitkow et al. [2007] proposed a Markov decoder model for visual input, which incorporates the drift movement as a random process with a distinct diffusion constant on a grid of neurons with a multiplicative update of the firing rates of a neuron by use of the firing rate in adjacent neurons. The decoder was able to detect the orientation of tiny bars (1×2 arcmin.) as long as the bars performed a random walk across the decoder. They further describe that the investigated persistence on short time scales [Mergenthaler and Engbert, 2007] is beneficial for such a decoder model. Nevertheless, they argue that the anti-persistence on long time scales is due to the microsaccades, which contradicts the results presented in Section 3.2 and [Mergenthaler and Engbert, 2007]. This could be one of the reasons why humans still perform better than the Markov decoder model.

Generally, detailed investigation of drift is commonly neglected. However, Steinman et al. [1973] have shown that the role of microsaccades can be at least partially carried over to the drift, which suggests that drift by itself plays a role for both described functions of fixational eye movements. Thus, the specific investigation of periods of drift contains additional information that reveals properties like feedback control [Mergenthaler and Engbert, 2007]. Nevertheless, the analyses investigating local scaling inquire global properties of the eye movement trajectories. Such analyses cannot be used to detect possible local triggering mechanisms for microsaccades. With the box-counting algorithm (Section 3.5), we supply an new tool to characterize the drift during small time windows [Engbert and Mergenthaler, 2006] that could possibly address the question of microsaccade triggering. Microsaccades can be generated by a random process, by locking to brain activity, e.g., phase locking to alpha rhythms [Gaarder et al., 1966; Lehmann et al., 1965], or by a dynamical process on the basis of certain properties of the drift [Engbert and Mergenthaler, 2006; Mergenthaler and Engbert, subm]. With the box-counting approach, we could at least detect if microsaccades are preceded by a reduction in the box count, and clearly they are: Around 300 ms before microsaccade onset, the number of boxes necessary to cover the trajectory is reduced. We still cannot decide if microsaccade programming reduced the drift before the microsaccade or if microsaccades are triggered by the reduced drift. Furthermore, we cannot decide if the reduced drift coincides with a certain phase in the alpha rhythm. Nevertheless, the box-counting approach appears to be a analysis that could reveal several interesting properties concerning relations between brain activity, drift behavior and microsaccade occurrence.

5.2 Theoretical model of fixational eye movements

For larger eye movements like saccades and smooth pursuit, numerous computational models exist [Girard and Berthoz, 2005]. This is different for fixational eye movements where only two earlier models are available (Section 4.2), which were based on direct control of the eye position [Vasudevan et al., 1972; Seung, 1996]. However, it was pointed out by Epelboim and Kowler [1993] that the control of fixational eye movements has to be at the level of velocity control. We proposed the first model based on velocity control (Section 4.3, [Mergenthaler and Engbert, 2007]). It is set up as a stochastic model motivated by Ohira [1997] and Yao et al. [2001], with a delayed feedback term, a noise source, and an autoregressive term in the velocity related variable. This is summed up with an additional noise source to represent motoneuron activity (Eq. (4.3)). Currently, the model nicely reproduces the local scaling properties within the data for the vertical and horizontal drift movements. The largest success of the model is that the estimated delays for the feedback control in the horizontal component concur with the duration of a physiological feedback loop from the retina trough the brain stem to the eye muscles [Sparks, 2002; Moschovakis et al., 1996]. For the vertical component, the delays are shorter; this could indicate that an internal feedback loop, which has only been reported for the vertical component, replaces the external feedback control. The model as proposed in this dissertation is generally diffusive, due to the added noise in the position related equation. This is in accordance with the lack of a decay to zero of the scaling exponent for towards the largest scales [Moreau and Sontag, 2003]. Nevertheless, the longest timescale could be missed by the relatively short (20 ms) fixations. The existence of such a third timescale coincides with a stable dynamic within the position related equation; it is still not yet clear whether, in addition to velocity related feedback, control mechanisms within the position related activity are active. Finally, we were able to corroborate the local scaling properties by a semi-analytic approximation of the scaling properties on long and short timescales.

5.3 Outlook

The experiments, analyses and modeling presented in this dissertation offer numerous possibilities to advance the research on fixational eye movements.

Experiments which would strongly contribute to the knowledge of fixational eye movement control are experiments with different stimuli and with more natural postures. The experiments with different stimuli could contain experiments that investigate how strongly the control of fixational eye movement is governed by luminance or contrast information. It could be that fixations on a spot that is

isoluminant to the background [Valsecchi and Turatto, 2007] are controlled with longer feedback delays due to the color-blind retinotectal pathway. Further, it would be useful to perform experiments where the visual information that is used for fixation control is only available in the periphery, e.g., a light blue annulus as in the Troxler fading experiments [Martinez-Conde et al., 2006]. Another batch of experiments could target the two counteracting functions of fixational eye movements, the stabilization of stimuli and the counteraction of retinal fatigue. This issue can be addressed by experiments with different postures like sitting with a free head and standing, where the influence of head movements is increased, which shifts the emphasis towards stabilization. However, further experiments should also be performed that could reveal more about the possible microsaccade triggering by properties of the drift [Engbert and Mergenthaler, 2006], or by locking to alpha activity in the EEG [Gaarder et al., 1966]. It is still unclear if microsaccades are generated fully randomly by a point process or by a triggering mechanism like retinal image slip; in the first case, it would be necessary to explain the reduction of retinal image slip before microsaccades. Experiments where subjects are instructed to produce reactive saccades with the same small amplitudes as microsaccades could be a useful tool to explain the mechanisms of microsaccade generation.

The presented analyses could then be performed on different data sets. Nevertheless, the advancement of the presented analyses and the application of further analyses are exptected to contribute to the understanding of fixational eye movements. The separate investigation of the box count in inter-microsaccade intervals of different lengths could supply evidence for control mechanisms. In addition, the use of wavelet-based methods to classify fixational eye movements into drift and microsaccades [Holschneider et al., 2006] would be beneficial. Another necessary analysis is direct delay estimation to confirm the indirect estimated delays via comparison of model and data. For linear systems, the method by Ohira and Sawatari [1997] (see also: Appendix B) could be applied; for fixational eye movements, the approach by Siefert [2007] could be pursued.

A first next step to develop our model is to incorporate microsaccades; this can also be used to evaluate the triggering of microsaccades. The model has to follow the observed behavior of reduces retinal image slip before a microsaccade. The properties of microsaccades, i.e., amplitude, rate, and direction, should then be incorporated. However, alternative approachs to the modeling will be developped. For example on the basis of self-avoiding random walks as introduced by Freund and Grassberger [1992]. Such a model would be motivated by the exhaustion of re-growing resources and inherently prevents the fatigue of photoreceptors.

Appendix A

Map of connections between oculomotor nuclei

For completeness, and to integrate the smaller figures for horizontal (Figure 4.2) and vertical (Figure 4.3) into the circuitry of the brainstem, we give a full picture of the known connections that contribute to the saccade generation (Figure A.1). The figure is adapted from [Moschovakis et al., 1996]. It shows the excitatory and inhibitory connections in the brain stem. The brain stem areas receive input input from the retina, the cortex, and the cerebellum and propagate to the three pairs of motoneurons, which directly actuate the extraocular muscles.

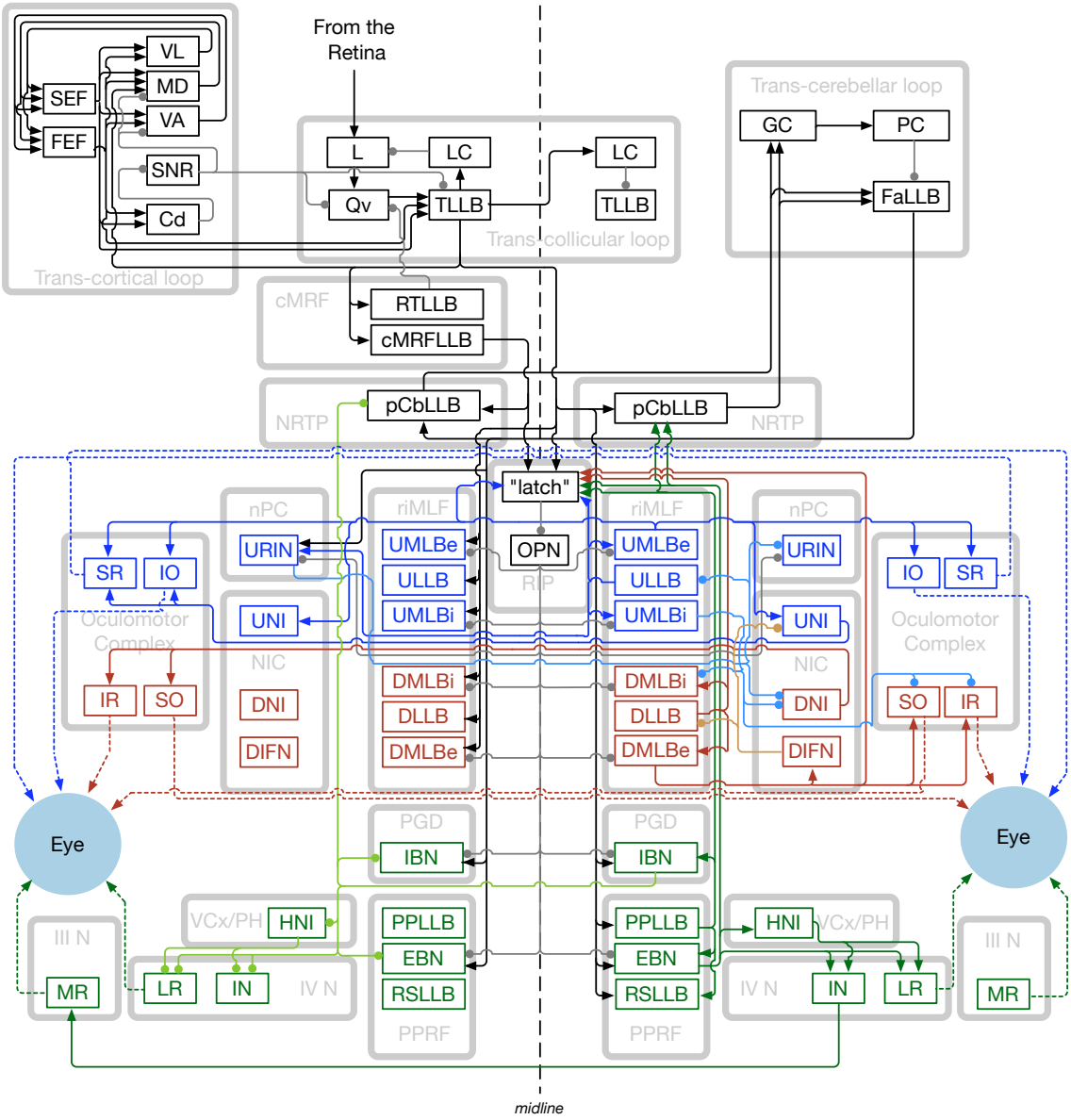

Figure A.1: The full control loop for saccadic eye movements [Moschovakis et al., 1996]. A clear physiological separation of vertical (blue: up and red: down) and horizontal (green) in the brain stem is made. Connections ending with an arrow head are excitatory while connections ending with a bullet are inhibitory. The light gray boxes denote the higher order brain structures in the upper part and the different nuclei in the lower part. The smaller black or colored boxes describe smaller areas of brain structures in the upper part and areas of neurons with a certain firing property in the lower part. For abbreviations see next page.

III N	oculomotor nucleus
VI N	abducens nucleus
Cd	caudate
CbLLB	cerebellar long lead burst neurons
cMRF	central mesencephalic reticular formation
cMRFLLB	long lead burst neurons of the cMRF
DIFN	downward inhibitory feedback neuron
DLLB	downward long lead burst neurons
DMLBe	excitatory downward medium lead burst neurons
DMLBi	inhibitory downward medium lead burst neurons
DNI	downward neural integrator
EBN	excitatory burst neuron
FaLLB	fastigial long lead burst neurons
FEF	frontal eye field
GC	granule cells of the oculomotor vermis
HNI	horizontal neural integrator
IBN	inhibitory burst neuron
IN	internuclear neuron
IO	inferior oblique
IR	inferior rectus
L	lateral neurons of the superior colliculus
LC	local circuit neuron
LR	lateral rectus
MD	mediodorsal nucleus of the thalamus
MR	medial rectus
NIC	interstitial nucleus of Cajal
nPC	nucleus of posterior commissure
NRTP	nucleus reticularis tegmenti pontis
OPN	omnipause neuron
pCbLLB	precerebellar long lead burst neurons
PC	posterior commissure
PGD	nucleus paragigantocellularis dorsalis
PH	nucleus prepositus hypoglossi
PPLLB	pontopontine long lead burst neurons
PPRF	paramedian pontine reticular formation
Qv	quasivisual neurons
riMLF	rostral interstitial nucleus of the median longitudinal fasciculus
RIP	nucleus raphé interpositus
RSLLB	reticulospinal long lead burst neurons
RTLLB	reticulotectal long lead burst neurons
SEF	supplementary eye fields
SNR	substantia nigra pars reticulata
SO	superior oblique
SR	superior rectus
TLLB	thalamic long lead burst neurons
ULLB	upward long lead burst neurons
UMLBe	excitatory upward medium lead burst neurons
UMLBi	inhibitory upward medium lead burst neurons
UNI	upward neural integrator
URIN	upward resettable integrator neuron
VA	nucleus ventralis anterior of the thalamus
VCx	vestibular complex
VL	nucleus ventralis lateralis of the thalamus.

Appendix B

Delay estimation - Ohira method

The delay estimation for the model was performed indirectly by fitting the parameters to the data. A more direct way to estimate control delay would be preferable. A possibility of performing a delay estimation is proposed in [Ohira and Sawatari, 1997]. The method is described to be applied to time series that are approximately generated by a noisy linear feedback system. Nevertheless, as delayed random walk models seem the appropriate choice of model type for fixational eye movements, we applied the method to the data of horizontal, vertical eye movements, and simulations of our model.

The analysis, described in [Ohira and Sawatari, 1997], consists of several steps:

1. Compute the autocorrelation function $C(u)$ from the time series. It should be oscillating with some $C(u) < 0$. Otherwise the method is not directly applicable.

2. A "normalized set" is built from the autocorrelation function $C(u)$.

$$K(u) = \frac{C(u)}{2[C(0) - C(1)]} \tag{B.1}$$

3. Identify τ_i, the first point where $K(u) \approx 0$.

4. Choose a τ_e which is close to τ_i and evaluate its quality according to the next steps.

5. With the chosen τ_e, compute:

$$y_1(u) = \frac{K(u)}{K(|\tau_e - u|)}, \qquad z_1(u) = \frac{K(u+1)}{K(|\tau_e - u|)} \tag{B.2}$$

$$y_2(u) = \frac{K(|\tau_e - u|)}{K(u)}, \qquad z_2(u) = \frac{K(u+1)}{K(u)} \tag{B.3}$$

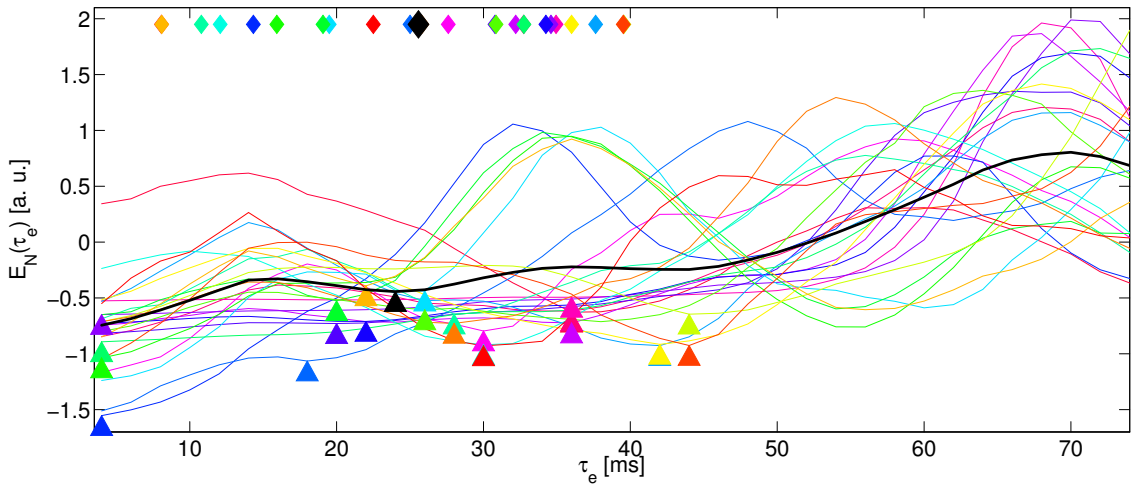

Figure B.1: Horizontal eye movements: The diamonds at the upper edge denote the τ_i estimated from the first zero crossing of the autocorrelation function. The triangles denote the individual local minimum of $E_N(\tau_e)$ closest to τ_i. Their horizontal position gives the individual τ_e. Each colored line corresponds to the mean of one participant. The black diamond and triangle denote the means over all.

6. For a linear system and optimal choice of τ_e, the values y_1, z_1, y_2, z_2 should obey the following linear relations:

$$z_1(u) = (1-\alpha)y_1(u) - \beta, \qquad z_2(u) = -\beta y_2(u) - (1-\alpha). \tag{B.4}$$

   For choices that are less optimal, the values should deviate more from the linear relation. The parameters α and β can be estimated via linear regression.

7. To quantify the deviation from the linear relation, compute the χ^2 error of the two relations and define:

$$E(\tau_e) = \chi_1^2 + \chi_2^2. \tag{B.5}$$

8. The best estimate of the intrinsic delay is the one that minimizes $E(\tau_e)$.

The described procedure (step 1 to 8) is performed on the velocity signals obtained from Experiment 1 separately for horizontal (Figure B.1) and vertical (Figure B.2) eye movements and on the velocity signal obtained by model simulations (Figure B.3) with the optimized parameters for the horizontal component (see Subsection 4.3.2). For the linear regression a robust fit procedure is used to minimize the effect of extreme outliers. In step 7 the two obtained χ^2 errors are summed up via (B.5). In addition to the described procedure for obtaining the $E(\tau_e)$ a normalized $E_N(\tau_e)$ is computed via $E_N(\tau_e) = (E(\tau_e) - \overline{E(\tau_e)})/\sigma_{E(tau_e)}$, where $\overline{E(\tau_e)}$ denotes the mean of $E(\tau_e)$ over all τ_e and $\sigma_{E(\tau_e)}$ give the standard deviation of $E(\tau_e)$ over all τ_e. The

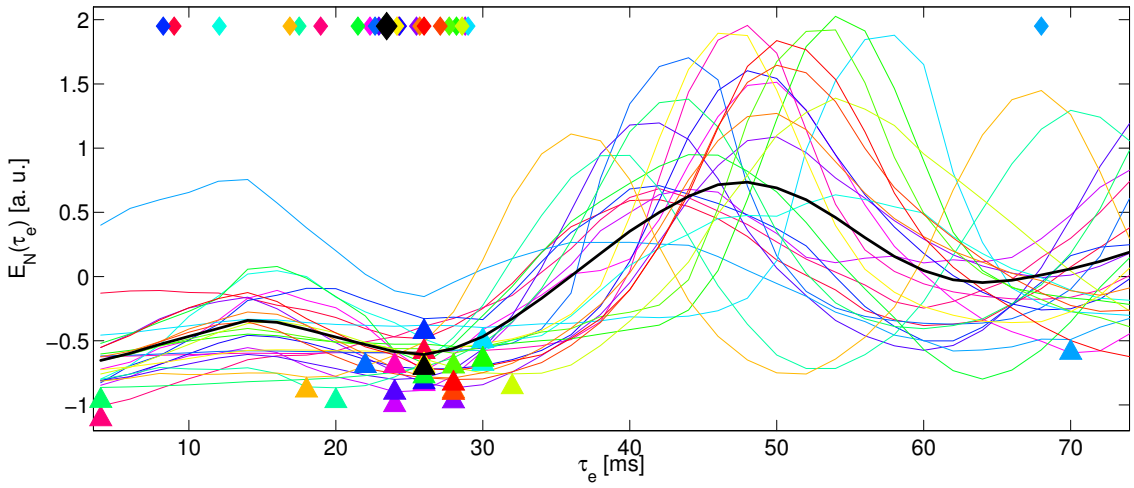

Figure B.2: Vertical eye movements: The diamonds at the upper edge denote the τ_i estimated from the first zero crossing of the autocorrelation function. The triangles denote the individual local minimum of $E_N(\tau_e)$ closest to τ_i. Their horizontal position gives the individual τ_e. Each colored line corresponds to the mean of one participant. The black diamond and triangle denote the means over all.

computation of the normalized errors $E_N(\tau_e)$ does not change the position of the minimum, which are detected in step 8, but it allows a better comparison across participants and allows the plotting in a single graph.

In simulations with the linear model proposed in [Ohira and Sawatari, 1997], we find that noise sources which are added to the feedback system, but are not feedback, i.e. measurement noise, leads to delay estimations which strongly underestimates the intrinsic delay. The simulations further suggest that in principle the noise dependent displacement of the minimum could be evaluated for the linear system. But if the displacement obeys a manageable relation to the noise strength has to be investigated. While for models the evaluation of the displacement is possible, as the parameters including the delay are known, for the eye movement data the displacement and therefore the underlying delay could not be accessed by the method described above. Thus, we argue that the appraisal of the delay via comparison of the location of the trough in SDA and DFA between the data and the model gives a more stable estimate than the method proposed by Ohira and Sawatari.

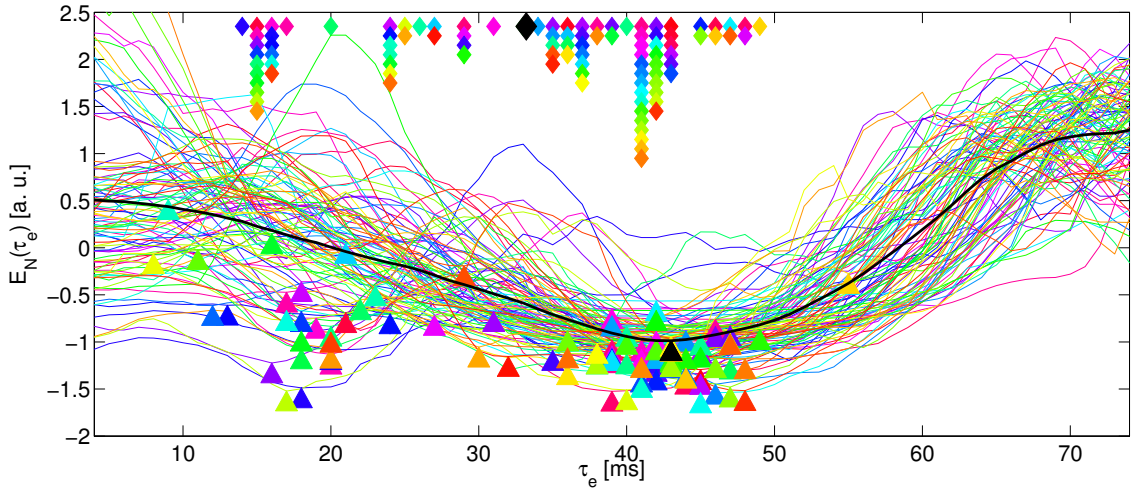

Figure B.3: Modeling horizontal data: The diamonds at the upper edge denote the τ_i estimated from the first zero crossing of the autocorrelation function. The triangles denote the local minimum of $E_N(\tau_e)$ closest to τ_i. Their horizontal position gives the τ_e. Each colored line corresponds to one model simulation. The black diamond and triangle denote the mean over all simulations.

Appendix C

Publications and conference presentations

Publications

Engbert, R. and Mergenthaler, K. (2006). Microsaccades are triggered by low retinal image slip. *Proceedings of the National Academy of Sciences of the United States of America, 103*(18), 7192-7197.
Even during visual fixation of a stationary target, our eyes perform rather erratic miniature movements, which represent a random walk. These "fixational" eye movements counteract perceptual fading, a consequence of fast adaptation of the retinal receptor systems to constant input. The most important contribution to fixational eye movements is produced by microsaccades; however, a specific function of microsaccades only recently has been found. Here we show that the occurrence of microsaccades is correlated with low retinal image slip approximate to 200 ms before microsaccade onset. This result suggests that microsaccades are triggered dynamically, in contrast to the current view that microsaccades are randomly distributed in time characterized by their rate-of-occurrence of 1 to 2 per second. As a result of the dynamic triggering mechanism, individual microsaccade rate can be predicted by the fractal dimension of trajectories. Finally, we propose a minimal computational model for the dynamic triggering of microsaccades.

Mergenthaler, K. and Engbert, R. (2007). Modeling the control of fixational eye movements with neurophysiological delays. *Physical Review Letters, 98*, **128104.**
We propose a model for the control of fixational eye movements using time-delayed random walks. Fixational eye movements produce random displacements of the retinal image to prevent perceptual fading. First, we demonstrate that a transition

from persistent to antipersistent correlations occurs in data recorded from a visual fixation task. Second, we propose and investigate a delayed random-walk model and get, by comparison of the transition points, an estimate of the neurophysiological delay. Differences between horizontal and vertical components of eye movements are found which can be explained neurophysiologically. Finally, we compare our numerical results with analytic approximations.

Mergenthaler, K. and Engbert, R. (submitted). Microsaccade detection and its impact on rate and amplitude under different visual conditions. Miniature (or fixational) eye movements are performed involuntarily during visual fixation. Microsaccades represent the fastest component of fixational eye movements which are modulated by visual stimulus type, experimental instructions, and visual attention. Therefore accurate detection of microsaccades is crucial for basic research on fixational eye movements. Here we propose an improved microsaccade detection algorithm taking into account individual differences. We show that the influence of the choice of the detection algorithm on scientific questions, i.e. the rate and the amplitude of binocular microsaccades in two visual conditions is strong. We found a significant difference between visual fixations on a stimulus (condition 1) and fixations in darkness (condition 2). Additionally, using our new statistical procedure we reject the hypothesis of the existence of monocular microsaccades.

Selected presentations

Mergenthaler, K. and Engbert, R. (2005). A model of fixational eye movements. *Poster at: DYBIO 05, 20th June - 15th July 2005, Dresden.*

Mergenthaler, K. and Engbert, R. (2007). Control principles underlying the generation of fixational eye movements. *Talk at: ECEM 07, 19th - 22th August 2007, Potsdam.*

Mergenthaler, K. and Engbert, R. (2007). Control mechanisms of fixational eye movements. *Poster at: ESF-EMBO Symposium: Three Dimensional Sensory and Motor Space: Perceptual Consequences of Motor Action, 6th - 10th October 2008, Sant Feliu de Guixols, Spain.*

Mergenthaler, K. and Engbert, R. (2008). Precursory retinal image motion before small-amplitude saccades. *Poster at: ECVP 08, 24th - 28th August 2008, Utrecht, Netherlands.*

Bibliography

Adler, F. H., & Fliegelman, M. (1934). Influence of fixation on the visual acuity. *Archives of Opthalmology*, *12*, 475–483. Cited on page: 4, 5, 7, 15

Aizawa, H., & Wurtz, R. W. (1998). Reversible inactivation of monkey superior colliculus. I. Curvature of saccadic trajectory. *Journal of Neurophysiology*, *79*, 2082–2096. Cited on page: 45

Angelaki, D. E., & Hess, B. J. M. (2004). Control of eye orientation: Where does the brain's role end and the muscle's begin? *European Journal of Neuroscience*, *19*, 1–10. Cited on page: 3

Applebaum, D. (2004). Lévy processes—from probability to finance and quantum groups. *Notices of the AMS*, *51*(11), 1337–1347. Cited on page: 3, 7

Bahill, A. T., Clark, M. R., & Stark, L. (1975). The main-sequence, a tool for studying human eye movements. *Mathematical Bioscience*, *24*, 191–204. Cited on page: 36

Barlow, H. B. (1963). Slippage of contact lenses and other artifacts in relation to fading and regeneration of supposedly stable retinal images. *Quarterly Journal of Experimental Psychology*, *15*, 36–51. Cited on page: 8

Beatty, J., & Lucero-Wagoner, B. (2000). The pupillary system. In J. T. Cacioppo, L. G. Tassinary, & G. G. Berntson (Eds.) *Handbook of Psychophysiology*, (pp. 142–146). Cambridge University Press, Cambridge, UK. Cited on page: 11

Bengi, H., & Thomas, J. G. (1973). Studies on human ocular tremor. In R. M. Kenedi (Ed.) *Perspectives in biomedical engineering*, (pp. 281–292). Macmillan, London. Cited on page: 5, 49

Bergeron, A., & Guitton, D. (2000). Fixation neurons in the superior colliculus encode distance between current and desired gaze positions. *Nature Neuroscience*, *3*, 932–939. Cited on page: 45, 49

Betta, E., & Turatto, M. (2006). Are you ready? I can tell by looking at your microsaccades. *Neuroreport*, *10*, 1001–1004. Cited on page: 7, 63

Bouchaud, J.-P., & Georges, A. (1990). Anomalous diffusion in disordered media: Statistical mechanisms, models and physical applications. *Physics Reports*, *195*(4-5), 127–293. Cited on page: 3, 7

Boyce, P. R. (1967). Monocular fixation in human eye movement. *Proceedings of the Royal Society of London*, *167*, 293–315. Cited on page: 6, 7, 15, 41, 50

Brainard, D. H. (1997). The psychophysics toolbox. *Spatial Vision*, *10*, 433–436. Cited on page: 12

Brockmann, D., & Geisel, T. (2000). The ecology of gaze shifts. *Neurocomputing*, *32*, 643–650. Cited on page: 3

Chen, Z., Ivanov, P. C., Hu, K., & Stanley, E. (2002). Effects of nonstationarities on detrended fluctuation analysis. *Physical Review E*, *65*, 041107. Cited on page: 26, 27

Churilla, A., Gottschalke, W. A., Liebovitch, L. S., Selector, L. Y., Todorov, A. T., & Yeandle, S. (1996). Membrane potential fluctuations of human t-lymphocytes have fractal characteristics of fractional brownian motion. *Annals of Biomedical Engineering*, *24*(1), 99–108. Cited on page: 22

Ciuffreda, K. J., & Tannen, B. (1995). *Eye movement basics for the clinician*. Mosby, St. Louis. Cited on page: 18

Collewijn, H., & van der Mark, F. (1972). Ocular stability in variable visual feedback conditions in the rabbit. *Brain Research*, *36*, 47–57. Cited on page: 6

Collins, J. J., & De Luca, C. J. (1993). Open-loop and closed-loop control of posture - a random-walk analysis of center-of-pressure trajectories. *Experimental Brain Research*, *95*(2), 308–318. Cited on page: 7, 22, 23, 24

Collins, J. J., & De Luca, C. J. (1994). Random walking during quiet standing. *Physical Review Letters*, *73*(5), 764–767. Cited on page: 22, 23, 24

Coppola, D., & Purves, D. (1996). The extraordinary rapid disappearance of entoptic images. *Proceedings of the National Academy of Sciences of the USA*, *93*, 8001–8004. Cited on page: 8

Cornelissen, F. W., Peters, E. M., & Palmer, J. (2002). The eyelink toolbox: Eyetracking with matlab and the psychophysics toolbox. *Behavioral Research Methods, Instruments and Computers*, *34*, 613–617. Cited on page: 12

Cornsweet, T. N. (1956). Determination of the stimuli for involuntary drifts and saccadic eye movements. *Journal of the Optical Society of America*, *46*(11), 987–995. Cited on page: 5, 33

Curcio, C. A., Sloan, K. R., Kalina, R. E., & Hendrickson, A. E. (1990). Human photoreceptor topography. *The Journal of Comparative Neurology*, *292*(4), 497–523. Cited on page: 2

Darwin, R. W. (1786). New experiments on the ocular spectra of light and colors. *Philosophical Transactions of the Royal Society*, *76*, 313–348. Cited on page: 4

de Bie, J., & van den Brink, G. (1986). A model for the slow control system during monocular fixation. *Vision Research*, *26*(7), 1129–1142. Cited on page: 49

Delignières, D., Deschamps, T., Legros, A., & Caillou, N. (2003). A methodological note on nonlinear time series analysis: Is the open- and closed-loop model of Collins and De Luca (1993) a statistical artefact? *Journal of Motor Behavior*, *35*(1), 86–96. Cited on page: 22, 23, 24

Dimigen, O., Valsecchi, M., Sommer, W., & Kliegl, R. (subm). Microsaccades generate visual brain activity that superimposes on event-related EEG measurements. Cited on page: 64

Ditchburn, R. W. (1955). Eye movements in relation to retinal action. *Optica Acta*, *1*, 171–176. Cited on page: 33, 34, 37, 39

Ditchburn, R. W. (1980). The function of small saccades. *Vision Research*, *20*, 271–272. Cited on page: 7

Ditchburn, R. W., Fender, D. H., & Myne, S. (1959). Vision with controlled movements of the retinal image. *Journal of Physiology*, *145*, 98–107. Cited on page: 8, 39

Ditchburn, R. W., & Ginsborg, B. L. (1952). Vision with a stabilized retinal image. *Nature*, *170*(4314), 36–37. Cited on page: 8

Ditchburn, R. W., & Ginsborg, B. L. (1953). Involuntary eye movements during fixation. *Journal of Physiology-London*, *119*(1), 1–17. Cited on page: 6, 49

Donaldson, I. M. L. (2000). The functions of the proprioceptors of the eye muscles. *Philosophical Transactions of the Royal Society B: Biological Sciences*, *355*(1404), 1685–1754. Cited on page: 3

Edwards, A. M., Phillips, R. A., Watkins, N. W., Freeman, M. P., Murphy, E. J., Afanasyev, V., Buldyrev, S. V., da Luz, M. G. E., Raposo, E. P., Stanley, H. E., & Viswanathan, G. M. (2007). Revisiting levy flight search patterns of wandering albatrosses, bumblebees and deer. *Nature*, *449*(7165), 1044–1048. Cited on page: 37, 38

Einstein, A. (1905). Über die von der molekularkinetischen Theorie der Wärme geforderte Bewegung von in ruhenden Flüssigkeiten suspendierten Teilchen. *Annalen der Physik*, *322*, 549–560. Cited on page: 21

Eizenman, M., Hallet, P. E., & Frecker, R. C. (1985). Power spectra for ocular drift and tremor. *Vision Research*, *25*(11), 1635–1640. Cited on page: 5, 9

Engbert, R. (2006). Microsaccades: A microcosm for research on oculomotor control, attention, and visual perception. In *Visual Perception, Part 1, Fundamentals of Vision: Low and Mid-Level Processes in Perception*, vol. 154 of *Progress in Brain Research*, (pp. 177–192). Amsterdam: Elsevier Science Bv. Cited on page: 1, 8, 18, 36, 38, 63

Engbert, R., & Kliegl, R. (2003). Microsaccades uncover the orientation of covert attention. *Vision Research*, *43*(9), 1035–1045. Cited on page: 6, 7, 16, 17, 64, 65

Engbert, R., & Kliegl, R. (2004). Microsaccades keep the eyes' balance during fixation. *Psychological Science*, *15*(6), 431–436. Cited on page: 18, 22

Engbert, R., & Mergenthaler, K. (2006). Microsaccades are triggered by low retinal image slip. *Proceedings of the National Academy of Sciences of the USA*, *103*(18), 7192–7197. Cited on page: 15, 17, 39, 40, 66, 68

Epelboim, J., & Kowler, E. (1993). Slow control with eccentric targets: Evidence against a position-corrective model. *Vision Research*, *33*(3), 361–380. Cited on page: 51, 67

Eurich, C. W., & Milton, J. G. (1996). Noise-induced transitions in human postural sway. *Physical Review E*, *54*(6), 6681–6684. Cited on page: 53

Feder, J. (1988). *Fractals*. Plenum Pr., New York. Cited on page: 21

Fermüller, C., Pless, R., & Aloimonos, Y. (1997). Families of stationary patterns producing illusory movement: Insights into the visual system. *Proceedings of the Royal Society B: Biological Sciences*, *264*(1383), 795–806. Cited on page: 63

Findlay, J. M., & Gilchrist, I. D. (2003). *Active Vision*. Oxford University Press. Cited on page: 2

Fiorentini, A., & Ercole, A. M. (1966). Involuntary eye movements during attempted monocular fixation. *Atti della Fondazione Giorgio Ronchi*, *21*, 199–217. Cited on page: 34

Freund, H., & Grassberger, P. (1992). The red queens walk. *Physika A*, *190*(3-4), 218–237. Cited on page: 68

Gaarder, K., Koresko, R., & Kropfl, W. (1966). The phasic relation of a component of alpha rhythm to fixation saccadic eye movements. *Electroencephalography and Clinical Neurophysiology*, *21*, 544–551. Cited on page: 66, 68

Girard, B., & Berthoz, A. (2005). From brainstem to cortex: Computational models of saccade generation circuitry. *Progress in Neurobiology*, *77*, 215–251. Cited on page: 44, 45, 67

Goltz, H. C., Irving, E. L., Steinbach, M. J., & Eizenman, M. (1997). Vertical eye position control in darkness: Orbital position and body orientation interact to modulate drift velocity. *Vision Research*, *37*(6), 789–798. Cited on page: 6

Guitton, D. (1992). Control of eye head coordination during orienting gaze shifts. In R. H. S. Carpenter (Ed.) *Eye Movements*, (p. 244). Mc Millan, London. Cited on page: 48, 53

Hafed, Z. M., & Clark, J. J. (2002). Microsaccades as an overt measure of covert attention shifts. *Vision Research*, *42*(22), 2533–2545. Cited on page: 7, 63, 64

Hanes, D. P., Patterson, W. F., & Schall, J. D. (1998). Role of frontal eye fields in countermanding saccades: Visual, movement, and fixation activity. *Journal of Neurophysiology*, *79*, 817–834. Cited on page: 49

Hansen, R. M., & Skavenski, A. A. (1977). Accuracy of eye position information for motor control. *Vision Research*, *17*, 919–926. Cited on page: 50

Harris, C. H., & Wolpert, D. M. (2006). The main sequence of saccades optimizes speed-accuracy trade-off. *Biological Cybernetics*, *95*, 21–29. Cited on page: 36, 43

Hartigan, J. A., & Hartigan, P. M. (1985). The dip test of unimodality. *The Annals of Statistics*, *13*(1), 70–84. Cited on page: 36

Hartigan, P. M. (1985). Computation of the dip statistic to test for unimodality. *Applied Statistics*, *34*(3), 320–325. Cited on page: 36

Hartline, H. K. (1940). The nerve messages in the visual pathway. *Journal of the Optical Society of America*, *30*, 239–247. Cited on page: 39

Helmholtz, H. v. (1867). *Handbuch der physiologischen Optik*. Leopold Voss, Leipzig. http://vlp.mpiwg-berlin.mpg.de/library/data/lit3858. Cited on page: 4, 5, 8

Hermann, L. (1870). Eine Erscheinung des simultanen Contrastes. *Pflügers Archive Gesamte Physiologie*, *3*, 13–15. Cited on page: 63

Holschneider, M., Paladini, C., Kliegl, R., & Engbert, R. (2006). Automatic detection and characterization of microsaccades. *Perception (ECVP06 Abstracts)*, *35*, 230. Cited on page: 68

Hotson, J. . R. (1982). Cerebellar control of fixational eye movements. *Neurology*, *32*, 31–36. Cited on page: 46

Hu, K., Ivanov, P. C., Chen, Z., Carpena, P., & Stanley, H. E. (2001). Effects of trends on detrended fluctuation analysis. *Physical Review E*, *64*, 011114. Cited on page: 27

Hung, G. K. (2001). *Models of Oculomotor Control*. World Scientific Publishing Co. Pte. Ltd. Cited on page: 3

Hurst, H. E. (1951). Long-term storage capacity of reservoirs. *American Society of Civil Engineers Transactions*, *116*, 770–799. Cited on page: 21, 22, 23

Hurst, H. E., Black, R. P., & Simaika, Y. M. (1965). *LongTerm Storage: An Exerimental Study*. Constable, London. Cited on page: 22, 23

ISI Web of Knowledge (n.d.). Website. http://apps.isiknowledge.com. Cited on page: 64

Kantelhardt, J. W., Koscielny-Bunde, E., Rego, H. H. A., Havlin, S., & Bunde, A. (2001). Detecting long-range correlations with detrended fluctuation analysis. *Physica A*, *295*(3-4), 441–454. Cited on page: 31

Keller, E. L., & Missal, M. (2003). Shared brainstem pathways for saccades and smooth-pursuit eye movements. *Annals of the New York Academy of Sciences*, *1004*, 29–39. Cited on page: 48

Kelly, D. H. (1979). Motion and vision: I. Stabilized images of stationary gratings. *Journal of the Optical Society of America*, *69*, 1266–1274. Cited on page: 8

Kitaoka, A. (n.d.). Akiyoshi's illusion pages. Website. http://www.ritsumei.ac.jp/~akitaoka/index-e.html. Cited on page: 4, 63

Kitaoka, A., & Ashida, H. (2003). Phenomenal characteristics of the peripheral drift illusion. *Vision*, *15*, 261–262. Cited on page: 63

Kohama, T., & Usui, S. (2002). Attentional effects on microsaccadic eye movements. *Cahiers de Psychologie Cognitive / Current Psychology of Cognition*, *21*(4-5), 377–395. Cited on page: 7, 16, 64

Kowler, E., & Steinman, R. M. (1979). Miniature saccades: Eye movements that do not count. *Vision Research*, *19*, 105–108. Cited on page: 64

Kowler, E., & Steinman, R. M. (1980). Small saccades serve no useful purpose - Reply. *Vision Research*, *20*(3), 273–276. Cited on page: 7, 64

Krauskopf, J., Cornsweet, T. N., & Riggs, L. A. (1960). Analysis off eye movements during monocular and binocular fixation. *Journal of the Optical Society of America*, *50*, 572–578. Cited on page: 49

Kumar, T., & Glaser, D. A. (2006). Illusory motion in Enigma: A psychophysical investigation. *Proceedings of the National Accademy of Sciences of the USA*, *103*, 1947–1952. Cited on page: 63

Laubrock, J., Engbert, R., & Kliegl, R. (2005). Microsaccade dynamics during covert attention. *Vision Research*, *45*(6), 721–730. Cited on page: 7

Laubrock, J., Engbert, R., Rolfs, M., & Kliegl, R. (2007). Microsaccades are an index of covert attention. Commentary on Horowithz, Fine, Fencsik, Yurgenson, and Wolfe (2007). *Psychological Science*, *18*(4), 364–366. Cited on page: 63

Lefévre, P., Quaia, C., & Optican, L. M. (1998). Distributed model of control of saccades by superior colliculus and cerebellum. *Neural Networks*, *11*, 1175–1190. Cited on page: 44

Lehmann, D., Beeler Jr., G. W., & Fender, D. H. (1965). Changes in patterns of the human electroencephalogram during fluctuations of perception of stabilized retinal images. *Electroencephalography and Clinical Neurophysiology*, *19*, 336–343. Cited on page: 66

Leopold, D. A., & Logothetis, N. K. (1998). Microsaccades differentially modulate neural activity in the striate and extrastriate visual cortex. *Experimental Brain Research*, *123*, 341–345. Cited on page: 64

Lettvin, J. Y., Maturana, H. R., McCulloch, W. S., & Pitts, W. H. (1959). What the frog's eye tells the frog's brain. *Proceedings of the Institute of Radio Engineers*, *47*, 1940–1951. Cited on page: 1

Leviant, I. (1996). Does "brain-power" make enigma spin? *Proceedings of the Royal Society B: Biological Science*, *263*, 997–1001. Cited on page: 63

Liang, J. R., Moshel, S., Zivotofsky, A. Z., Caspi, A., Engbert, R., Kliegl, R., & Havlin, S. (2005). Scaling of horizontal and vertical fixational eye movements. *Physical Review E*, *71*, 031909. Cited on page: 25

Liebovitch, L. S., & Yang, W. M. (1997). Transition from persistent to antipersistent correlation in biological systems. *Physical Review E*, *56*(4), 4557–4566. Cited on page: 22

Longtin, A., Milton, J. G., Bos, J. E., & Mackey, M. C. (1990). Noise and critical-behavior of the pupil light reflex at oscillation onset. *Physical Review A*, *41*(12), 6992–7005. Cited on page: 52

Mandelbrot, B. B. (1967). How long is the coast of britain? Statistical self-similarity and fractal dimensions. *Science*, *156*, 636–638. Cited on page: 39

Mandelbrot, B. B., & van Ness, J. W. (1968). Fractional brownian motions, fractional noise and applications. *SIAM Reviews*, *10*, 422–436. Cited on page: 21

Martinez-Conde, S. (2006). Fixational eye movements in normal and pathological vision. *Progress in Brain Research*, *154*, 151–176. Cited on page: 63, 65

Martinez-Conde, S., & Macknik, S. L. (2007). Windows on the mind. *Scientific American*, (pp. 56–63). Cited on page: 63

Martinez-Conde, S., Macknik, S. L., & Hubel, D. H. (2000). Microsaccadic eye movements and firing of single cells in the striate cortex of macaque monkeys. *Nature Neuroscience*, *3*(3), 251–258. Cited on page: 16, 63, 64, 65

Martinez-Conde, S., Macknik, S. L., & Hubel, D. H. (2002). The function of bursts of spikes during visual fixation in the awake primate lateral geniculate nucleus and primary visual cortex. *Proceedings of the National Academy of Sciences of the USA*, *99*(21), 13920–13925. Cited on page: 63, 64

Martinez-Conde, S., Macknik, S. L., & Hubel, D. H. (2004). The role of fixational eye movements in visual perception. *Nature Reviews Neuroscience*, *5*(3), 229–240. Cited on page: 4, 5, 7, 45

Martinez-Conde, S., Macknik, S. L., Troncoso, X. G., & Dyar, T. A. (2006). Microsaccades counteract visual fading during fixation. *Neuron*, *49*(2), 297–305. Cited on page: 63, 65, 68

Matin, L., Matin, E., & Pearce, D. G. (1970). Eye movements in dark during attempt to maintain a prior fixation position. *Vision Research*, *10*(9), 837–857. Cited on page: 6

McPeek, R. M., & Keller, E. L. (2002). Saccade target selection in the superior colliculus during a visual search task. *Journal of Neurophysiology*, *88*, 2019–2034. Cited on page: 33

Mergenthaler, K., & Engbert, R. (2007). Modeling the control of fixational eye movements with neurophysiological delays. *Physical Review Letters*, *98*, 138104. Cited on page: 15, 18, 22, 25, 44, 63, 66, 67

Mergenthaler, K., & Engbert, R. (subm). Microsaccade detection and its impact on rate and amplitude under different visual conditions. Cited on page: 15, 18, 40, 65, 66

Metzler, R., & Klafter, J. (2004). The restaurant at the end of the random walk: Recent developments in the description of anomalous transport by fractional dynamics. *Journal of Physics A*, *37*, R161. Cited on page: 39

Michalik, M. (1987). Spectral-analysis of the ocular microtremor in patients with brain-stem disorders. *EEG-EMG-Zeitschrift für Elektroenzephalographie Elektromyographie und verwandte Gebiete*, *18*(1), 20–26. Cited on page: 5, 9, 49

Møller, F., Laursen, M. L., & Sjolie, A. K. (2006). The contribution of microsaccades and drifts in the maintenance of binocular steady fixation. *Graefe's Archive for Clinical and Experimental Ophthalmology*, *244*, 465–471. Cited on page: 6, 7, 18, 65

Møller, F., Laursen, M. L., Tygesen, J., & Sjolie, A. K. (2002). Binocular quantification and characterization of microsaccades. *Graefe's Archive for Clinical and Experimental Ophthalmology*, *240*, 765–770. Cited on page: 7, 16, 18, 41

Moreau, L., & Sontag, E. (2003). Balancing at the border of instability. *Physical Review E*, *68*, 020901. Cited on page: 53, 67

Moschovakis, A. K., Scudder, C. A., & Highstein, S. M. (1996). The microscopic anatomy and physiology of the mammalian saccadic system. *Progress in Neurobiology*, *50*(2-3), 133. Cited on page: 3, 44, 46, 47, 52, 53, 55, 67, 69, 70

Munoz, D. P., & Wurtz, R. H. (1993a). Fixation cells in monkey superior colliculus. I. Characteristics of cell discharge. *Journal of Neurophysiology*, *70*, 559–575. Cited on page: 49

Munoz, D. P., & Wurtz, R. H. (1993b). Fixation cells in monkey superior colliculus. II. Reversible activation and deactivation. *Journal of Neurophysiology*, *70*, 576–589. Cited on page: 49

Murphy, B. J., Kowler, E., & Steinman, R. M. (1975). Slow oculomotor control in the presence of moving backgrounds. *Vision Research*, *15*, 1263–1268. Cited on page: 49

Nachmias, J. (1959). 2-dimensional motion of the retinal image during monocular fixation. *Journal of the Optical Society of America*, *49*(9), 901–908. Cited on page: 6, 7, 15

Nachmias, J. (1961). Determiners of the drift of the eye during monocular fixation. *Journal of the Optical Society of America*, *51*(7), 761–766. Cited on page: 6, 34, 49

Newman, M. E. J. (2005). Pareto distributions and Zipf's law. *Contemporary physics*, *46*, 323–351. Cited on page: 38

Ohira, T. (1997). Oscillatory correlation of delayed random walks. *Physical Review E*, *55*(2), R1255–R1258. Cited on page: 52, 66, 67

Ohira, T., & Milton, J. G. (1995). Delayed random-walks. *Physical Review E*, *52*(3), 3277–3280. Cited on page: 52

Ohira, T., & Sawatari, R. (1997). Delay estimation from noisy time series. *Physical Review E*, *55*(3), R2077 – R2080. Cited on page: 68, 73, 75

Ohira, T., & Yamane, T. (2000). Delayed stochastic systems. *Physical Review E*, *61*(2), 1247–1257. Cited on page: 52

Ölveczky, B. P., Baccus, S. A., & Meister, M. (2003). Segregation of object and background motion in the retina. *Nature*, *423*(6938), 401–408. Cited on page: 2, 10, 39

Ouchi, H. (1977). *Japanese Optical and Geometrical Art*. Dover, New York. Cited on page: 10, 63

Pack, C., Grossberg, S., & Mingolla, E. (2001). A neural model of smooth pursuit control and motion perception by cortical area MST. *Journal of Cognitive Neuroscience*, *13*(1), 102–120. Cited on page: 49

Pelli, D. G. (1997). The VideoToolbox software for visual psychophysics: Transforming numbers into movies. *Spatial Vision*, *10*, 437–442. Cited on page: 12

Peng, C. K., Buldyrev, S. V., Havlin, S., Simons, M., Stanley, H. E., & Goldberger, A. L. (1994). Mosaic organization of DNA nucleotides. *Physical Review E*, *49*(2), 1685–1689. Cited on page: 22, 24

Peng, C. K., Havlin, S., Stanley, H. E., & Goldberger, A. L. (1995). Quantification of scaling exponents and crossover phenomena in nonstationary heartbeat time series. *Chaos*, *5*(1), 82–87. Cited on page: 25

Percival, D. B., & Walden, A. T. (2000). *Wavelet Methods for Time Series Analysis*. Cambridge, University Press, Cambridge, England. Cited on page: 22, 27

Pitkow, X., Sompolinsky, H., & Meister, M. (2007). A neural computation for visual acuity in the presence of eye movements. *Public Library of Science Biology*, *5*(12), 2898–2911. Cited on page: 63, 66

Prichard, D., & Theiler, J. (1994). Generating surrogate data for time-series with several simultaneously measured variables. *Physical Review Letters*, *73*(7), 951–954. Cited on page: 18

Quaia, C., Aizawa, H., Optican, L. M., & Wurtz, R. H. (1998). Reversible inactivation of superior culliculus. II. Maps of saccadic deficits. *Journal of Neurophysiology*, *79*, 2097–2110. Cited on page: 45

Ratliff, F., & Riggs, L. A. (1950). Involuntary motions of the eye during monocular fixation. *Journal of Experimental Psychology*, *40*(6), 687–701. Cited on page: 4, 5, 15

Rattle, J. D. (1969). Effect of target size on monocular fixation. *Optica Acta*, *16*, 183–192. Cited on page: 50

Riggs, L. A., Armington, J. C., & Ratliff, F. (1954). Motions of the retinal image during fixation. *Journal of the Optical Society of America*, *44*, 315–321. Cited on page: 49

Riggs, L. A., & Ratliff, F. (1952). The effect of counteracting the normal movements of the eye. *Journal of the Optical Society of America*, *42*, 872–873. Cited on page: 8

Riggs, L. A., Ratliff, F., Cornsweet, J. C., & Cornsweet, T. N. (1953). The disappearance of steadily fixated visual test objects. *Journal of the Optical Society of America*, *43*(6). 11. Cited on page: 8

Rolfs, M., Kliegl, R., & Engbert, R. (2008). Towards a model of microsaccade generation: The case of microsaccadic inhibition. *Journal of Vision*, *8*(11), 1–23. Cited on page: 33

Rolfs, M., Laubrock, J., & Kliegl, R. (2006). Shortening and prolongation of saccade latencies following microsaccades. *Experimental Brain Research*, *169*, 369–376. Cited on page: 65

Rucci, M., & Desbordes, G. (2003). Contribution of fixational eye movements to the discrimination of briefly presented stimuli. *Journal of Vision*, *3*, 852–864. Cited on page: 8

Rucci, M., Iovin, R., Poletti, M., & Santini, F. (2007). Miniature eye movements enhance fine spatial detail. *Nature*, *447*(7146), 851–855. Cited on page: 9, 39, 63

Scafetta, N., & Grigolini, P. (2002). Scaling detection in time series: Diffusion entropy analysis. *Physical Review E*, *66*, 036130. Cited on page: 22, 27

Schiller, P. H., & Stryker, M. (1972). Single-unit recording and stimulation in superior colliculus of the alert rhesus monkey. *Journal of Neurophysiology*, *35*, 915–924. Cited on page: 33

Schiller, P. H., True, S. D., & Conway, J. L. (1980). Deficits in eye movements following frontal eye field and superior colliculus ablation. *Journal of Neurophysiology*, *44*, 1175–1189. Cited on page: 45

Schulz, E. (1984). Binocular micro-movements in normal persons. *Graefe's Archive Clinical Experimental Optalmology*, *222*, 95–100. Cited on page: 7, 18

Seung, H. S. (1996). How the brain keeps the eyes still. *Proceedings of the National Academy of Sciences of the USA*, *93*, 13339–13344. Cited on page: 51, 67

Shlesinger, M. F. (2006). Search research. *Nature*, *443*, 281–282. Cited on page: 39

Shlesinger, M. F., Zaslavsky, G. M., & Frisch, U. (Eds.) (1995). *Lévy Flights and Related Topics in Physics*. Springer, Berlin. Cited on page: 8, 39

Siefert, M. (2007). Practical criterion for delay estimation using random perturbations. *Physical Review E*, *76*, 026215. Cited on page: 68

Skavenski, A. A. (1972). Inflow as a source of extraretinal eye position information. *Vision Research*, *12*(2), 221. Cited on page: 6

Skavenski, A. A., Hansen, R. M., Steinman, R. M., & Winterson, B. J. (1979). Quality of retinal image stabilization during small natural and artificial body rotations in man. *Vision Research*, *19*(6), 675–683. Cited on page: 9

Skavenski, A. A., & Steinman, R. M. (1970). Control of eye position in dark. *Vision Research*, *10*(2), 193–203. Cited on page: 34

Sparks, D. L. (1986). Translation of sensory signals into commands for control of saccadic eye-movements—Role of primate superior colliculus. *Physiological Reviews*, *66*(1), 118–171. Cited on page: 47, 54

Sparks, D. L. (2002). The brainstem control of saccadic eye movements. *Nature Reviews Neuroscience*, *3*(12), 952–964. Cited on page: 44, 45, 52, 53, 67

Spauschuss, A., Marsden, J., Halliday, D. M., Rosenberg, J. R., & Brown, P. (1999). The origin of ocular microtremor in man. *Experimental Brain Research*, *126*, 556–562. Cited on page: 5, 9, 49

Stampe, D. M. (1993). Heuristic filtering and reliable calibration methods for video-based pupil-tracking systems. *Behavior Research Methods, Instruments, & Computers*, *23*(2), 137–142. Cited on page: 11

St.Cyr, G. J., & Fender, D. H. (1969). The interplay of drift and flicks in binocular fixation. *Vision Research*, *9*, 245–269. Cited on page: 6

Steinman, R. M. (1965). Effect of target size, luminance, and color on monocular fixation. *Journal of the Optical Society of America*, *55*, 1158–1165. Cited on page: 50

Steinman, R. M., Cunitz, R. J., Timberla.Gt, & Herman, M. (1967). Voluntary control of microsaccades during maintained monocular fixation. *Science*, *155*(3769), 1577–1579. Cited on page: 6

Steinman, R. M., Haddad, G. M., Skavenski, A. A., & Wyman, D. (1973). Miniature eye movements. *Science*, *181*(4102), 810–819. Cited on page: 6, 9, 66

Steinman, R. M., Pizlo, Z., Forofonova, T. I., & Epelboim, J. (2003). One fixates accurately in order to see clearly not because one sees clearly. *Spatial Vision*, *16*, 225–241. Cited on page: 9

Theiler, J., Eubank, S., Longtin, A., Galdrikian, B., & Farmer, J. D. (1992). Testing for nonlinearity in time-series— The method of surrogate data. *Physica D*, *58*(1-4), 77–94. Cited on page: 18, 19

Timberlake, G., Wyman, D., Skavensky, A., & Steinman, R. (1972). The oculomotor error signal in the fovea. *Vision Research*, *12*, 1059–1064. Cited on page: 50

Tulunay-Keesey, U. (1960). Effects of involuntary eye movements on visual acuity. *Journal of the Optical Society of America*, *50*, 769–774. Cited on page: 8

Valsecchi, M., Betta, E., & Turatto, M. (2007). visual oddballs induce prolonged microsaccadic inhibition. *Experimental Brain Research*, *177*, 196–208. Cited on page: 65

Valsecchi, M., & Turatto, M. (2007). Microsaccadic response to visual events that are invisible to the superior colliculus. *Behavioral Neuroscience*, *121*(4), 786–793. Cited on page: 33, 68

Vasudevan, R., Phatak, A. V., & Smith, J. D. (1972). A stochastic model for eye movements during fixation on a stationary target. *Kybernetik*, *11*, 24–31. Cited on page: 50, 67

Viswanathan, G. M., Afanasyev, V., Buldyrev, S., Murphy, E., Prince, P. A., & Stanley, H. E. (1996). Lévy flight search patterns of wandering albatrosses. *Nature*, *381*(6581), 413–415. Cited on page: 37

Wei, L., Levi, D. M., Li, R. W., & Klein, S. A. (2007). Feasibility study on a hyperacuity device with motion uncertainty: Two-point stimuli. *IEEE Transactions on Systems, Man, and Cybernetics - Part B: Cybernetics*, *37*(2), 385–397. Cited on page: 63

Wyman, D., & Steinman, R. M. (1973). Small step tracking: Implications for the oculomotor "dead zone". *Vision Research*, *13*(11), 2165–2172. Cited on page: 50

Yao, W., Yu, P., & Essex, C. (2001). Delayed stochastic differential model for quiet standing. *Physical Review E*, *63*(2), 021902. Cited on page: 52, 67

Yuval-Greenberg, S., Tomer, O., Keren, A. S., Nelken, I., & Deouell, L. Y. (2008). Transient induced gamma-band response in EEG as a manifestaion of miniature saccades. *Neuron*, *58*, 429–441. Cited on page: 64

Zuber, B. L., Stark, L., & Cook, G. (1965). Microsaccades and velocity-amplitude relationship for saccadic eye movements. *Science*, *150*(3702), 1459. Cited on page: 36, 45